Fall 1-31-2001

Numerical stimulation of stress-induced crystallization of injection molded semicrystalline thermoplastics

Jianxin Guo
New Jersey Institute of Technology

ABSTRACT

NUMERICAL SIMULATION OF STRESS-INDUCED CRYSTALLIZATION OF INJECTION MOLDED SEMICRYSTALLINE THERMOPLASTICS

by
Jianxin Guo

Injection molded semicrystalline plastic products exhibit variable morphology along their thickness directions. The processing conditions have a significant effect on the crystallinity distribution in the final parts. However, because of the lack of sound theoretical models for stress-induced crystallization kinetics in thermoplastics, simulations of the injection molding process of semicrystalline plastics with the consideration of stress-induced crystallization have been scarce.

A stress-induced crystallization model for semicrystalline plastics is proposed based on the theory that stress induced orientation of polymer chains increase the melting temperature of the plastics, and hence, the supercooling which is the driving force for crystallization. By assuming that the effect of stress on crystallization is only by increasing the equilibrium melting temperature, the basic quiescent state crystallization equation can be directly applied to model stress-induced crystallization kinetics. A simple experimental technique such as rotational rheometric measurement, can be used to determine the melting temperature shift. The model predicts the most prominent features of stress-induced crystallization: with the application of shear stress, crystallization rate becomes higher, the crystallization temperature range is broadened and the peak of crystallization rate shifts to higher temperatures. The main advantage of the model is that the parameters in the quiescent state crystallization model do not change and the

parameters in the equilibrium melting temperature shift model are easy to determine. And the unknown constants are kept to a minimum.

The injection molding process of semicrystalline plastics was simulated with the proposed stress-induced crystallization model. A pseudo-concentration method was used to track the melt front advancement. The simple Maxwell stress relaxation model in combination with WFL equation was used to investigate the importance of stress relaxation on the development of crystallinity during the injection molding. Simulations were carried out under different processing conditions to investigate the effect of processing parameters on the crystallinity of the final part. Other results such as skin layer build-up and mold pressure were also simulated. The simulation results reproduced most of the features that were obtained by the experiments reported in the literature.

NUMERICAL SIMULATION OF STRESS-INDUCED CRYSTALLIZATION OF INJECTION MOLDED SEMICRYSTALLINE THERMOPLASTICS

by
Jianxin Guo

A Dissertation
Submitted to the Faculty of
New Jersey Institute of Technology
In Partial Fulfillment of the Requirements for the Degree of
Doctor of Philosophy in Mechanical Engineering

Department of Mechanical Engineering

January 2001

APPROVAL PAGE

NUMERICAL SIMULATION OF STRESS-INDUCED CRYSTALLIZATION OF INJECTION MOLDED SEMICRYSTALLINE THERMOPLASTICS

Jianxin Guo

Dr. Kwabana A. Narh, Dissertation Advisor — Date
Associate Professor of Mechanical Engineering, NJIT

Dr. Rong Y. Chen, Committee Member — Date
Professor of Mechanical Engineering, NJIT

Dr. Costas G. Gogos, Committee Member — Date
Professor of Chemical Engineering, NJIT
President of Polymer Processing Institute, Newark, NJ

Dr. Zhiming Ji, Committee Member — Date
Associate Professor of Mechanical Engineering, NJIT

Dr. Pushpendra Singh, Committee Member — Date
Assistant Professor of Mechanical Engineering, NJIT

Dr. Marino Xanthos, Committee Member — Date
Professor of Chemical Engineering, NJIT
Director of Research, Polymer Processing Institute, Newark, NJ

BIOGRAPHICAL SKETCH

Author: Jianxin Guo

Degree: Doctor of Philosophy in Mechanical Engineering

Date: January 2001

Undergraduate and Graduate Education:

- Doctor of Philosophy in Mechanical Engineering,
  New Jersey Institute of Technology, Newark, New Jersey, 2000

- Master of Science in Mechanical Engineering,
  Beijing University of Chemical Technology, Beijing, P. R. China, 1987

- Bachelor of Science in Mechanical Engineering,
  Beijing University of Chemical Technology, Beijing, P. R. China, 1984

Major: Mechanical Engineering

Presentations and Publications:

Guo, J. and K. A. Narh (2000)
"Computer Simulation of Stress-Induced Crystallization in Injection Molded Thermoplastics Part I: A Model for Stress Induced Crystallization Kinetics and Parameter Formulation," submitted to *Polymer Engineering and Science.*

Guo, J. and K. A. Narh (2000)
"Computer Simulation of Stress-Induced Crystallization in Injection Molded Thermoplastics Part II: Result of Simulation," submitted to *Polymer Engineering and Science.*

Guo, J. and K. A. Narh (2000)
"On the Prediction of Crystallinity Distribution in Injection Molded Semicrystalline Thermoplastics" Proceedings of SPE-ANTEC Conference, May 7-11, 2000, Orlando, Florida, pp538-542 (selected for publication by *Journal of Reinforced Plastics and Composites*).

Guo, J. (2000)
"A New Finite Difference Formulation of 2-D Partial Differential Equations", Ninth Annual Uni-Tech Conference, April 28, 2000, Newark, New Jersey.

Guo, J. and Narh, K. A. (2000)
"Buckling Analysis on the Stud Assembly and Simulation on the Spacer Punching Process", *Simulations*, in press.

Narh, K. A., J. Guo, M. Xanthos, U. Yilmazer and V. Tan (1999)
"Product Design with High Value Recyclable Plastics Waste Streams," Proceedings of SPE-ANTEC Conference, May 2-6, 1999, New York, pp3294-3298.

Narh, K. A., J. Guo and Z. Li (1998)
"Measurement and Molding of Flow and Mechanical Properties of ASR-Filled Polymer Composites," *Polymer Composites*, vol. 19, pp787-792.

Guo, J. and K. A. Narh,
"Evaluation of Rheological and Mechanical Properties of ASR/PE Composites," Eighth Annual Uni-Tech Conference, April 24, 1998.

Guo, J. (1998)
"Characterization of ASR-Filled Plastics and Simulation of Some Application on Recycled Plastics", Presentation at monthly student meeting, Multi-life-cycle Engineering Research Center, NJIT, March 1998.

To my beloved family

ACKNOWLEDGEMENT

I would like to thank my dissertation advisor, Dr. Narh, for his valuable guidance and suggestions during my dissertation research. I would also like to thank Dr. R. Chen, Dr. Gogos, Dr. Z. Ji, Dr. P. Singh and Dr. M. Xanthos for serving as dissertation committee members, and for providing many valuable suggestions for my doctoral research.

Special thanks to the Multi-life-cycle Engineering Research Center, New Jersey Institute of Technology, for providing financial support for my PhD studies from September 1997 to May 2000, and thanks also to the Mechanical Engineering Department, NJIT, for funding an assistantship from September 1996 to August 1997, as well as the Fall semester, 2000.

Also, I would like to express my appreciation to Dr. Gogos, Dr. Xanthos and Dr. Tan of the Polymer Processing Institute, for providing useful information and suggestions for this study.

TABLE OF CONTENTS

Chapter		Page
1	INTRODUCTION	1
	1.1 Injection Molding Process	1
	1.2 Crystallization in Polymers	5
	1.2.1 Amorphous and Crystalline States	5
	1.2.2 Crystallization Under Quiescent State	6
	1.2.3 Stress Induced Crystallization	11
	1.2.4 Effect of Crystallinity on the Properties of Polymers	13
	1.3 Injection Molded of Semicrystalline Plastics	15
2	LITERATURE REVIEW	18
	2.1 Simulation of Injection Molding Process	18
	2.2 Simulation of Injection Molding of Semicrystalline Plastics	20
3	MOTIVATION AND OBJECTIVES	29
4	A MODEL FOR STRESS-INDUCED CRYSTALLIZATION KINETICS OF POLYMERS	31
	4.1 Crystallization in Quiescent State	33
	4.2 Determination of Parameters for Quiescent State Crystallization	36
	4.2.1 Brief Description of the Experiment	36
	4.1.2 Determination of the Kinetic Parameters Using Experimental Data	37
	4.3 Shear Induced Crystallization	42
	4.4 Determination of Parameters for the Kinetics of Stress Induced Crystallization	46

TABLE OF CONTENTS
(Continued)

Chapter	Page
4.5 Summary	56
5 MELT FRONT TRACKING TECHNIQUE	58
5.1 Problem Statement	58
5.2 F-Smooth Technique	62
5.3 Special Treatment during Advancement of Melt Front	64
6 MATHEMATICAL MODEL	67
6.1 Hypothesis and Assumptions	67
6.2 Governing Equations	68
6.3 Initial and Boundary Conditions	72
6.4 The Rheological Model	74
6.5 Transport Equations of Induction Time Index and Crystallinity	76
6.6 Governing Equations for Post Filling Stage	77
6.7 Stress Relaxation Model	77
7 FINITE ELEMENT EQUATION FORMULATION	79
7.1 Introduction	79
7.2 Finite Element Equations	82
7.2.1 Finite Element Equations for Velocities and Pressure	82
7.2.2 Finite Element Formulation for Pseudo-Fluid, Temperature, Crystallinity and Induction Time Index	86
7.3 Computation Procedure	86
7.4 Computation Time Saving Consideration	88

TABLE OF CONTENTS
(Continued)

Chapter		Page
8	SIMULATION RESULTS AND DISCUSSIONS	90
	8.1 Simulation of Injection Molding of PET	90
	8.1.1 Parameters Used in the Simulation	90
	8.1.2 Crystallinity at the End of Filling Stage	92
	8.1.3 The Effect of Stress Relaxation on the Development of Crystallinity	97
	8.1.4 Effect of Injection Speed	100
	8.1.5 Effect of Mold Temperature	105
	8.1.6 Effect of Holding Time	110
	8.1.7 Effect of Melt Temperature	112
	8.1.8 The Effect of TCR	116
	8.2 Simulation of Stress-Induced Crystallization in Injection Molded Polypropylene	118
	8.2.1 The Material Properties of PP	120
	8.2.2 Filling Stage	124
	8.2.3 Crystallinity in the Final iPP Part	127
	8.2.4 Crystallization Evolution During the Injection Molding Process of iPP	129
9	CONCLUSIONS AND FUTURE WORK	132
	9.1 Conclusions	132
	9.2 Recommended Future Work	135
APPENDIX A	TAYLOR GALERKIN METHOD FOR THE HYPERBOLIC EQUATIONS	136

TABLE OF CONTENTS
(Continued)

Chapter	Page
APPENDIX B TAYLOR-GALERKIN METHOD FOR ENERGY EQUATION, INDUCTION TIME INDEX AND CRYSTALLINITY DISTRIBUTION EQUATIONS.....	139
APPENDIX C COMPUTER PROGRAM.....	143
REFERENCES.....	171

LIST OF TABLES

Table **Page**

1.1 Comparison of general characteristics of semicrystalline and amorphous thermoplastics (Belofsky, 1995)..... 14

4.1 Equilibrium temperature shift with the shear stress..... 49

8.1 Induction times and equilibrium melting point shifts of PP..... 121

LIST OF FIGURES

Figure		Page
1.1	A schematic drawing of an injection molding machine (Johannaber, 1985).....	2
1.2	A Schematic illustration of polymer flow in mold cavity (Osswald and Menges, 1995).....	3
1.3	Configuration of amorphous and crystalline states of plastics (Belofsky, 1995).....	5
1.4	Crystallization process: (a) Nucleation State; (b) Growth and Nucleation; (c) Growth; (d) Impingement of crystals and completion of crystallization process.....	7
1.5	Microscope cross-polarized pictures taken during evolution of spherulities. Left: During isothermal growth; Right: Upon completion of primary crystallization (Baer and Moet 1991).....	7
1.6	Two-dimensional fringed-micelle model of semicrystalline plastics (Mandelkern, 1964).....	8
1.7	Crystallization rate versus temperature.....	9
1.8	Crystallization process in polymers.....	10
1.9	Experiment shows the effect of shear stress on crystallization of isotactic polypropylene at different shear rates (Titomanlio et al. 1997).....	11
1.10	Induction time for flow-induced crystallization as a function of shear rate for HDPE with $M_w = 1.89 \times 10^4$, $\overline{M}_n = 1.38 \times 10^4$, A: T=125°C; B: T=126°C; C: T=129°C (Lagasse and Maxwell, 1976).....	13
1.11	Microstructure in the thickness direction of injection molded HDPE, depicting various morphology regions (Tan and Kamal, 1977).....	16
2.1	Hsiung and Cakmak's crystallization model shows increased crystallization rate and temperature shift under shear stresses.....	23
2.2	The stress induced crystallization model of Titomanlio et al. for Polypropylene shows broadened crystallization temperature, fixed maximum crystallization rate.....	25

LIST OF FIGURES
(Continued)

Figure		Page
4.1	Plot of isothermal crystallization rate constant as a function of temperature. Solid circles represent the experimental data (Narh et al.,1995a). The solid line represents the best fit according equations (4.4) and (4.5).....	39
4.2	Avrami plots for isothermal crystallization at various temperatures.....	40
4.3	Comparison of prediction result using isothermal parameters with the experimental data: lines are predictions, points are experimental result.....	41
4.4	Shear stress versus shearing time showing the effect of Shear rate and temperature on the onset of crystallization (Narh et al. 1995b): (a) shows the shear dependence and (b) shows the temperature dependence.....	48
4.5	Temperature shift as a function of shear stress: data points are calculated from the experiment work of Narh et al.(1995b), line is the best fit result.....	50
4.6	Kinetics of crystallization of PET under effect of shear stress. The results show the crystallization process shift to higher temperatures with increased crystallization rate.....	52
4.7	Crystallization process of PET with/without the application of shear stress under constant cooling rate of 20°C/min.....	53
4.8	Comparison of Hsiung and Cakmak's model with present model. Dotted lines are Hsiung and Cakmak's model, solid lines are present model with the parameters formulated from parameters given by Hsiung and Cakmak (1991).....	54
4.9	Equilibrium temperature shift versus shear stress according Hsiung and Cakmak's model for PPS. Solid line represents the fitting function given by: $T_{shift} = 73\left[\exp\left(-\frac{50000}{\tau}\right)\right]$.....	55
5.1	Representation of the Flow field in pseudo-concentration technique	60

LIST OF FIGURES
(Continued)

Figure		Page
5.2	Smoothing and updating of the F-space	63
5.3	Triple points	64
5.4	Non -slip condition at the triple point shows no advancement at the contact point	65
5.5	Melt Front Advancement with 0.1 cm free slip length apart from the triple point	66
5.6	Melt front advancement with 0.2 cm free slip length	66
6.1	Mold cavity dimensions	68
6.2	Calculation Domain	69
6.3	Boundary conditions for the mold flow analysis using pseudo-concentration technique	74
7.1	Finite element model	81
7.2	Flow chart of computation procedure	88
7.3	Computation region during the filling process	89
8.1	Induction time index distribution at the end of filling stage	94
8.2	Crystallinity distribution at the end of filling stage with different injection speeds	96
8.3	Comparison of different stress relaxation models: A: No stress relaxation is considered; B: Stress effect is not considered in the cooling stage; C: Stress remains constant in the skin layer, but relaxed completely outside skin layer; D: Stress relaxation follows the WFL model. Injection rate: Q=5 cm^3/s, Mold temperature: 90°C	98

LIST OF FIGURES
(Continued)

Figure		Page
8.4	Comparison of different parameter selections for stress relaxation: Injection rate: Q=5 cm^3/s ; Mold temperature:90°C.....	99
8.5	Effect of Injection speed on the final crystallinity distribution across the thickness: material PET; melt temperature 270°C; mold temperature 90°C	102
8.6	Skin layer thickness at the end of filling with different injection speeds. PET: melt temperature 270 °C, mold temperature 90 °C.....	103
8.7	Cavity pressure at the end of filling for different injection speeds. Material: PET; Melt temperature: 270 °C ; Mold temperature: 90 °C.....	104
8.8	Effect of mold temperature on the final distribution of crystallinity. Material: PET; Injection rate: Q=5 cm^3/s	107
8.9	Effect of mold temperature on the build-up of skin layer at the end of filling stage. Material: PET; Injection rate: Q=5 cm^3/s	108
8.10	Pressure in the mold cavity under various mold temperatures. Material: PET; Injection rate: Q=5 cm^3/s	109
8.11	Effect of packing time on the crystallinity distribution across the specimen thickness at geometrical center of the molding: Injection rate: 5 cm^3/s ; Melt temperature: 270°C; Mold temperature: 90°C; TCR in packing stage: 1×10^{-5} m^2-K/W ; TCR in cooling stage: 1×10^{-3} m^2-K/W	111
8.12	Effect of melt temperature on the final crystallinity distribution in the final part. Injection rate: 5 cm^3/s ; Mold temperature: 90°C	113
8.13	Effect of melt temperature on the skin layer build-up at the end of filling.....	114
8.14	Pressure in the mold cavity at different melt temperatures.....	115

LIST OF FIGURES
(Continued)

Figure		Page
8.15	Effect of TCR on the crystallinity distribution. Injection rate: 5 cm^3/s ; Melt temperature: 270°C; Mold temperature 90°C.....	117
8.16	Comparison of crystallization rate of PP and PET.....	119
8.17	Equilibrium melting temperature shift for PP as a function of shear stress.....	122
8.18	The effect of shear stress on the crystallization rate of PP.....	123
8.19	Induction time index at the end of filling stage. x--flow direction, y--distance to the center, z--induction time index.....	125
8.20	Crystallinity at the end of filling stage: x—flow direction, y—distance from the center, z—crystallinity(%).....	126
8.21	Final crystallinity of Injection molded PP at different processing Conditions. X: Flow direction; Y: Distance from center; Z: crystallinity (%).....	128
8.22	Crystallinity evolution during the post filling stage with the consideration of shear stress. Injection rate Q=5 cm^3/s, Mold temperature: T=50°C.....	130
8.23	Crystallinity evolution in the post-filling stage without considering the effect of shear stress Injection rate: Q=5 cm^3/s, Mold temperature: 50°C.....	131

LIST OF SYMBOLS

a	Material constant for induction time
B_1, B_2	Material constants in WFL model (°C)
C_1	Material constant in melting temperature shift model (°C)
C_2	Material Constant in melting temperature shift model (Pa)
C_p	Heat capacity (J/Kg-K)
C_c	Heat of fusion of 100% crystals (J/Kg)
F	Pseudo-concentration for imaginary fluids
F_c	Cut-off value of pseudo concentration for determining the melt front
G	Shear modulus (Pa)
G_m	Gibbs free energy of the melt (J/Kg)
G_c	Gibbs free energy of the crystalline phase (J/Kg)
H_c	Enthalpy of the crystalline phase (J/Kg)
H_m	Enthalpy of the melt (J/Kg)
ΔH	Heat of fusion (J/Kg)
k	Avrami isothermal crystallization rate constant
K	Nonisothermal crystallization rate constant
K_h	Thermal conductivity (J/s-m-K)
k_g	Spherulite growth rate (K^2)
$\overline{M}_n$	Number average molecular weight
$\overline{M}_w$	Weight average molecular weight

LIST OF SYMBOLS
(Continued)

n	Avrami index
$\tilde{n}$	Power law index for viscosity
P	Pressure (Pa)
Q	Injection speed (cm^3 / s)
R	Gas constant (J/mol)
S_c	Entropy of the crystalline phase (J/Kg-°C)
S_m	Entropy of the melt (J/Kg-°C)
ΔS_f	Entropy of fusion (J/Kg-°C)
t	Time (s)
$t_{\frac{1}{2}}$	Crystallization half time (s)
t_i	Induction time (s)
$\bar{t}$	Induction time index
T_b	Material constant in cross-exponential model, reflecting the effect of temperature on viscosity (°C)
T_g	Glassy transition temperature (°C)
T_m^0	Equilibrium melting temperature (°C)
T_m	Melting temperature for stressed material (°C)
T_{shift}	Melting temperature shift from equilibrium melting temperature by shear stress (°C)

LIST OF SYMBOLS
(Continued)

T_s	Reference temperature in WFL model (°C)
T_0	Reference temperature in cross-exponential viscosity model (°C)
T_w	Mold wall temperature (°C)
T_∞	Temperature under which crystallization process ceases (°C)
t_m	Material constant for induction time (s)
T	Temperature (°C)
T_m^0	Equilibrium melting temperature (°C)
T_m	Melting temperature under shear stress (°C)
u, **u**	Velocity in x direction (m/s)
U^*	Activation constant (J/mol)
v, **v**	Velocity in y direction (m/s)
ρ	Density (Kg/m^3)
η	Apparent viscosity (Pa-s)
η_0	Zero shear rate viscosity (Pa-s)
η_x	Viscosity enhancement factor by crystallinity
χ	Absolute crystallinity (%)
χ_∞	Ultimate absolute crystallinity (%)
θ	Relative crystallinity
τ	Stress (Pa)

τ^*	Shear stress at which shear thinning begins (Cross-Exponential model) (Pa)
γ	Shear strain
$\dot{\gamma}$	Shear rate (1/s)
λ	Relaxation time (s)
λ_0	Relaxation time at reference temperature (s)
Φ	Degree of orientation

CHAPTER 1

INTRODUCTION

1.1 Injection Molding Process

Injection molding process is one of the most widely used operations in the polymer processing industry. It is characterized by high production rate, high automation, accurate dimensional precision. Products ranging from as small as small plastic gears to as large as automobile bumpers and bathtubs can be injection molded. Injection molding process is accomplished in an injection molding machine (Fig. 1.1) which basically consists of two essential components: the injection unit and the clamping unit. The function of the former is to melt the polymer and inject it into the mold cavity, whereas the clamping unit holds the mold, opens and closes it automatically, and ejects the finished products.

The most common type of injection molding machine is the in-line reciprocating screw type. The screw both rotates and undergoes axial reciprocating motion. When the screw rotates, it acts like a screw extruder, melting and pumping the polymer. When it moves axially, it acts like an injection plunger, pushing the polymer melts into the mold cavity. The screw is generally driven by a hydraulic motor and its axial motion is activated and controlled by a hydraulic system. The raw material is supplied to the injection molding machine through the feed hopper, which is located on top of the injection unit. The screw takes in the material and conveys it to the screw tip. On its way, the plastic passes through heated barrel zones, while the rotation of the screw results in a continuous rearrangement of the plastic material in the flights of the screw. Shear and heating from the barrel wall cause a largely homogeneous heating of the material. The conveying action of the screw builds up pressure in front of the tip. This pressure pushes

back the screw. As soon as there is enough supply of melt in front of the screw, the nozzle thrusts against the sprue bushing of the mold and the screw moves forward to inject the molten material into the mold cavity.

The injection molding process can be divided into three stages: filling, packing and cooling.

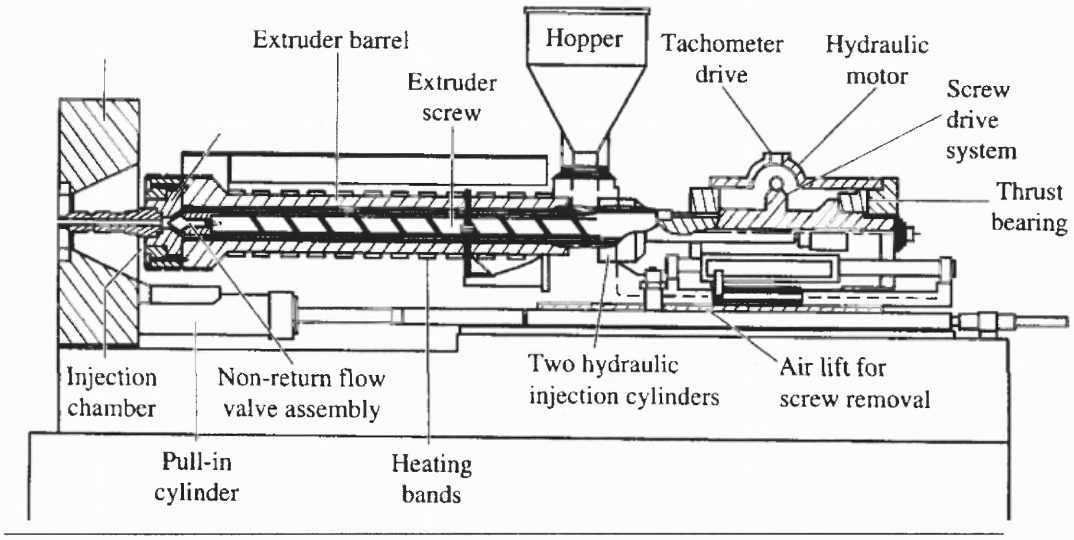

Figure 1.1 A schematic drawing of an injection molding machine (Johannaber, 1985)

During the filling stage the molten material is injected into the mold cavity under high pressure by the piston movement of the screw. As the polymer melt enters the mold cavity, the pressure in the mold rises slowly. The flow is unsteady and the polymer starts cooling as soon as it touches the mold wall. Polymer flow into the cavity does not cease when the melt fills the whole cavity of the mold. Extra polymer melt should be introduced into the cavity to compensate for the shrinkage during the cooling. At this

stage, the viscous polymer is compressed and the cavity pressure rises to its maximum. This stage is called packing stage. During the cooling stage, through the heat exchange with the walls of the mold, the polymer melt solidifies to form the final shape of the part. A continuous decrease of the pressure in cavity can be observed at this stage.

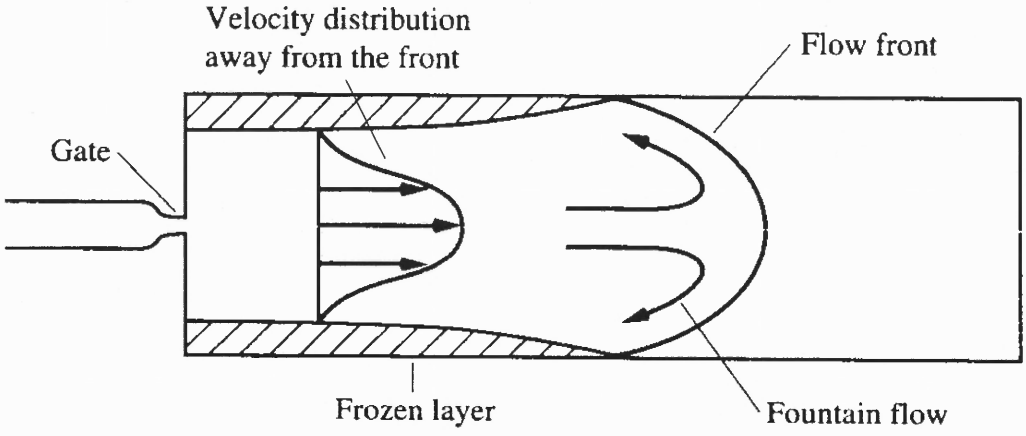

Figure 1.2 A schematic illustration of polymer melt flow in mold cavity (Osswald and Menges, 1995).

The mold filling process itself involves all the interesting and complicating aspects of polymer processing: non-isothermal, transient flow of non-Newtonian fluids in complex geometries with simultaneous structuring and solidification. The polymer melt flow in the mold cavity during the filling stage can be roughly divided into two regions: a fountain flow region and pure shear flow region (Fig. 1.2). In the fountain flow region, the polymer melt flows from the cavity center towards the wall of the mold due to the fountain effect. Once the melt touches the cold mold wall, it cools down and solidifies into a frozen layer. The fluid far behind the fountain front is under pure shear flow.

The fountain effect during the filling stage can have significant influence on the mechanical properties of the final product. According to the model proposed by Tadmor (1974), both the orientation in the close neighborhood of the wall and the transverse orientation originate from the fountain type of flow in the advancing front region, whereas the source of the rest of the orientation is primarily from the shear flow upstream the front. Within the fountain flow region, the melt has approximately undergone a steady elongational flow. As a result of the fountain type of flow, an oriented polymer layer is deposited on the cold wall of the mold. The surface layer solidifies upon contact with the cold wall, retaining the maximum elongational orientation. Further away from the surface, the fully developed shear flow behind the front is responsible for any molecular orientation that may be present in the final product.

The mechanical and physical properties of the injection molded parts do not depend only on the chemical constitution of the material and its corresponding properties. The processing conditions such as temperature, pressure and velocity distribution in the mold cavity during the molding cycle, exert a considerable influence on the mechanical and physical properties of the final parts. The polymer properties and molding conditions interact to produce the thermo-mechanical history experienced by the polymer melt, which determine the microstructure distribution and, therefore, the ultimate properties of the molded parts.

1.2 Crystallization in Polymers

1.2.1 Amorphous and Crystalline State

The basic distinguishing feature of the structure of a high polymer is a long molecular chain or backbone. The many unusual and valuable physical properties of polymers arise directly from this feature of their molecular structure.

There are two possible order types between molecular segments and their neighbors: amorphous and crystalline. An amorphous state is defined as having a purely random structure, or implies the absence of the characteristic regular arrangement of the polymeric chains, as illustrated in figure 1.3a, while the crystalline state corresponds to the highly organized pack of molecule chains (Fig.1.3b).

(a) amorphous state (b) crystal

Figure 1.3 Configuration of amorphous and crystalline states of plastics (Belofsky, 1995)

Practically, all polymers can be found in the amorphous state at sufficiently high temperatures. When the polymer melt is rapidly cooled to below its glass transition temperature, the molecules do not have the time to rearrange their conformation and their

random structure will be frozen and the polymer will maintain their amorphous state. In highly amorphous polymers, there may be some preferred orientation induced by stresses in processing, as in drawn fibers or films. Injection molded amorphous plastics may show local areas of orientation due to frozen-in flow patterns.

1.2.2 Crystallization under Quiescent State

When a semi-crystalline polymer melt is cooled down into its crystallization temperature range, crystallization starts around discrete points called 'nuclei', and the crystals grow around nuclei to form what is referred to as 'spherulites'. Once all the spherulites meet their neighbors, the crystallization process is complete. This process is illustrated in Figure 1.4. Figure 1.5 shows the picture taken during the crystallization process. It clearly shows the crystal growth and completion of the crystallization.

Many observations have indicated that the microstructure of semicrystalline plastics can be adequately represented by the so-called fringed-micelle model (Fig. 1.6). The molecular chains arrange themselves in thin, plate-like lamellae. In polymer that has been crystallized from the melt, those ordered, planar domains are separated, and the spaces between lamellae are filled with amorphous and randomly arranged macromolecules. The function of the amorphous material is to tie all of the lamellae together. In the single lamella the molecular chains are folded to form organized microstructure (Fig 1.3b). The combination of the lamellae is a spherulite, tending to grow spherically outward.

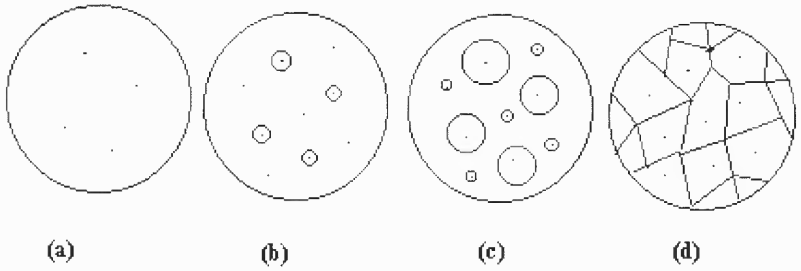

Figure 1.4 Crystallization process: (a) Nucleation stage; (b) Growth and nucleation; (c) Growth; (d) Impingement of crystals and completion of crystallization process.

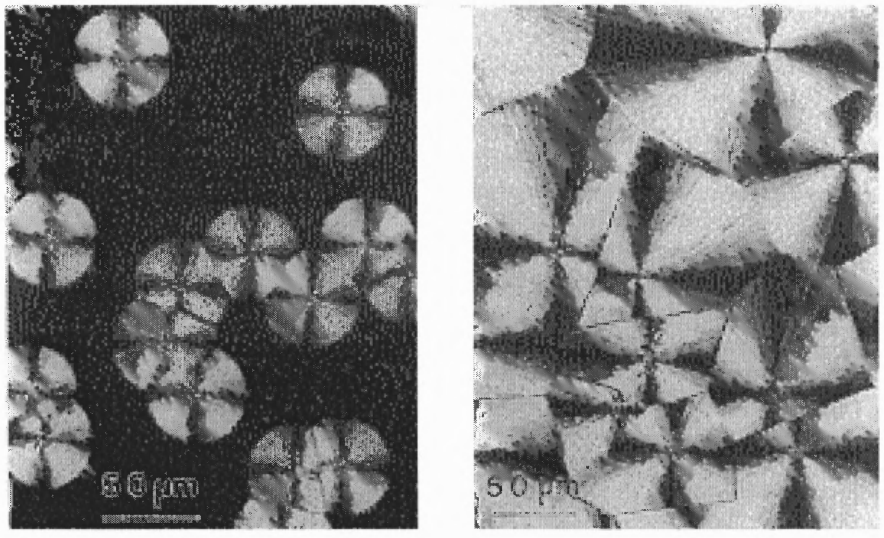

Figure 1.5 Microscope cross-polarized pictures taken during evolution of sperulities. Left: During isothermal growth. Right: Upon completion of primary crystallization (Baer and Moet, 1991)

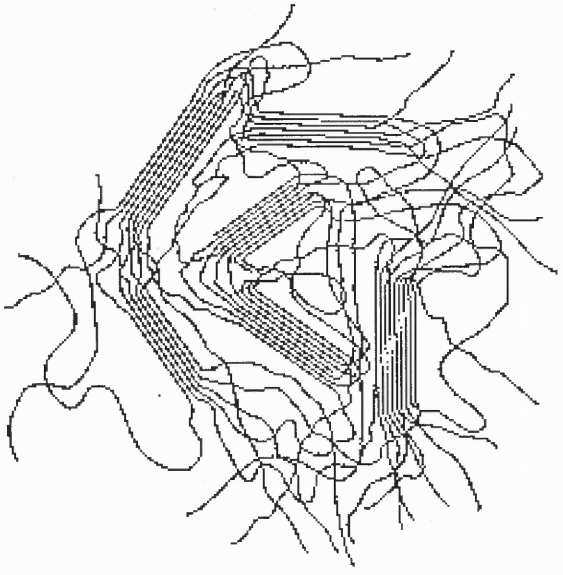

Figure 1.6 Two-dimensional fringed-micelle model of semicrystalline plastics (Mandelkern, 1964)

In bulk polymers, crystallization does not extent throughout because of the long chain nature and irregularities, such as molecular branches. Bulk polymer can be semicrystalline at most. The non-crystalline part is amorphous. Also not all polymers are able to form the close-packed, ordered structures called crystallites or spherulites; only molecules that have regular, periodic location of chemical groups can pack closely enough. For a given polymer, the extent of crystallization attained during melt processing depends upon the rate of crystallization and the time during which the temperature is maintained.

The rate of crystallization in pure polymers depends on the product of the rate of two processes: nucleation and crystal growth. Nucleation rates are high at low crystallization temperatures, where the chains are characterized by low energy levels. On the other hand, high crystallization temperatures favor rapid crystal growth rates. It is

expected that the rate of crystallization will have a maximum at some crystallization temperature, as illustrated in Figure 1.7.

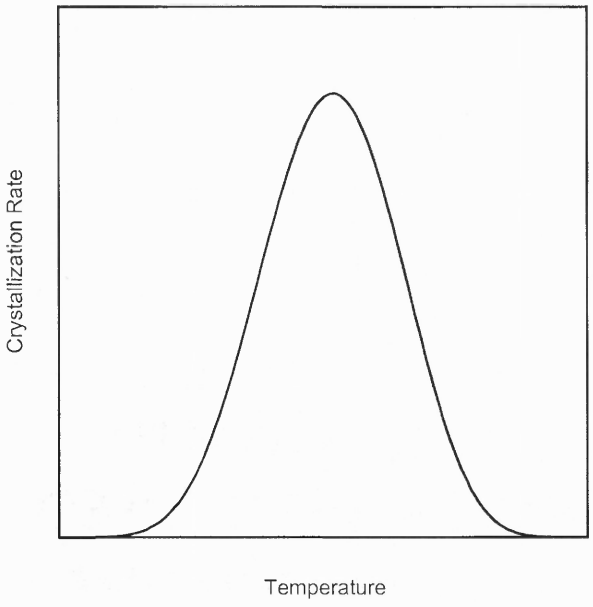

Figure 1.7 Crystallization rate versus temperature

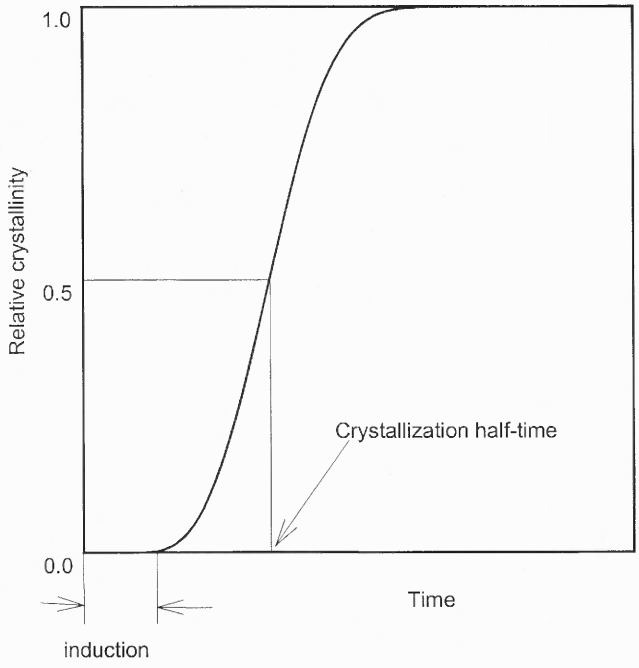

Figure 1.8 Crystallization process in polymers

Figure 1.8 shows a typical plot of crystallization process in polymers. Unlike low molecular materials, polymers do not crystallize immediately once they reach their crystallization temperature. The molecular chains need time to rearrange their configuration to favor the formation of crystals. This time is called induction time, as illustrated in Fig. 1.8. The crystallization process usually starts slowly and the crystals grow rapidly. The time at which the crystallinity reaches half of the maximum crystallinity that can be attained by the polymer is usually used to determine the crystallization rate of the polymers. At the end of the crystallization process, because of the impingement of the growing crystals and decreased non-crystallized regions, the crystallization rate decreases.

1.2.3 Stress Induced Crystallization

The shear stress and molecular orientation have significant influence on the crystallization process in polymers. Since most of the polymer processing operations always involve the application of shear to the polymer material, shear induced crystallization is a very common feature in semicrystalline plastics. The effect of shear stress on the crystallization process in plastics can be observed by a simple experiment.

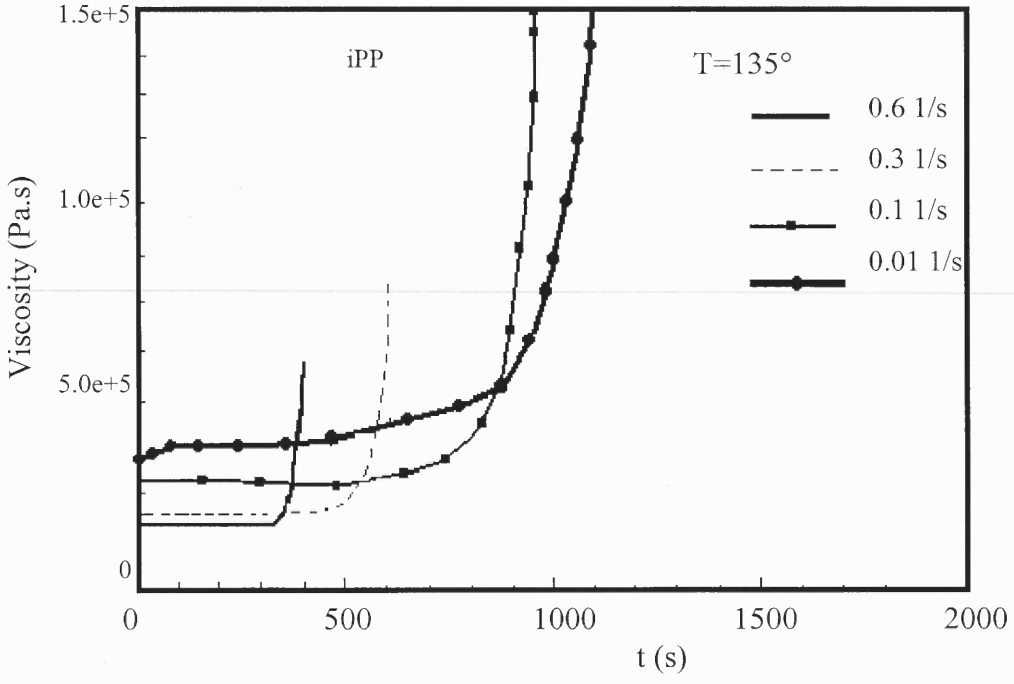

Figure 1.9 Experiment shows the effect of shear stress on crystallization of isotactic polypropylene at different shear rates (Titomanlio et al. 1997)

Fig. 1.9 shows a typical experimental result on the stress induced crystallization process of isotactic polypropylene (iPP), which is a semicrystalline thermoplastic (Titomanlio et al. 1997). The experiment was performed in a rotational rheometer under constant shear rate at 135°C. Under quiescent state at a temperature of 135°C, it takes

several hours for iPP to start crystallizing. It was seen from the experiment that, after a time, which decreases as shear rate increases, the stress undergoes a sharp increase, indicating the start of crystallization. The larger the shear stress imposed on the polymer melt, the sooner the start of the crystallization and the faster the crystallization process. Actually, the crystallization temperature range becomes broader and the crystallization rate becomes higher as the shear stress increases. Similar results were observed by Haas and Maxwell (1969) and Narh et al. (1995a).

Optical microscopy observations (Haas and Maxwell, 1969) showed that the application of a shear stress to a polymer melt leads to large increases in the number of crystalline structures formed and to the formation of oriented morphologies. The shear stresses cause the chain alignment in the molecules and favor the formation and growth of crystals. The driving force for the polymer crystallization is the supercooling, which is the difference between the melting temperature and the crystallization temperature. In accordance with the theories of Flory (1956) and Krigbaum and Roe (1964), the associated decrease in entropy of the melt may be considered to increase the supercooling. Under high stresses, crystallization occurs more rapidly at high temperatures because of the increased supercooling. At extremely low shear stresses, the molecules relax faster than the stress induced orientation. In that case, no significant effect can be observed on the crystallization process by the stress. Figure 1.10 indicates the nucleation induction time as a function of shear rate (Lagasse and Maxwell, 1976). It shows that the induction time decreases with increasing shear rate, while the crystallization rate increases. This is because the chain alignment favors the formation of

nuclei. At low shear rates, the induction time is not affected, because the chains relax during the flow process.

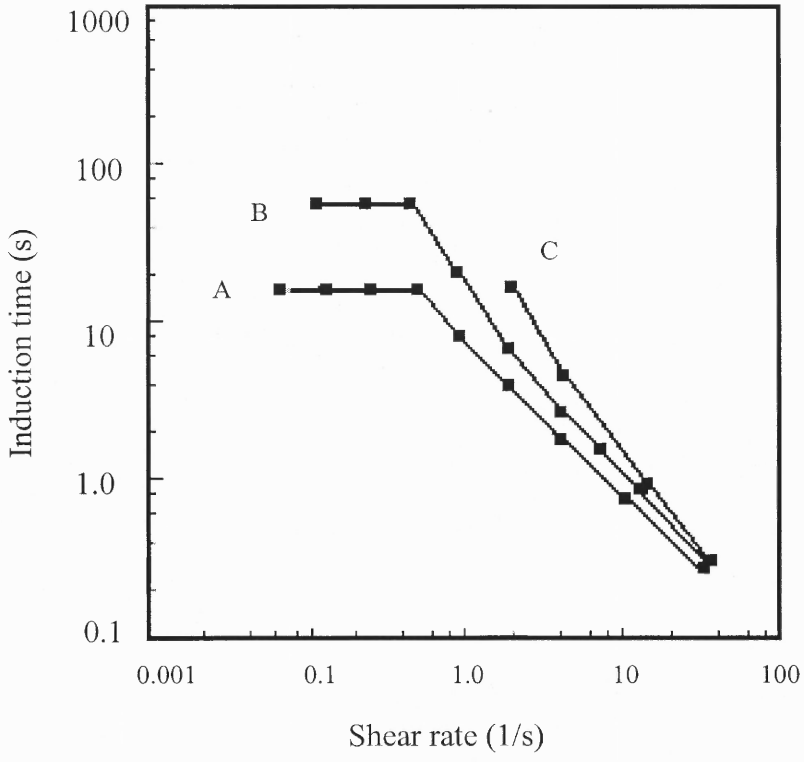

Figure 1.10 Induction time for flow-induced crystallization as a function of shear rate for HDPE with $M_w = 1.89 \times 10^4$, $\overline{M}_n = 1.38 \times 10^4$, A: T=125°C; B: T=126°C; C: T=129°C. (Lagasse and Maxwell, 1976)

1.2.4 Effect of Crystallinity on the Properties of Polymers

The crystalline nature of a bulk polymer has a major effect on its properties. Table 1.1 is the comparison of general characteristics of semicrystalline and amorphous plastics. The crystalline phase is highly ordered and compacted; the crystallized polymer has higher strength and higher stiffness than that of the amorphous polymer. Other properties such as service temperature and stress relaxation properties are also improved. Since the

crystallization process is closely related to the thermal history and processing conditions, to some extent, the morphologies or the properties of the semicrystalline plastics can be controlled by varying processing parameters. For example, injection blow molding is generally used to produce PET bottles. The injection speed must be limited to prevent stress-induced crystallization. Then the preform must be quenched on the chilled core pin and mold wall to retain the amorphous state. In the stretching and blowing stage, the preform is reheated to about 100°C and is simultaneously stretched and inflated, small and uniformly distributed crystallites form, and the product retains the transparency of the amorphous state. However, it is much stronger and tougher than either the amorphous state or the spherulitic crystalline forms.

Table 1.1 Comparison of general characteristics of semicrystalline and amorphous thermoplastics (Belofsky, 1995)

Semicrystalline	**Amorphous**
High strength	High toughness
High stiffness	High ductility
High density	Low density
High mold shrinkage	Low mold shrinkage
Opacity	Transparency
Resistance to fatigue	Lower residual stresses
Higher service temperature	Closer molding tolerance
Higher energy to process	Lower post-mold shrinkage

1.3 Injection Molded Semicrystalline Plastics

The semicrystalline plastic products from the injection molding process may exhibit a range of morphologies resulting from the processing conditions. A typical skin-core morphology is generally developed in the moldings. The high shear stress near the mold wall gives a high orientation in the polymer crystallites, while the low shear stresses in the core region of the mold allow the melt to crystallize three dimensionally to form spherulites. The injection molded semicrystalline plastics have unique microstructure across the thickness, since the stress and heat effect vary dramatically from the skin to the core region. In the skin layer or near the skin surface, row nuclei are formed by chains aligned in the direction of flow (extensional flow) on which lamellae grow in the plane perpendicular to the filling direction. At the layer just below, row nucleation still persists, but there the lamellae are perpendicular to the mold surface, but randomly oriented with respect to the filling direction. Shear flow orientation in combination with the prevailing temperature gradients is probably responsible for this morphology. Both shear and elongational flows are capable of producing chain orientation that is intense enough to create row nucleation. Spherulitic morphology, indicative of little or no orientation, is observed in the core region. An example of complex morphologies of injection molded plastics is shown in Fig. 1.11.

Generally, the following features can be observed from an injection molded plastics part at different processing conditions (Hsiung et al. 1990):

(i) At low mold temperature and high injection speed, a uniform amorphous product can be obtained.

(ii) At intermediate mold temperatures above the glass transition temperature and low injection speed, a three-layer structure can be observed in the final product: (a) amorphous skin layer, (b) crystallized layer and, (c) amorphous or semi-crystallized core.

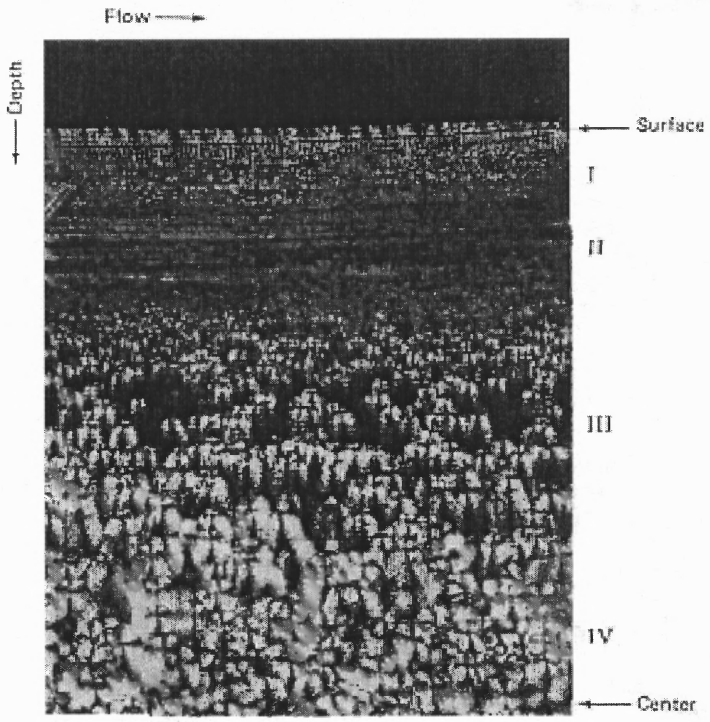

Figure 1.11 Microstructure in the thickness direction of injection molded HDPE, depicting various morphology regions (Tan and Kamal, 1977)

(iii) At a processing temperature near the cold crystallization temperature, the products exhibit uniformly crystalline morphology, where the structure development is primarily dominated by the thermally induced crystallization.

These structural features are a result of complex interactions between flow behavior and thermal effects such as fast cooling and crystallization. It is therefore clear

order to simulate the injection molding process of semi-crystalline polymers, the stress effects and non-isothermal effects should be considered.

In order to quantitatively analyze the behavior of the polymer melt as it interacts with a processing system, it is necessary to formulate and solve the equations which describe the process. The governing equations include the general conservation equations (mass, momentum, and energy) and the constitutive equations which describe the properties of the material being processed. For the semi-crystalline plastics, the kinetics of crystallization should also include the effect of the shear stress during the injection process, as well as the stress evolution in the post filling period. Furthermore, the influence of crystallinity on the flow behavior of the melt should also be included.

CHAPTER 2

LITERATURE REVIEW

2.1 Simulation of Injection Molding Process

In the past few decades, the injection molding process has widely been studied experimentally and theoretically. The analysis of mold filling in injection molding, started with the work of Spencer and Gilmore (1950) in the early 50's. They employed an empirical equation for capillary flow and coupled it with a quasi steady-state approximation to calculate the filling time. Since then, different models have been proposed to describe the molding cycle with varying degrees of complexity. One-dimensional rectangular flow was proposed by Ballman, et al. (1959) and Staub (1961). Harry and Parrot (1970) considered a one-dimensional quasi-steady state flow analysis coupled with an energy balance equation. Williams and Lord (1975) made a significant contribution by considering all the components of a one-dimensional non-isothermal flow. A similar model was presented by Thienel and Menges (1978) - using a different solution technique.

In order to study a more representative one-dimensional flow, a number of analyses were carried out on the radial filling of a center gated disc mold. Kamal and Kenig (1972) proposed an integrated mathematical treatment of the filling, packing, and cooling stages of the injection molding cycle. Similar simulations were carried out by Berger and Gogos (1973), Wu et al. (1974), and Stevenson (1978). An analytical solution for a two-dimensional flow in a rectangular cavity was presented by Kuo and Kamal (1976), and Kamal et al. (1975). Ryan and Chung (1980) used a conformal mapping technique to solve a similar set of equations. A combined finite element/finite difference

method for the solution of a two-dimensional flow was presented by Hieber and Shen (1980). A modified version with an improved numerical scheme for the solution of the pressure field has been provided by Hieber et al. (1983). Van Wijingearden and Dijiksman (1982) analyzed the non-isothermal two dimensional flow into a rectangular cavity, taking into account the orientation and corrective effect due to the formation of the solid layer at the wall.

None of the above models took into account the fountain effect due to the transient surface flow in the cavity during the filling process. Tadmor and Gogos (1979) presented a semi-quantitative model to describe the molecular orientation in injection molding, in which the effect of fountain flow was considered. The flow was analyzed in two parts: a fully developed flow away behind from the flow front, and a planar stagnation flow in the vicinity of the flow front. By assuming isothermal and incompressible flow, the complex flow near an advancing fluid front was taken into consideration for reacting fluids by Domine and Gogos (1980), and Gogos et al. (1986), using a Marker-and-Cell (MAC) finite difference method. They were able to predict, by simulation, the experimental result by Schmdit (1977) which clearly revealed the fountain flow existence. Kamal et al. (1986) used the MAC method to simulate the fountain flow with viscoelastic rheological model. Their results showed that the temperature distribution in the front region is dramatically modified by the fountain effect. Fountain flow also influences the stress distributions near the melt front. Papathanasiou and Kamal (1993) and Kamal and Papathanasiou (1993) used a finite difference method to simulate the filling stage of injection molding. By using Boundary Fitted Curvilinear Coordinates technique, they were able to extend the finite difference method to complex shaped mold

geometries. Mavridis and Hrymak (1986) investigated the free surface shape of the melt front using finite element method. They used a moving boundary system and assumed isothermal viscous flow. Sato and Richardson (1995) simulated isothermal fountain flow for viscoelastic fluids.

2.2 Simulation of Injection Molding of Semicrystalline Plastics

Although there have been many studies to simulate the injection molding process, the efforts to simulate the injection molding of semicrystalline polymers are rather rare because of the lack of practical model for crystallization kinetics that incorporates the influence of stress or strain. Eder et al. (1988) proposed a theoretical explanation for shear-induced crystallization. In this theory, the nucleation rate, as well as the crystalline growth rate, were supposed to be functions of the dis-entanglement or the orientation fraction in the melt. The orientation fraction of the melt depends on the shear rate, shearing time and stress relaxation. The theory can qualitatively explain the mechanism of shear-induced crystallization at isothermal conditions with constant shear rate. With practical injection molding, the shear rate changes continuously with time along the flow path of a fluid particle under non-isothermal conditions. Under these circumstances, the solutions to the theory will not be straight-forward and the method may fail. Moitzi and Skalicky (1993) used Eder's theory to fit the experimental results for isotactic polypropylene under isothermal conditions and constant shear rate. The parameters in the theory were derived by curve fitting to experimental data. For non-isothermal conditions, the parameters in the theory such as nucleation rate and growth rate, as well

as the relaxation time, are all coupled together. It is very difficult to get the parameters involved in the theories, hence, they are rarely applied to the real process.

Several attempts were made to include crystallization kinetics into the process simulation of injection molding of semicrystalline polymers in order to predict the microstructure development in the moldings or to incorporate the heat release due to crystallization during processing. Lafleur and Kamal (1986) used a MAC (Maker-and-Cell) type finite difference method for a non-isothermal viscoelastic fluid, and considered a kinetic equation of crystallization combined with heat transfer to simulate the injection molding process. They were able to predict the melt front progression as well as the residual stress and crystallinity distribution. Since a fast crystallizing polymer was considered in their model, the stress effect was not included. Chiang et al. (1991) simulated the filling and post filling stages of the injection molding process by using temperature dependent thermal properties of the polymers to account for the heat generated by crystallization. Han and Wang (1997) predicted the volumetric shrinkage of slow-crystallizing thermoplastics in injection molding. The crystallization kinetics and their effect on the viscosity were considered, but flow induced crystallization was neglected.

The kinetics of crystallization models involved in the above simulation studies are quiescent state models. Because of the nature of the injection molding process, the polymer melt undergoes high shear rate and high cooling rate. Many observations have shown that the shear stress has significant effect on the crystallization kinetics and, consequently, affect the microstructure distribution in the molded part. To successfully simulate the injection molding process of a semi-crystalline polymer, the effect of shear

stress on the kinetics of crystallization should be included. Hsiung and Cakmak (1991) developed a simple model for the simulation of slow-crystalline polymers. Based on the observation of the crystallization behavior of semi-crystallizing polymers, they proposed a computational model of crystallization kinetics, in which parabolic log functions for crystallization rate constant, K, and the shear stress, τ, were expressed in the form:

$$\log K = \log K_p - A(T - T_p)^2 \tag{2.1a}$$

$$T_p = T_{Pq} + \tau \times B \tag{2.1b}$$

$$\log K_p = \log K_{pq} + \tau \times C \tag{2.1c}$$

where subscript q represents the parameter value under quiescent state, subscript p represents the peak value, T crystallization temperature. A, B and C are material constants that can be estimated from literature.

Figure 2.1 shows the overall crystallization rate as a function of temperature under the effect of shear stress according to the model of Hsiung and Cakmak (Eq. 2.1a-c). It can be seen that the model predicts that shear stress increases the crystallization rate and shifts the crystallization process to higher temperatures. The same relations were used between the crystallization rate constant and temperature, induction time and stress, and induction time and temperatures. Hsiung and Cakmak also considered the crystallization heat by relating the specific heat capacity to the evolution of crystallinity. They were able to evaluate the effect of major operating parameters such as injection speed, mold temperature and holding time on the crystallinity gradients. However, the

material constants involved in the model were estimated from literature data, some of which were not from the same material.

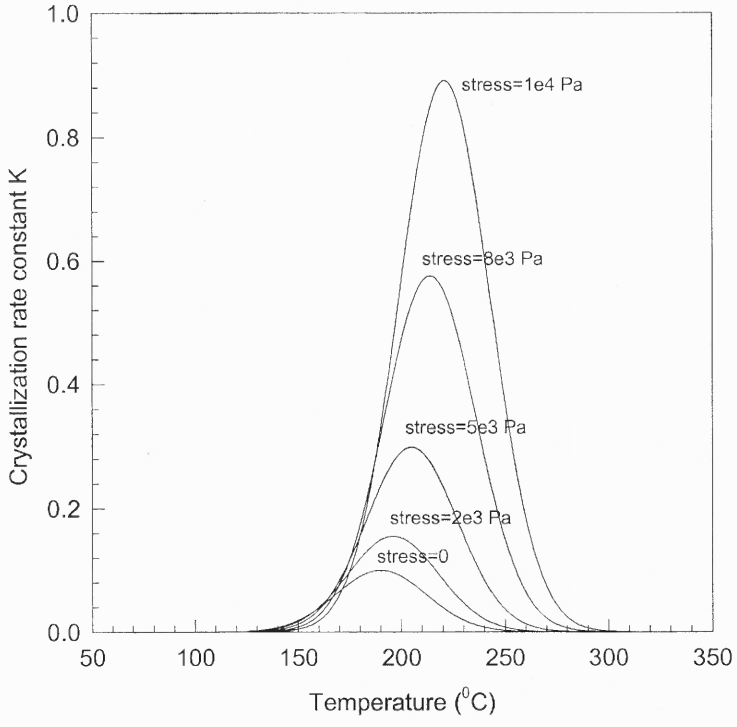

Figure 2.1 Hsiung and Cakmak's crystallization model shows increased crystallization rate and temperature shift under shear stresses.

Considering the enhancement of crystallization kinetics as a consequence of flow as well as during solidification, Titomanlio et al. (1997) simulated the injection molding process on the basis of Lord and Williams model. Titomanlio's model was derived from the quiescent state model, in which only one parameter of the model was modified according to the effect of stress. The model may be expressed as follows:

$$K(T,\tau) = K_c \exp\left(-\frac{4\ln 2(T - T_{max})^2}{D^2}\right) \tag{2.2}$$

where $K(T,\tau)$ the crystallization rate constant; is a function of temperature and shear stress. K_c is the maximum crystallization rate, T_{max} the maximum crystallization temperature, and D a parameter that considers the effect of stress. According to Titomanlio et al. (1997), D can be expressed as:

$$D = D_0 + b\tau^s \tag{2.3}$$

where, D_0 is the value in quiescent state. s and b are material constants that can be estimated from experimental results.

Figure 2.2 shows the crystallization rate as the function of temperature with the effect of stress in Titomanlio's model for polypropylene. It is clear from the model that the shear stress increases the crystallization rate by broadening the distribution of the crystallization rate over temperature, while the maximum crystallization rate and maximum crystallization temperature remain constant. The main advantage of Titomanlio's model is that it has only one extra material constant to be determined by experiment. However, the model can not predict the fact that the peak crystallization rate temperature shifts to higher temperatures.

In the most recent work of Guo et al. (1999), a so-called unified approach (Isayev et al. 1995) was employed to model the crystallization kinetics of isotactic polypropylene (iPP) during the injection molding process. In the unified approach, it was assumed that the effect of shear stress on the crystallization kinetics is only on the induction period, i.e., once the crystallization starts, the crystallization process follows the crystallization kinetics under quiescent states. Thus, the basic quiescent state crystallization kinetics

equation does not need to be modified, and can be applied directly to the stress induced process.

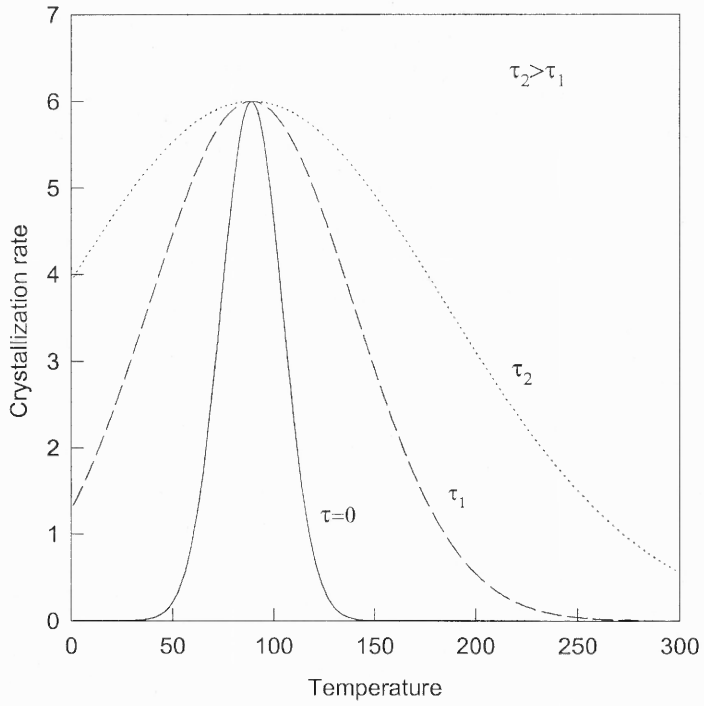

Figure 2.2 The stress induced crystallization model of Titomanlio et al. (1997) for polypropylene shows broadened crystallization temperature, fixed maximum crystallization rate

For the effect of stress on the induction period, Guo et al. (1999) introduced an extra term in the induction time expression. This extra term takes into account the effect of shear induced molecular orientation:

$$t_i(T,\Phi) = \frac{t_{qi}(T)}{1+\kappa\Phi} \tag{2.3}$$

where $t_i(T,\Phi)$ is the induction time under effect of stress, $t_{qi}(T)$ the induction time in the quiescent state, Φ shear-induced orientation factor, and κ a material constant called flow enhanced coefficient.

According to the work by Eder et al. (1988), the orientation factor Φ can be expressed as:

$$\Phi(T,\dot{\gamma},t_s)=\frac{(\dot{\gamma}/\dot{\gamma}_a)}{1+(\dot{\gamma}/\dot{\gamma}_a)}\left\{1-\exp\left[-\left(1+\left(\frac{\dot{\gamma}}{\dot{\gamma}_a}\right)^s\right)\frac{t_s}{\lambda}\right]\right\} \tag{2.4}$$

where $\dot{\gamma}_a$ is the activation shear rate, λ is the molecular relaxation time, t_s is the shear time. Expression (2.4) was obtained by assuming that the initial value of orientation factor is zero.

To characterize the molecular deformation of polymer melt due to flow, Guo et al. (1999) set up two sets of extrusion experiments: extrusion-quenching and extrusion-relaxation-quenching. By observing the microstructure on the cross section of the extrudate, the thickness of the skin layer was determined. By calculating the shear rate at the interface of the skin-core layer, the material constants involved in equation (2.4) were obtained. To determine the flow enhancement coefficient κ in Eq. (2.3), a separate instrument -parallel plate rheometer was used. Using the unified model, they were able to predict the crystallinity distribution as well as the microstructure gradient in the injection moldings. The unified model has a few advantages:

(i) Since it is assumed that the effect of shear stress on the crystallization process is only on the induction period, it is possible to make use of quiescent state crystallization kinetics to model the process.

(ii) It is possible to use the model to predict the crystal size distribution. The detailed microstructure can be simulated.

However, the model still has some disadvantages that need to be addressed:

(a) Although the model seems to be simple compared with other stress-induced crystallization model, extra complication is introduced in the model since there are too many parameters that needed to be experimentally determined.

(b) To determine the material constants in the model, two separate experiments need to be set up. One is the extrusion experiment to determine the constants involved in the orientation factor. The other is the determination of flow enhancement coefficient. It is generally difficult to accurately control the extrusion experiment. Therefore, the parameters thus obtained are subject to significant errors.

(c) The simplification that the stress has no effect on the crystal growth stage can not be applied for most polymers. Several reported experimental results have shown that shear stress not only accelerates the nucleation rate, but also increases the crystal growth rate (Haas and Maxwell, 1969; Tan and Gogos, 1976).

In the injection molding process, high stresses are generated in the filling stage. However, in the cooling stage, the stresses would relax due to the nature of the polymer material. For the material still in the molten state at the end of filling, the stress vanishes immediately once the flow stops. Isayev and Hieber (1980) used a Leonov constitutive model and calculated idealized one dimensional flow, and non-isothermal stress

relaxation, after cessation of the flow. Their result showed that the shear stress relaxes rapidly, following the cessation of the flow. It remains frozen in the skin layer but relaxes in the core region. The relaxation of stress during the cooling stage implies a decreased effect of stress on the kinetics of crystallization after filling. Therefore, a realistic model of crystallization during injection molding should also consider the effect of stress relaxation.

CHAPTER 3

MOTIVATION AND OBJECTIVES

The injection molding process is a very complex process, which includes all the interesting aspects of polymer flow, heat transfer and solidification. As discussed in Chapters 1 and 2, the processing conditions have significant effect on the microstructure of injection molded semicrystalline plastic parts, and, consequently influence their ultimate mechanical properties of the final part. This is particularly important for high precision injection molding since the crystallinity will increase the shrinkage and cause dimensional variation. Therefore, it is important to take into account the kinetics of crystallization process during the simulation of injection molding process. Because of the lack of sound practical model for the crystallization kinetics that incorporates the effect of stress, most of the existing simulations did not include the kinetics of stress-induced crystallization. The available stress-induced crystallization models for the simulation of injection molding are either empirical (Hsiung and Cakmak 1991) or have difficulties in formulating the parameters involved in the model (Guo et al. 1999). The simple model of Titomanlio et al (1997), which has only two constants apart from quiescent crystallization model, did not clearly explain the crystallization behavior of the stress induced crystallization in polymers. So it is imperative to develop a realistic stress induced crystallization model for the numerical simulation of the injection molding process of semicrystalline plastics. The model should be able to predict the behavior of stress induced crystallization of plastics, and yet be easy enough to be incorporated into the numerical simulations.

The primary objective of this work is to simulate the injection molding process of semicrystalline plastics with the consideration of stress induced crystallization. The simulation work includes the following tasks:

(1) Develop a realistic model of stress induced crystallization for semicrystalline plastics, which not only can depict the stress induced crystallization process, but also has theoretical basis.

(2) The main feature of the mold filling stage is the fountain flow. Fountain flow influences the material distribution, temperature distribution, molecular orientation and crystallinity distribution. Consequently, the fountain flow was considered in this work.

(3) Since the ultimate microstructure of injection molded parts is significantly influenced by the processing conditions, simulations were carried out to simulate the effects of processing parameters on the development of microstructure in the final parts. The processing parameters considered include injection rate, melt temperature, mold temperature, holding time, as well as the thermal contact resistance (TCR) between the plastics and the mold wall.

(4) The crystallinity distribution and evolution during the injection molding process was also simulated.

CHAPTER 4

A MODEL FOR STRESS-INDUCED CRYSTALLIZATION KINETICS OF POLYMERS

Polymer processing always involves the application of shear or deformation and heat to transform the polymeric material into various shaped products. As a result, the products exhibit different microstructures at different locations. The mechanical properties of the product strongly depend on the microstructure of the material. Thus, it is important to take into account the structure development during the modeling of the processing operations. The kinetics of crystallization of polymers in quiescent state, i. e. in the absence of stress and flow, has received extensive investigation (Chan and Isayev, 1992, 1994; Eder et al., 1983; Hammani and Methrotra 1995; Hammani and Spruiell, 1995; Liu et al., 1997; Schneider and Koppel, 1988). And there have been theoretical models to describe the quiescent state crystallization, either isothermally (Avrami 1939, 1940, 1941; Hoffman et al., 1976) or non-isothermally (Nakamura et al., 1972). There have been some experimental studies on the stress-induced crystallinity in thermoplastics (Haas and Maxwell, 1969; Kim and Kim, 1993; Liedauer et al., 1993; Moitzi and Skalicky, 1993; Sherwood and Price, 1978; Stein, 1976; Narh et al., 1995b). However, due to the difficulties involved in the experimental measurement of the stress induced crystallization process, there has been no thorough study of the effect of shear or stress on the crystallization process in polymers. There have been some theoretical models to analyze the stress induced crystallization process (Eder et al., 1988). However, it is very difficult to incorporate the theoretical models into the modeling of real process. Some of the models used in the numerical process modeling are based solely on empirical model (Hsiung and Cakmak, 1991).

In the present studies, a stress induced crystallization model is proposed based on the kinetics of quiescent state crystallization. The model is based on the hypothesis that the equilibrium melting temperature will shift to higher temperatures in the stressed or oriented state.

It is important to note the following relative to the fountain flow:

(1) It certainly takes place during the mold filling process and may be " reasonably" simulated.

(2) By its very nature it forces the fluid near the advancing front to undergo extensional flow.

(3) The orientation induced because of such extensional flow is "frozen in" because of the contact of the melt with the cold wall, forming a "skin" with high orientation for amorphous polymers or of unique, nucleation dominated crystallizing morphology for crystallizing polymers.

(4) The skin region may have, as a result, distinct mechanical properties affecting the injection molded product properties.

Despite the above, it is also noted here that no experimental or theoretical work has been conducted to relate the effect of extensional flow on crystallization kinetics, that is, there is no extensional flow induced crystallization studies analogous to the work conducted in bi-conical flow (Tan and Gogos, 1976) or parallel plate flow (Narh et al. 1995a). It is for this reason that we decided to neglect the fountain flow entirely, noting that our simulation results do *not* hold for the skin region, rather than to produce fictitious results or results which were obtained under shear flows.

4.1 Crystallization in Quiescent State

The Avrami equation (Avrami, 1941) has been widely used to describe polymer crystallization kinetics under isothermal conditions in the form:

$$\theta(t) = \frac{\chi(t)}{\chi_\infty} = 1 - \exp(-kt^n) \tag{4.1}$$

where, $\theta(t)$ is the relative crystallinity at time t, $\chi(t)$ is the absolute crystallinity at time t, χ_∞ is the ultimate absolute crystallinity, n is the Avrami index, k is the Avrami isothermal crystallization rate of constant.

The Avrami equation (4.1) did not consider the induction time for the crystallization process in polymers. An empirical relation between induction time t_i and crystallization temperature T is generally used (Godovsky and Slonimsky, 1974):

$$t_i = t_m (T_m^0 - T)^{-a} \tag{4.2}$$

where t_m and a are material constants, T is the crystallization temperature, t_i the induction time at temperature T and T_m^0 the equilibrium melting temperature.

For non-isothermal conditions, on the basis of isokinetic conditions and the assumption that the number of activated nuclei is a constant, Nakamura et al. (1972) developed the following equation from the Avrami theory:

$$\theta(t) = \frac{\chi(t)}{\chi_{\infty}} = 1 - \exp\left[-\left(\int_0^t K(T)dt \right)^n \right] \tag{4.3}$$

where *K(T)* is the non-isothermal crystallization rate constant. Its relationship to the Avrami isothermal crystallization rate constant *k* can be expressed in the form:

$$K(T) = [k(T)]^{1/n} = \ln(2)^{1/n} \left(\frac{1}{t_{\frac{1}{2}}} \right) \tag{4.4}$$

where $t_{\frac{1}{2}}$ is the crystallization half-time. $\left(\frac{1}{t_{\frac{1}{2}}} \right)$ indicates the overall rate of isothermal crystallization. Assuming that the number of nucleation sites is independent of temperature and all sites are activated at the same time, Hoffman et al. (1976) developed the following expression to describe the overall rate of crystallization as a function of temperature:

$$\left(\frac{1}{t_{\frac{1}{2}}} \right) = \left(\frac{1}{t_{\frac{1}{2}}} \right)_0 \exp\left(-\frac{U^* / R}{T - T_{\infty}} \right) \exp\left(-\frac{K_g}{T \Delta T f} \right) \tag{4.5}$$

where T is the crystallization temperature, R is the universal gas constant, $\Delta T = T_m^0 - T$ is the supercooling, and $f = 2T/(T + T_m^0)$ is a correction factor accounting for the reduction in the latent heat of fusion as the temperature is decreased, U^* is the activation

energy for the transport of crystallizing units across the phase boundary, T_∞ is the temperature under which such transport ceases, K_g the spherulite growth rate. According to Hoffman et al. (1976), the parameters U^* and T_∞ can be assigned "universal" values of 6284 J/mol and $T_g - 30\,\mathrm{K}$, respectively. T_g is the glass transition temperature. The parameter $\left(\frac{1}{t_{\frac{1}{2}}}\right)_0$ is a pre-exponential factor that includes all the terms which are independent of temperature.

The original Nakamura equation did not consider the induction time for nucleation. Sifleet et al. (1973) suggested that "during a non-isothermal process any amount of time spent at a temperature increased the relative completion of the induction time by the amount of that time spent divided by the induction time at that temperature." When the accumulated induction time index $(\bar{t})$ reaches unity, the induction period is assumed to have been completed and the crystallization begins. Mathematically, this can be expressed in the form:

$$\bar{t} = \int_0^{t_I} \frac{dt}{t_i(T)} \tag{4.6}$$

where $t_i(T)$ is the isothermal induction time as a function of temperature. When $(\bar{t})$ reaches unity, the upper limit of integration is taken as the non-isothermal induction time t_I. In this approach, one essentially assumes that the non-isothermal process during the induction period consists of many infinitesimal isothermal steps.

Differentiation of Eq. (4.3) leads to the differential form of Nakamura equation:

$$\frac{d\theta}{dt} = nK(T)(1-\theta)[-\ln(1-\theta)]^{(n-1)/n} \tag{4.7}$$

which is more useful in process modeling.

The spontaneous formation of nuclei is not considered in Eq. (4.7), which gives a zero initial rate of crystallization, resulting in a zero solution. Therefore, a non-zero initial condition is required for a successful numerical treatment of Eq. (4.7). The non-zero initial value of relative crystallinity should be small enough so that it has no direct effect on the final solutions, generally in the range of 10^{-10}-10^{-15} (Patel and Spruiell, 1991).

4.2 Determination of Parameters for Quiescent State Crystallization

The parameters involved in the crystallization kinetics equation (4.5) can be determined experimentally. Narh et al. (1995a) conducted extensive experimental investigations on the kinetics of crystallization, including isothermal and non-isothermal crystallization of polyethylene terephthalate (PET). The experimental data used in the present studies are based on those experimental results.

4.2.1. Brief Description of the Experiment

The material used was polyethylene terephthalate (PET) resin (Kodapak 7532) supplied by Tennessee-Eastman. The isothermal and non-isothermal crystallization kinetic studies were carried out using a differential scanning calorimeter (DSC). All the samples were pre-dried in a vacuum oven at 120 °C for about 24 hours. Then, the samples were first

heated up to 300°C and kept for about 10 minutes in the DSC cell to completely melt any remaining crystals, and remove any orientation history. Isothermal crystallization experiment runs were carried out in the temperature range of 115-230°C. The melted samples were cooled down rapidly to the crystallization temperature and kept under that temperature for a desired period of time.

4.2.2 Determination of the Kinetics Parameters Using Experimental Data

By assigning the 'universal values' to U^* and T_∞ suggested by Hoffman et al. (Hoffman et al. 1972), there are only two unknown parameters, $\left(\frac{1}{t_{\frac{1}{2}}}\right)_0$ and K_g , which need to be determined. It is generally suggested (Chan and Isayev 1992) that a non-linear regression method is to be used to fit the experimental data by Eq. (4.5). The fitted values of the two parameters under isothermal condition according to Eq. (4.4) and Eq. (4.5) are represented by the solid line in Fig. 4.1, in which $\left(\frac{1}{t_{\frac{1}{2}}}\right)_0 = 4.25\times10^4$ (1/s), and $Kg=3.83\times10^5$ (K^2) are used.

The Avrami index was obtained by plotting *ln[-ln(1-θ)]* vs *ln(t)*. The slopes of the plotted lines are the Avrami indexes. Figure 4.2 shows reproduction of the experimental results, and the regression plots. The Avrami index so obtained was in the range 1.5-2.5 (Narh et al., 1995a). In the modeling of crystallization kinetics, an average value of $n=2$ is used.

The parameters involved in the induction time (Eq. 4.2) can be obtained from literature. Chan and Isayev (1992) have carried out similar experimental studies using the same grade of PET. By fitting Eq. (4.2) with their experimental data, the following constants were obtained:

$$t_m = 4.68 \times 10^{13} \text{ sec}$$

$$a = 6.40$$

For the non-isothermal conditions, the differential form of the Nakamura equation (4.7) can be used with the isothermal parameters. Figure 4.3 shows the predicted results from the isothermal parameters compared with the experimental results at various cooling rates. It is clear that the calculated results show a good agreement with the experimental data.

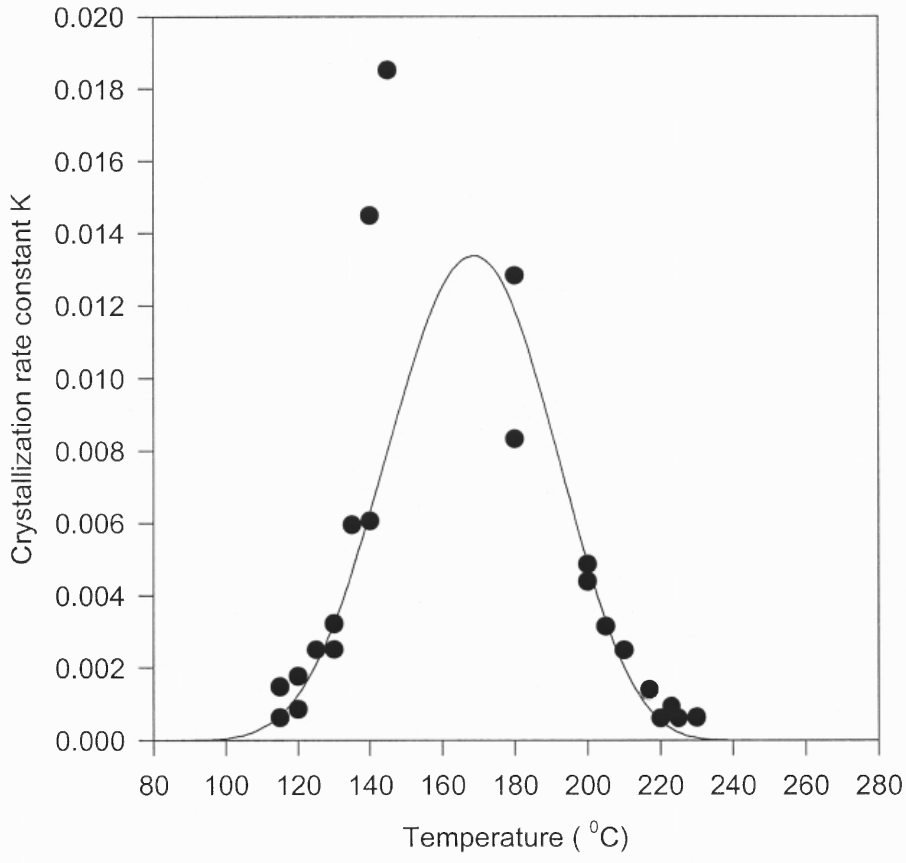

Figure 4.1 Plot of isothermal crystallization rate constant as a function of temperature. Solid circles represent the experimental data (Narh et al. 1995a). The solid line represents the best fit according to equations (4.4) and (4.5).

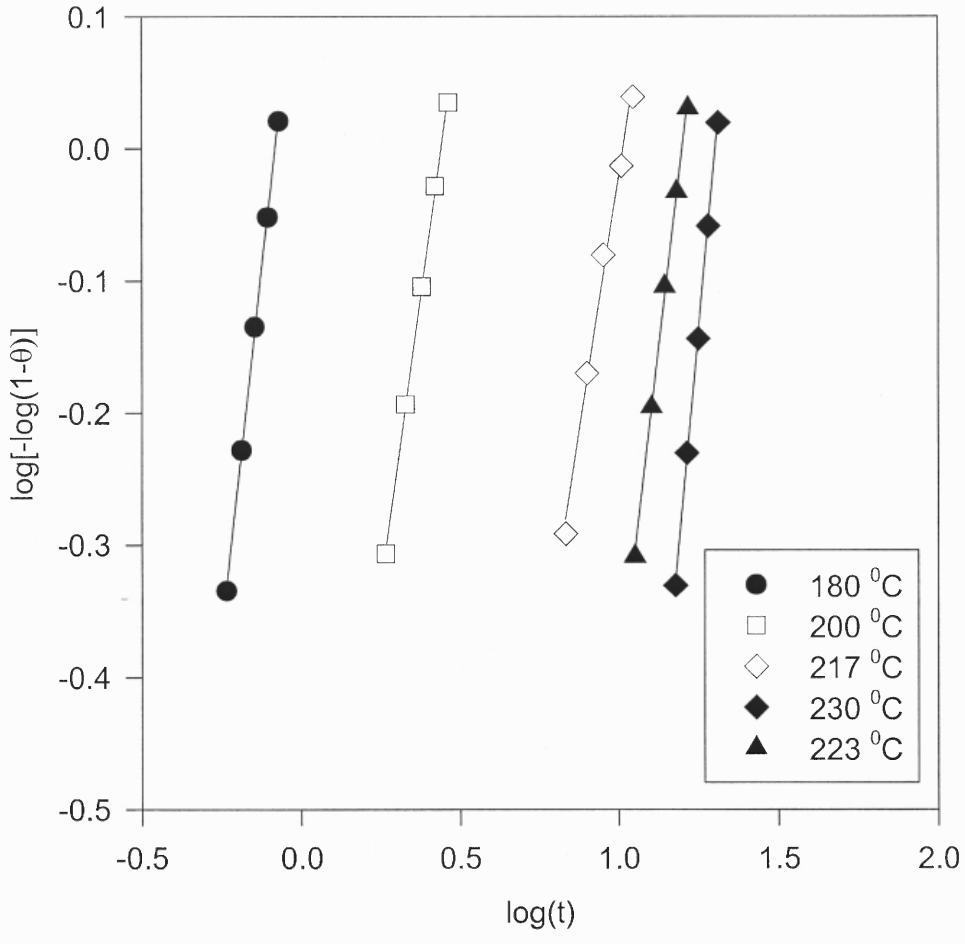

Figure 4.2 Avrami plots for isothermal crystallization of PET at various temperatures.

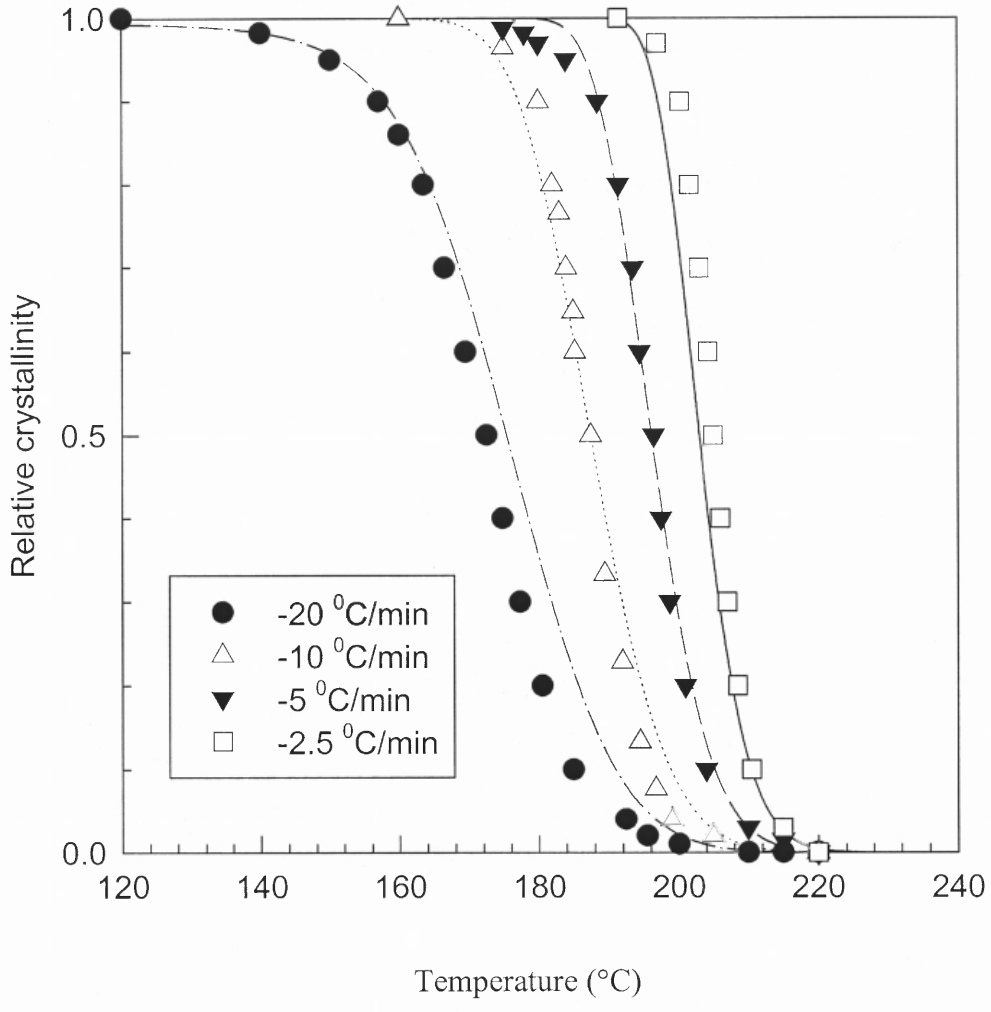

Figure 4.3 Comparison of prediction result using isothermal parameters with the experimental data: lines are predictions, points are experimental results.

4.3 Shear Induced Crystallization

All plastics processing operations involve the application of heat and stress, resulting in deformation of the polymer melt, often at a high shear rate. Due to the unique, long chain nature of the molecules of polymers, deformation of the melt will result in molecular orientations. This orientation process when acting during crystallization may affect the rate of crystallization and the morphology of the final product. The following discussion is based on the paper of Haas and Maxwell (1969).

A polymer melt at rest consists of coiled and intercoiled molecules which assume a "most random" set of conformations which maximize their entropy. The application of shear stress to the melt will result in the chain orientation of the polymer molecular chains. From statistical mechanics, it is known that an oriented polymer molecule has fewer possible conformations than a coiled one and, therefore, a lower entropy, i.e.,

$$S_m = k_m \log \Omega \tag{4.8}$$

where S_m is the entropy of the melt, k_m Boatsman's constant, and Ω number of conformations of the molecules.

At the equilibrium melting temperature, the Gibbs free energy of the crystal equals the free energy of the amorphous melt so that the melting temperature may be written as:

$$T_m^0 = \frac{\Delta H_f}{\Delta S_f} = \frac{H_m - H_c}{S_m - S_c} \tag{4.9}$$

where ΔH_f is the heat of fusion; ΔS_f is the entropy of fusion; H_m and H_c are the enthalpies of the amorphous melt and crystalline phases, respectively; S_m and S_c are the entropies of the melt and crystalline phases, respectively.

For an oriented melt, the decrease in entropy may be considered to increase the melting temperature and, therefore, the supercooling. Flory (1956) has applied this idea to the thermodynamics of a cross-linked system subjected to a tensile force by considering a model of axially oriented crystalline regions coexisting with an amorphous zone. Applying the requirement of thermodynamic equilibrium between the two phases, an expression was derived which predicts that the melting temperature increases with an increase in the applied tensile stress.

The polymer melt during crystallization under shear flow can be treated as a system of two independent phases (Krigbaum and Roe, 1964). Assuming that the free energy of the crystalline phase was independent of the shear strain so that:

$$G_c(T_m) = G_m(\gamma, T_m) \tag{4.10}$$

where G_c and G_m are the Gibbs free energy of the crystalline phase and melt phase, respectively. Then, we arrive at the following relationship:

$$G_m(\gamma, T_m) - G_m(0, T_m) = \Delta H_f \frac{T_m - T_m^0}{T_m^0} \tag{4.11}$$

When a polymer melt is deformed, a portion of the energy is dissipated in viscous flow and the remainder elastically stored. The left hand member of the above equation represents the stored energy, and for shear, may be written as:

$$G_m(\gamma, T_m) - G_m(0, T_m) = \int_0^{\gamma} \tau d\gamma \tag{4.12}$$

where γ is the elastic or recoverable shear strain. The integral can be approximated by assuming Hooke's law in shear, i.e., $\tau = G\gamma$, where G is the elastic shear modulus. Then Eq. (4.11) becomes:

$$T_m = \frac{T_m^0}{\Delta H_f}\left[\frac{\tau^2}{2G}\right] + T_m^0 \tag{4.13}$$

The first term on the right side can be thought of as the increase in the equilibrium melting temperature, that is:

$$T_{shift} = T_m - T_m^0 = \frac{T_m^0}{\Delta H_f}\left[\frac{\tau^2}{2G}\right] \tag{4.14}$$

If it is assumed that the effect of stress on the kinetics of crystallization is only to increase the equilibrium melting temperature, i. e., by increasing the supercooling, then, by replacing T_m^0 in Eq. (4.5) by T_m as expressed in Eq.(4.13), we can rewrite Eq.(4.5) as:

$$\left(\frac{1}{t_{\frac{1}{2}}}\right) = \left(\frac{1}{t_{\frac{1}{2}}}\right)_0 \exp\left(-\frac{U^*/R}{T-T_\infty}\right)\exp\left(-\frac{K_g}{T\Delta T' f'}\right) \tag{4.15}$$

where:

$$\Delta T' = T_m - T \tag{4.16}$$

$$T_m = T_m^0 + T_{shift} \tag{4.17}$$

$$f' = \frac{2T}{T+T_m} \tag{4.18}$$

$\left(\frac{1}{t_{\frac{1}{2}}}\right)_0$ and K_g have the same meanings as in equation (4.5). They are independent of stress.

The effect of shear stress on the induction time can also be obtained by replacing the equilibrium melting temperature in Eq. (4.2) with the increased equilibrium melting temperature, T_m, from Eq.(4.17):

$$t_i(T,\tau) = t_m(T_m - T)^{-a} \tag{4.19}$$

There have been experimental results to support the shift of equilibrium melting temperature by the effect of shear stress. In the work of Tan and Gogos (1979) on the crystallization behavior of polyethylene (PE) above its melting point, it was pointed out that a better fitting of the experimental data to the kinetic theory could be obtained by

shifting the equilibrium melting point to a higher temperature. For PE, a shift from 140.5 °C to 160 °C was recommended. And the authors also suggested that the best fit might be obtained by a functional relationship between the equilibrium melting temperature shift and shear stress. However, no model was proposed by these authors.

4.4 Determination of Parameters for the Kinetics of Stress Induced Crystallization

Since it is very difficult to follow the stress induced crystallization process, the efforts to investigate the effect of stress on the kinetics of crystallization have been scarce. By assuming that shear stress only affects the equilibrium melting point of the polymer, the parameters needed to be determined in the stress induced crystallization kinetics are kept to a minimum. Consequently, it is possible to model stress induced crystallization with the available experimental methods.

Equation (4.14) is based on the assumption that shear modulus is independent of applied shear stress. However, the relationship between the shear modulus and shear stress in a polymer is very complicated. Therefore, the equilibrium melting temperature shift may not necessarily follow the quadratic function expressed in Eq. (4.14).

At low shear stresses, the polymer molecules do not receive enough energy for their chains to extend. Hence, there is usually a critical stress or shear rate for the orientation of the molecules (Eder et al., 1988). The effect of shear stress on the crystallization process is prominent only when the stress exceeds a critical stress (Titomanlio et al., 1997). However, in an extremely high stress range, when the molecules are fully extended, any further increase in shear stress will not cause further orientation of the polymer molecules. The effect of stress on the crystallization process in

a high stress range should tend to a constant value. Consequently, we propose that the relationship between the equilibrium melting temperature shift and the shear stress τ, is of the form:

$$T_{shift} = C_1 e^{-\frac{C_2}{\tau}} \tag{4.20}$$

where C_1 and C_2 are material constants that can be determined by experiment.

Rotational viscometer is a common device used to study flow-induced crystallization in polymer melts (Titomanlio et al., 1994; Eder et al., 1989; Narh et al., 1995b). In the parallel plate rotational viscometer, constant shear is applied to the melt at constant temperatures by the relative rotation of the plates. The sudden rise in viscosity with time was interpreted as the onset of crystallization. Figure 4.4 shows typical stress-time plots for PET melt subjected to rotational shear (Narh et al., 1995b). The sudden rise in the stress-time plot gives us the critical time (induction time) for the onset of crystallization. This critical time can be used to determine the constants in Eq. (4.20). Table 4.1 lists the induction time for two shear rates at two different temperatures. The following formulation is used to derive the equilibrium melting temperature shift.

From Eq. (4.19), we have:

$$T_m = T + \left[\frac{t_i(T,\tau)}{t_m}\right]^{-\frac{1}{a}} \tag{4.21}$$

Then:

$$T_{shift} = T_m - T_m^0 = \left[\frac{t_i(T,\tau)}{t_m}\right]^{-\frac{1}{a}} - T_m^0 \tag{4.22}$$

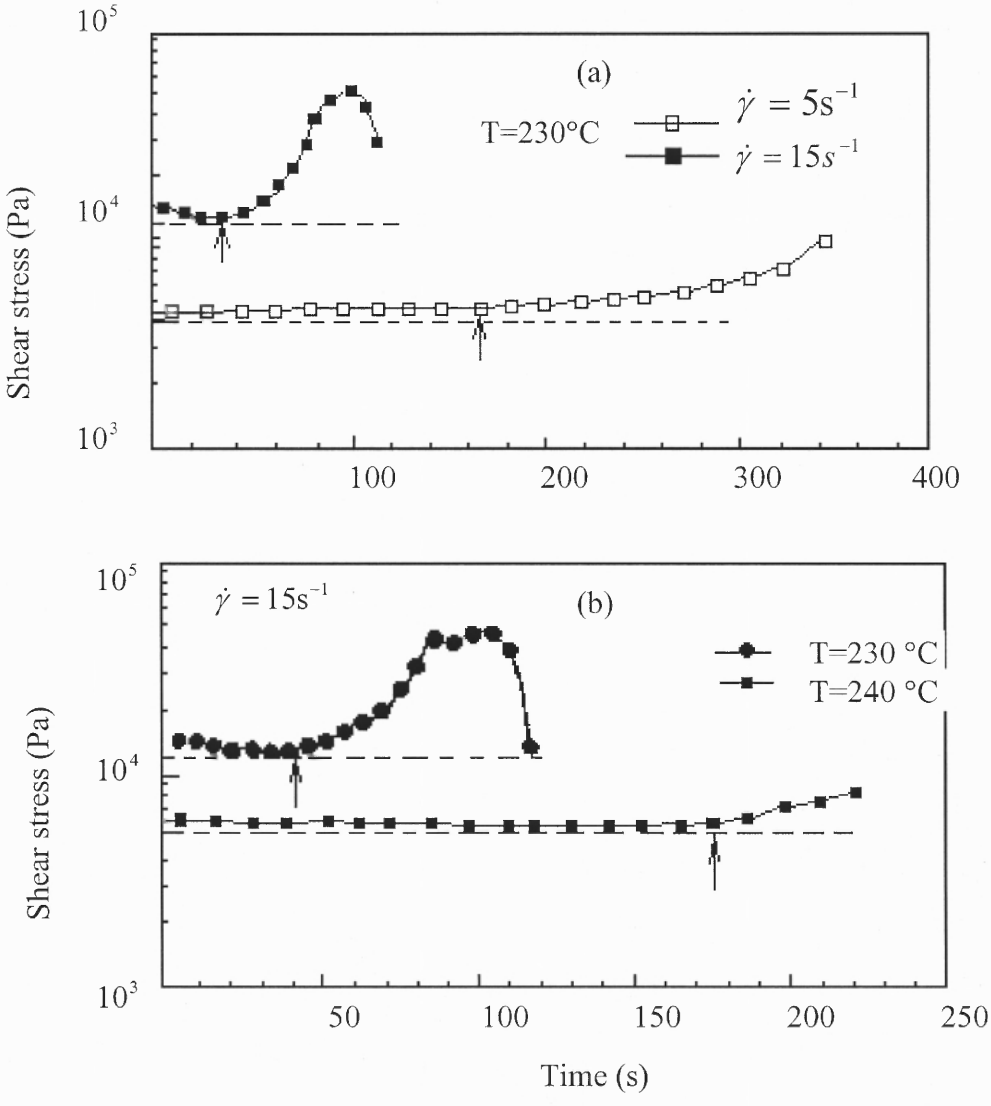

Figure 4.4 Shear stress versus shear time showing the effect of shear rate and temperature on the onset of crystallization (Narh et al., 1995b): (a) shows the shear dependence and (b) shows the temperature dependence.

The parameters t_m and a are chosen from the results of Chan and Isayev (1992) for the same grade of PET, which give $t_m = 4.68\times10^{13}$ s and a=6.40. The calculated values of T_{shift} are listed in table 4.1.

The constants C_1 and C_2 can be obtained by fitting the experimental results with Eq. (4.20). Figure 4.5 shows the best fitting result with the following constants:

$$C_1 = 37.3 \text{ °C} \text{ and } C_2 = 4\times10^3 \text{ Pa}$$

Table 4.1 Equilibrium temperature shift with the shear stress

Temperature (°C)	Shear stress (Pa)	t_i (s)	T_{shift} (°C)
230	14000	40	26.8
230	4500	133	13.9
240	6000	175	21.82

Figure 4.6 shows the effect of stress on the rate of crystallization of PET. It is clear that the shear stress increases the rate of crystallization. The distribution of the crystallization rate constant is broadened by the effect of shear stress. The highest crystallization rate shifts to higher temperatures. Figure 4.7 shows the crystallization process with and without the application of stress under constant cooling rate of 20 °C/min. It can be seen that the crystallization process is completed at a higher temperature and a faster rate in the stressed state than in the quiescent state.

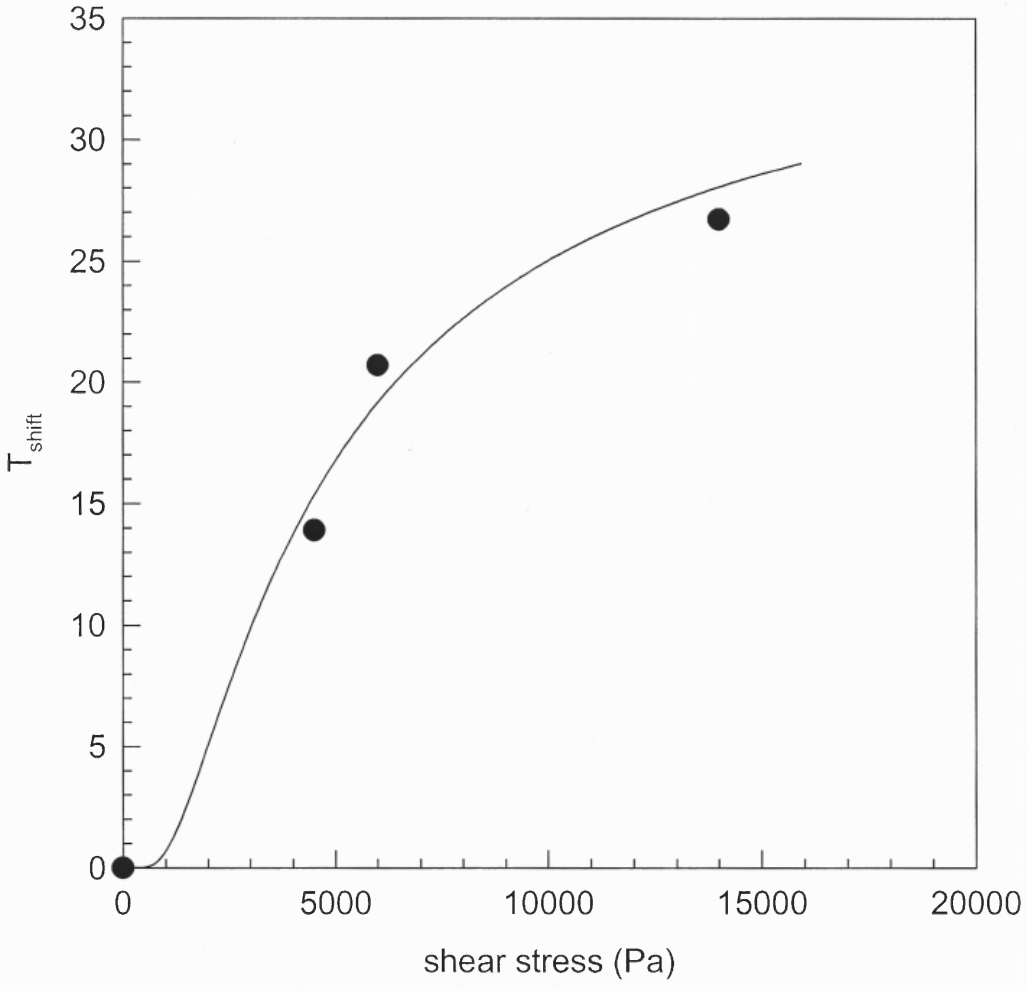

Figure 4.5 Temperature shift as a function of shear stress: data points are calculated form the experimental work of Narh (1995b), line is the best fitting result

The results of the present model are compared with Hsiung and Cakmak's empirical model (Hsiung and Cakmak, 1991) of stress-induced crystallization of polyphenylene sulfide (PPS). The equilibrium melting temperature shifts are obtained by fitting the present model to the same highest crystallization rate temperature as that in Hsiung's model. Using this approach, the following parameter values in the present model were obtained:

$$\left(\frac{1}{t_{\frac{1}{2}}}\right)_0 = 1.01\times10^{4}\,s^{-1} \text{ and } K_g = 2.29\times10^{5}\,K^2$$

Figure 4.8 shows the comparison of the two models. Figure 4.9 shows the equilibrium melting temperature shift with the effect of shear stress according to the data given by Hsiung and Cakmak for PPS. It can be seen that the proposed model shows good agreement with Hsiung and Cakmak's model, except that the proposed model shows the broadened distribution not only towards higher temperatures but also towards low temperatures. Compared with Hsiung and Cakmak's model, the proposed model also shows increased crystallization kinetics at low temperature range.

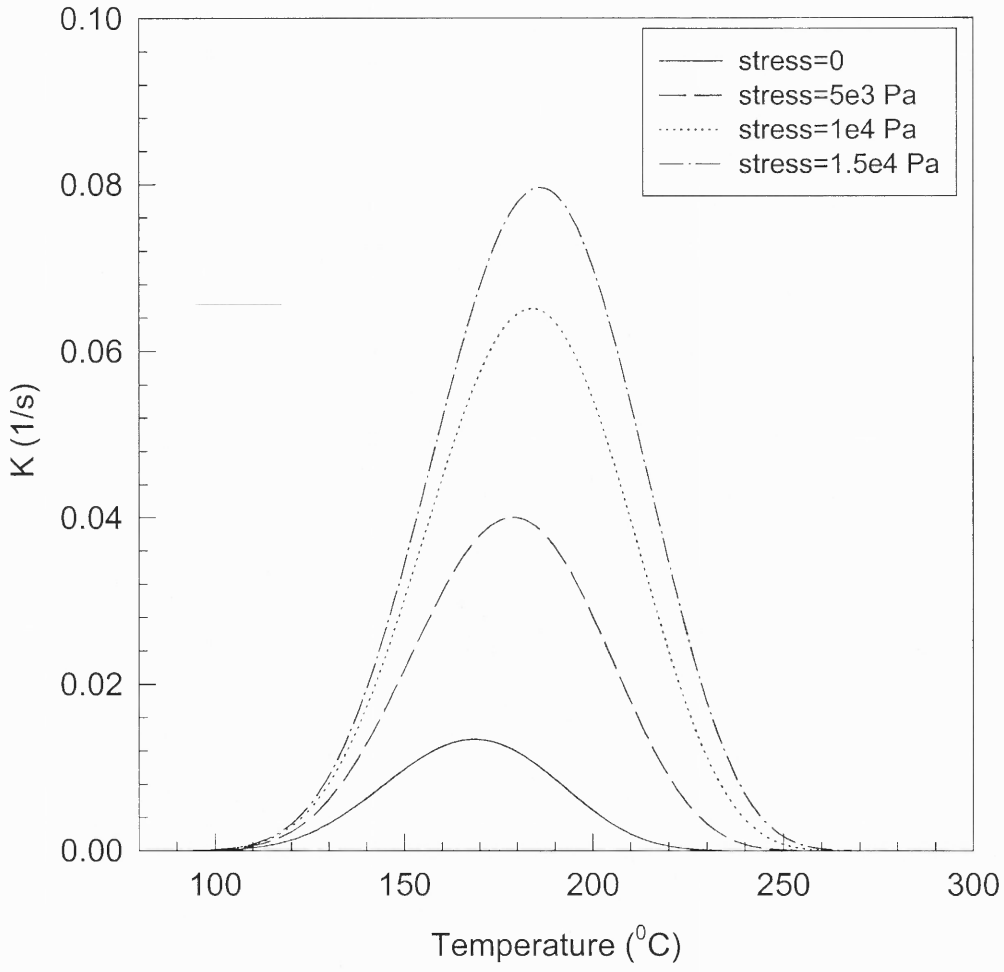

Figure 4.6 Kinetics of crystallization of PET under effect of shear stress. The results show the crystallization process shift to higher temperatures with increased crystallization rate

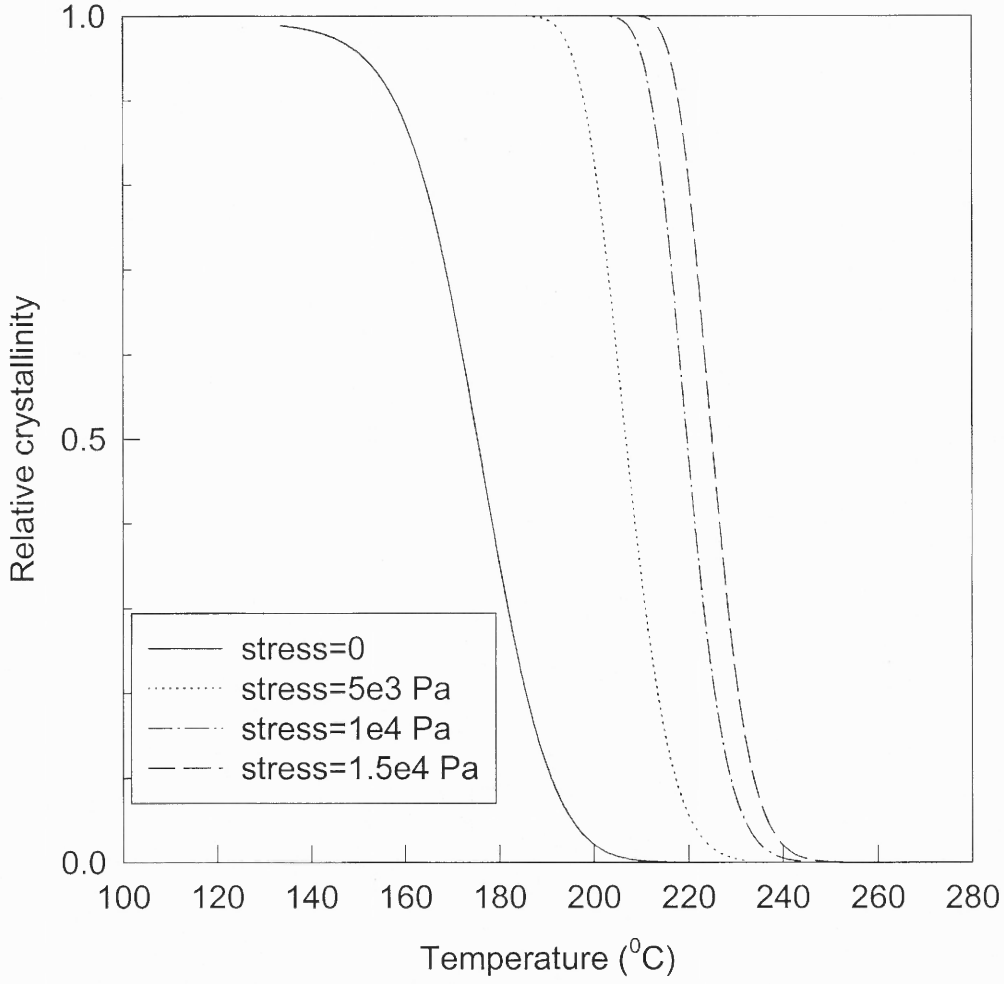

Figure 4.7 Crystallization process of PET with/without the application of shear stress under constant cooling rate of 20 °C/min

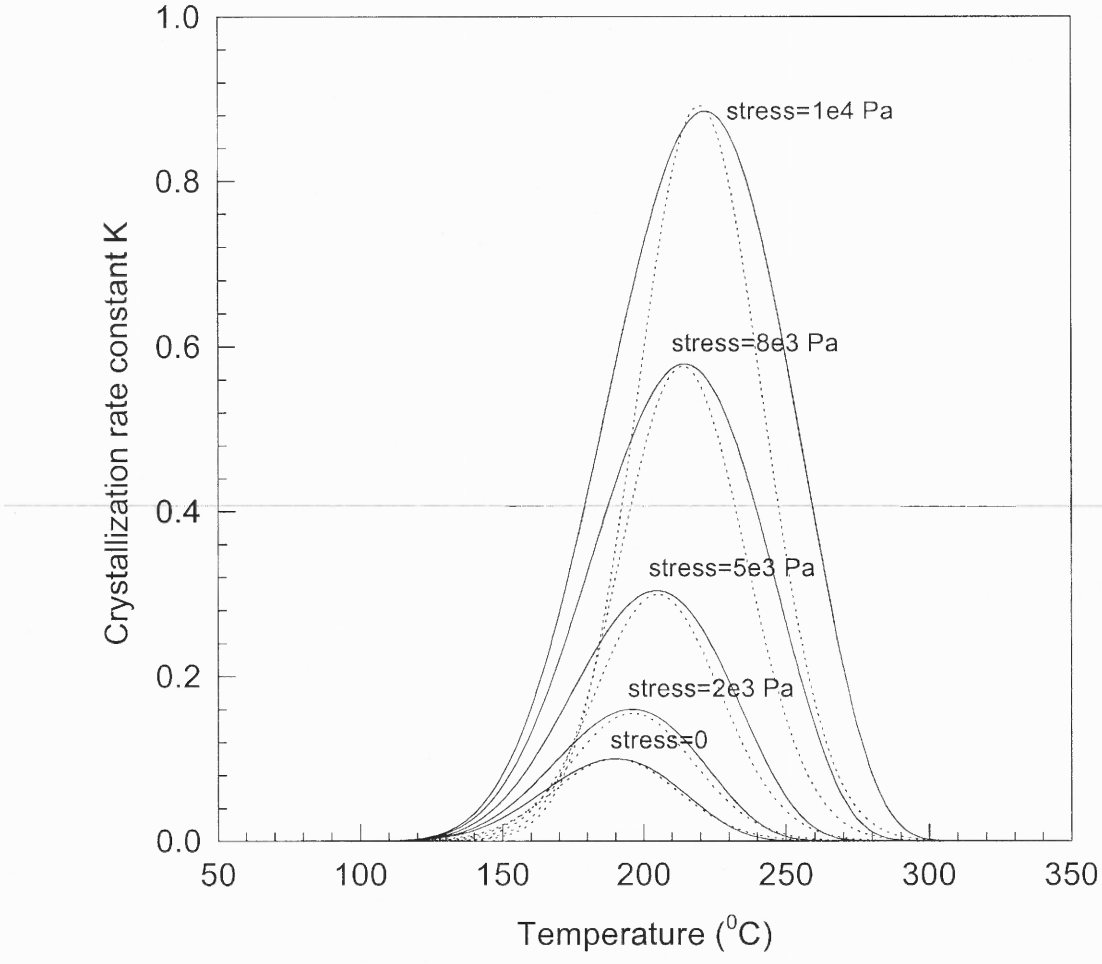

Figure 4.8 Comparison of Hsiung and Cakmak's model with present model. Dotted lines are Hsiung and Cakmak's model; solid lines are present model with the parameters obtained from Hsiung and Cakmak (1991).

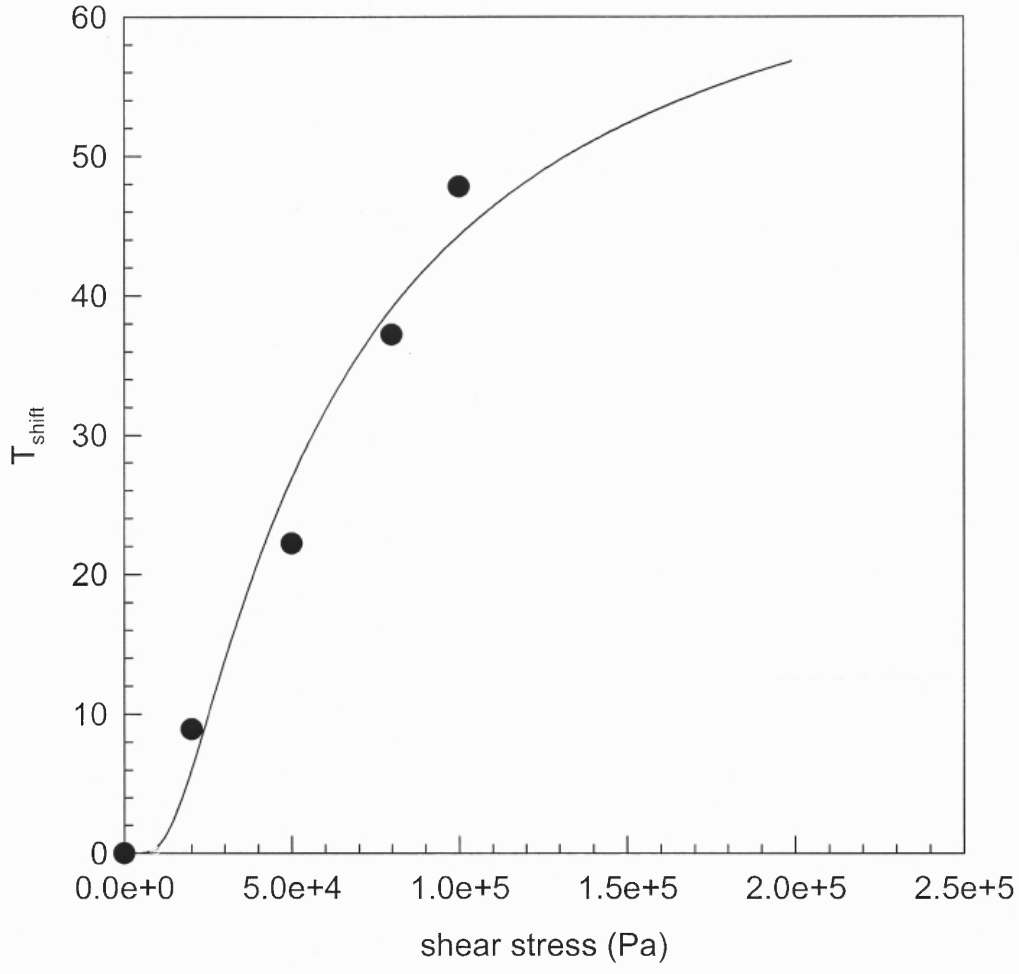

Figure 4.9 Equilibrium melting temperature shift with shear stress from Hsiung and Cakmak's model for PPS (solid points). Solid line represents the fitting function given by:

$$T_{shift} = 73\left[\exp\left(-\frac{50000}{\tau}\right)\right]$$

4.5 Summary

The proposed model is based on the hypothesis that the orientation of the polymeric chains caused by the shear stress lowers the entropy of the polymer, and, hence increases the equilibrium melting temperature and the supercooling. The model predicts that the application of shear stress not only increases the rate of crystallization, but also broadens the crystallization temperature range. The temperature corresponding to the highest crystallization rate shifts to higher temperatures with increasing shear stress. Since it is assumed that the effect of shear stress on the crystallization process is by increasing the supercooling, the basic kinetics equation by Hoffman et al (1976) is not changed and the parameters needed to be determined are kept to a minimum. This will certainly reduce the complexity of the modeling of the stress-induced crystallization process, which is generally very difficult to follow. Simple experimental methods such as rotational viscometer can be used to determine the parameters for the temperature shift model.

As stated in Chapter 1, elongational flow during the mold filling stage is the major cause of molecular orientation in the surface layer in injection molded plastic articles. The proposed model did not consider the elongational flow effect on the kinetics of crystallization. The main reason is that the no technique to measure the elongational flow effect on the kinetics of crystallization of plastics is available; nor is there a theoretical study for extensional flow. Thus, the application of the model to the injection molding process will fail to predict the crystallinity in the surface layer. However, due to the fast cooling in the skin layer, the melt temperature may fall below the crystallization temperature in a short time, and no significant amount of crystallinity forms. This is especially true for slow crystallizing thermoplastics molding in molds with temperature

below or near their glass transition temperature. On the other hand, the high elongational flow orientation surface layer will still be present of effect in a small portion of the thickness. The molecular orientational crystallization in the other portion across the thickness is mainly shear induced.

CHAPTER 5

MELT FRONT TRACKING TECHNIQUE

5.1 Problem Statement

The major challenge in modeling the mold filling stage is to accurately track the flow fronts. In the mold filling stage, two flow regimes can be distinguished: the main flow domain, and a front flow. The fountain effect occurs in the front flow, while a simple 2D flow exists only in the main flow. There are a number of techniques that have been presented in the literature dealing with free boundary problems. Marker-And-Cell (MAC) method (Harlow and Welch 1965) is a finite difference method. In MAC, every mesh cell in the flow field is marked with a flag that indicates the status of the cell: for example, E stands for the empty cell that needs to be filled, S represents the surface cell, B represents the boundary cell. The flow front is some where in the surface cell. This technique has been applied to the analysis of injection molding process (Domine and Gogos 1980; Manzione 1981; Gogos and Huang 1986; Kamal, Chu et al. 1986). The volume of fluid method (VOF) by Hirt and Nichols (1981) defines a function $F(x,y,t)$ that is equal to unity at any point occupied by fluid and zero elsewhere, and the discontinuity in F propagates according to the pure convection equation:

$$\frac{DF}{Dt} = \frac{\partial F}{\partial t} + u\frac{\partial F}{\partial x} + v\frac{\partial F}{\partial y} = 0 \tag{5.1}$$

which states that the interface is a material line. For the purpose of calculations, the interface is approximated by a straight line through the element or cell. This method has been used to simulate the injection molding processes (Isayev, 1991), as well as the gas-

assisted injection molding process (Gao, 1997), in which the gas penetration can also be tracked by VOF.

In the present studies, a pseudo-concentration technique derived from the VOF method is employed to track the flow front advancement. Using concentrations to follow the movement of an interface between two immiscible fluids was first used in the simulation of fluid flows associated with oil reservoirs (Argyris, 1984). Later on, Thompson (1986) extended this technique to the transient viscous flow analysis by assigning appropriate concentration values (pseudo-concentration) to the empty regions. A number of examples were presented, including injection molding and forging problems. The pseudo-concentration technique has been successfully applied to a metal casting problem (Usmani, 1992). Most recently, Hetu et al. (1998) used pseudo-concentration technique to simulate the filling stage in injection molding process with 3D finite element method. This approach was implemented in a fixed mesh system with flow fronts passing through it. An imaginary pseudo-concentration function F is assigned to the flow field, in which a critical value, F_c, represents the interface between the melt front and the vacant mold cavity. The transport of pseudo-concentration F is expressed in the Eulerian representation by Eq. (5.1)

The melt front position is explicitly expressed by the pseudo-concentration. For example, the region of $F > F_c$ is filled with polymer melt, and the in the region of $F < F_c$, the mold cavity is empty and need to be filled. The melt front is represented by $F = F_c$. The flow field for a pseudo-concentration technique is shown in figure 5.1

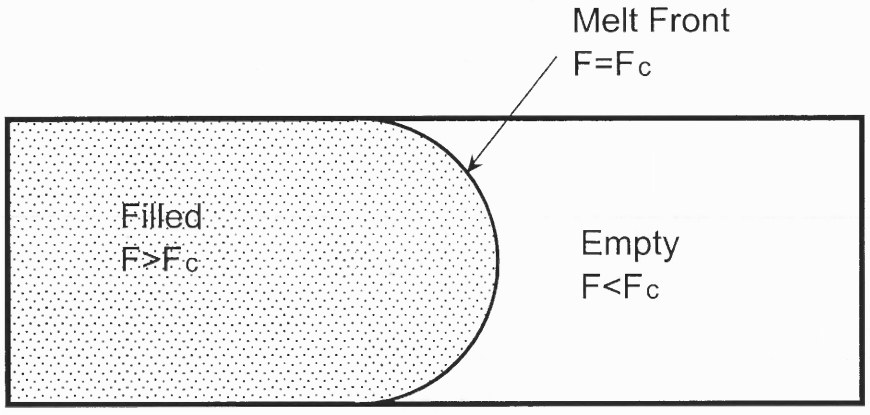

Figure 5.1 Representation of the flow field for pseudo-concentration technique

In order to model the flow of a fluid using a pseudo-concentration approach, it is necessary to define the fluid properties throughout the entire mesh and have it transported by an artificial fluid in regions where the real fluid is not present. It is possible to specify a viscosity for the artificial material to be low enough to ensure that its presence has no effect on the motion of the real fluid. Because the empty region is filled with air, the flow properties of air can be used. An alternate approach is to assign imaginary values of flow properties to the pseudo fluid. The imaginary values should be small enough so that no significant error occurs in the result. However, if too low a value is specified for the viscosity of the artificial fluid, the finite element equations become ill-conditioned. Generally, the suitable values of the viscosity of the artificial fluid should be two or three orders of magnitude smaller than the viscosity of real fluid without a noticeable difference in the resulting flow pattern.

The main advantage of the pseudo-concentration technique is that no special treatment is needed to deal with the melt front. The boundary conditions in the melt front are implicitly incorporated into the momentum equations. The position of the flow fronts is obtained directly by solving the hyperbolic equation. There is no need for treatment of special cases or the need to define how the volumes are filled.

The following boundary and initial conditions can be assigned for the transport equation of pseudo-concentration as follows:

$$F(x,y,t) = F_c + d \tag{5.2}$$

$$F(x,y,0) = 0 \tag{5.3}$$

where d represents the distance between the flow region and the melt front.

In the region where $F < F_c$, i. e. the empty region, a sufficiently small value for the material property is used, usually two or three order less than that of the real polymer melts. For example, the viscosity of polymer melt is usually in the order of $10^2 - 10^7 Pa \cdot s$ and the density is in the order of $10^3 kg/m^3$. The appropriate values for the pseudo-fluid are $\rho = 1kg/m^3$, $\eta = 1Pa \cdot s$.

The transport equation of F (Eq. 5.1) is a hyperbolic equation. The velocity field has direct influence on the transport of F. If the velocity is zero in some portions of flow field, then, by definition, F is not conveyed in such area. If no slip conditions are imposed on the mold walls, then the velocity field is such that F in these areas will be given by a solution at t=0. In other words, the value of F near the walls will not change as the fluid fills the cavity. The use of non-slip boundary conditions on the cavity walls, applied to

the polymer melt and pseudo-liquid, leads to unrealistic solutions where the melt would never touch the walls. Therefore, the boundary conditions for the vacant portion should be modified. In the present studies, a non-slip boundary condition will be imposed on the filled portion. In the pseudo-fluid portion of the mold cavity, the pseudo-fluid is free to move and leave the mold cavity by the advancing fluid. Mathematically, these can be expressed as:

$$u = 0 \text{ and } v=0 \text{ when } F \geq F_c \text{ (filled)} \tag{5.4}$$

$$\boldsymbol{\sigma \cdot n - pn} = 0 \text{ when } F < F_c \text{ (Empty)} \tag{5.5}$$

where $\boldsymbol{n}$ is the outward normal direction of the boundaries, σ the stress tensor and p the pressure.

5.2 F-Smoothing Technique

For a given F representation, one may obtain transport of F over a number of time steps without redefinition of F. When the variations of F in the neighboring zone of melt front become less smooth, it is necessary to redefine F. This treatment is called the smoothing of F. It involves:

1. Representation of abrupt melt front (melt-air interface) by a smoother function (F-space) via the introduction of F-values having smooth variations over the melt-air zones. A particular value of F, called the cut-off value F_c, defines the melt-air surface. The variation of F is a linear function of minimum distance from the melt front, $F > F_c$ in the filled zone and $F < F_c$ in the unfilled zone.

2. Transport of the melt front in F space by solving Eq. (5.1)

3. Tracking the new melt front from the transported values of F

4. If necessary, redefine the values of F (smoothing)

In this study, the values of F are updated at each time step in order to avoid error accumulation in the F values. The slope of F is adjusted as follows:

$$F(x,y) = F_c + A|d| \tag{5.6}$$

where A is positive for a node in the filled region and negative in the unfilled region. d is the distance of the node to the melt front. The redefinition of F is shown in Figure 5.2.

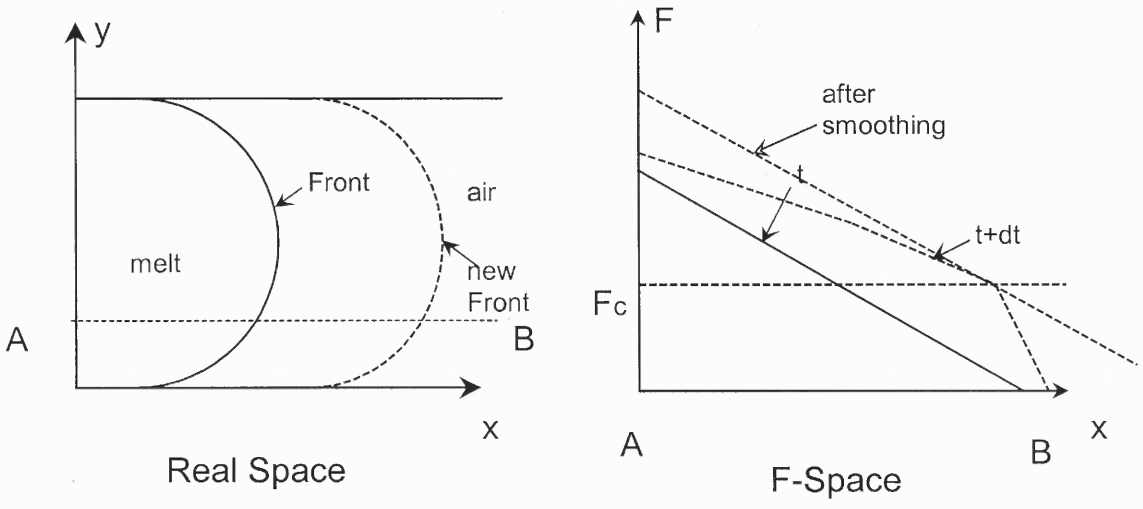

Figure 5.2 Smoothing and updating of the F-space

5.3 Special Treatment during Advancement of Melt Front

Using the above pseudo-concentration method to simulate the advancement of melt front during the filling stage, it is should be noted that the non-slip boundary condition can not be strictly applied on the point of melt front that contacts the wall, as shown in figure 5.3. This point is called triple point, at which melt, air (pseudo-fluid) and wall meet together. If the non-slip condition is imposed on this point, the values of F near this point will not change as the polymer melt fills the cavity. It is generally accepted that the triple point actually slides along the mold wall within a small distance of the interface. The length that is allowed to freely move along the wall will affect the shape of the melt front.

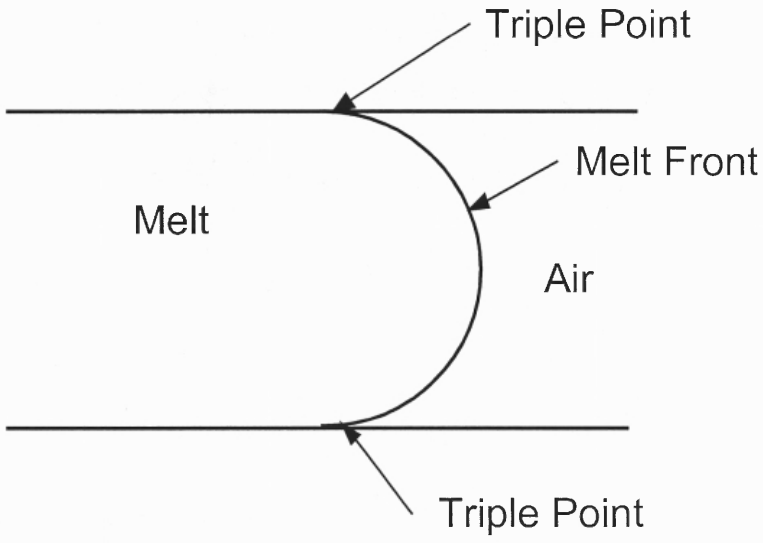

Figure 5.3 Triple points

Figure 5.4 shows the melt front advancement during the filling process at a time interval of about 0.0075 seconds with the non slip boundary condition applied to the triple point. The melt front curve remains in contact with the wall at the initial position, and will not move forward. Figure 5.5 shows the melt front advancement under the

condition that the free slip length within the contact point is 0.1 cm, at which the node closest to the triple point is set to be free to slip. If the length is increased to 0.2 cm, about 2 wall nodes near the triple point in the melt is free to slide, the melt front curve becomes flatter. Therefore, the selection of the free slipping length has influence on the final solution, and must be carefully determined. According to the test computation of the filling problem, a suitable selection of the free slipping length is about one element long.

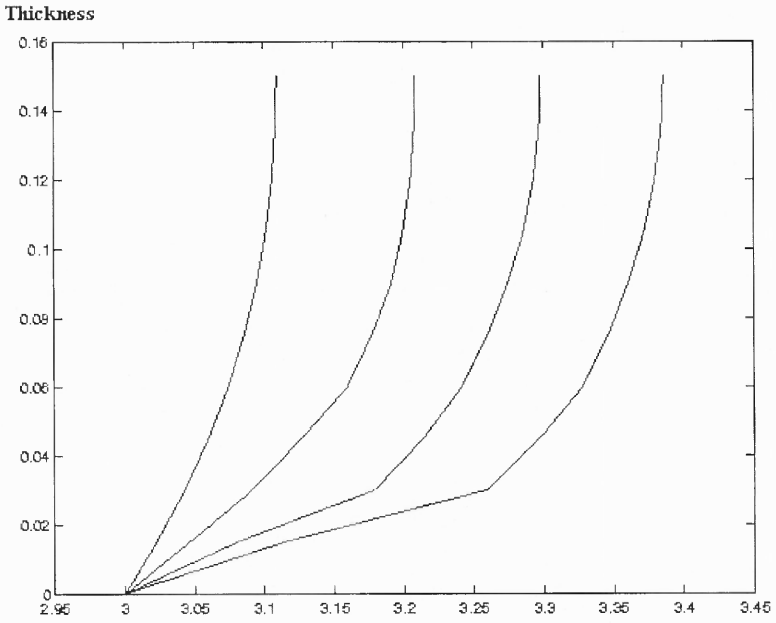

Figure 5.4 Non-slip condition at the triple point shows no advancement at the contact point

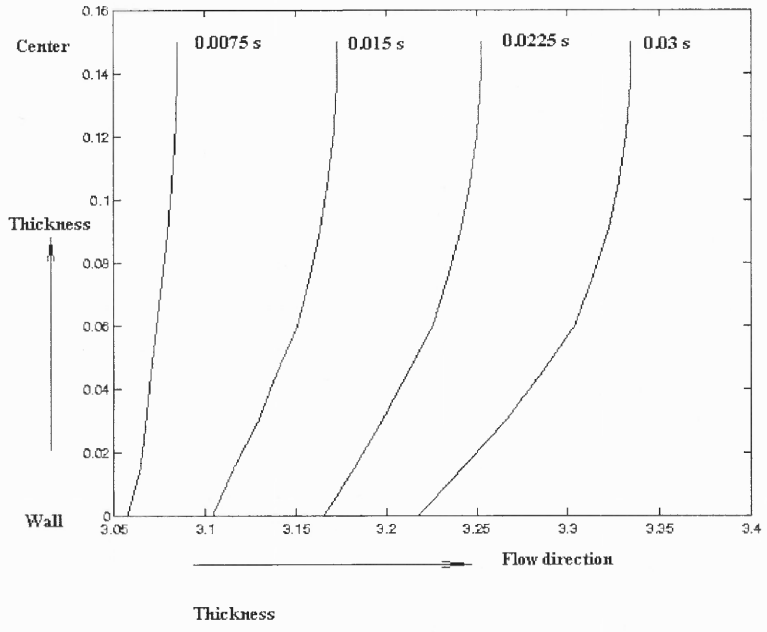

Figure 5.5 Melt Front Advancement with 0.1 cm free slip length apart from the triple point

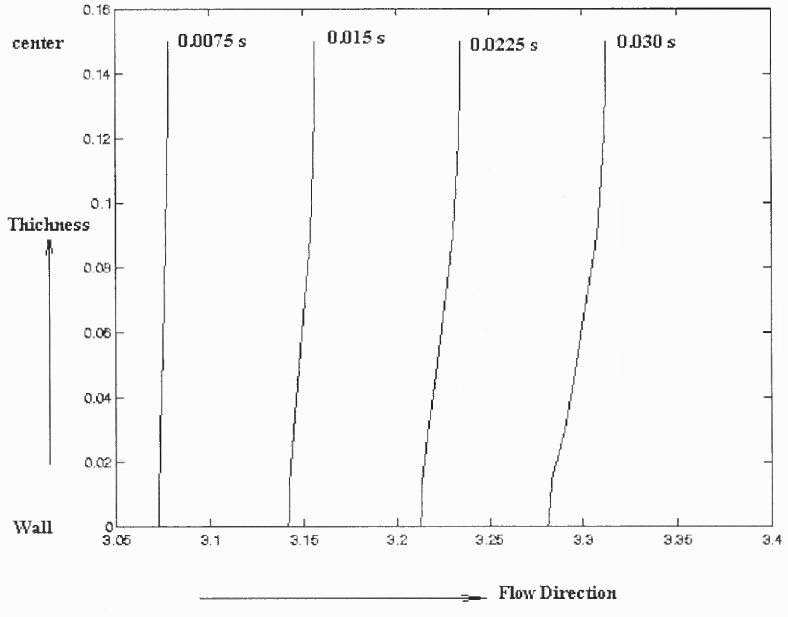

Figure 5.6 Melt front advancement with 0.2 cm free slip length

CHAPTER 6

MATHEMATICAL MODEL

6.1 Hypothesis and Assumptions

The hypothesis upon which this dissertation study is based presupposes that stress relaxation of high molecular weight polymers has a significant effect on the crystallization kinetics of semicrystalline polymers during the injection molding process. In particular, it is hypothesized that shear stresses have a significant effect on the crystallization in the filling stages of the injection molding process. However, the relaxation of stress during the cooling stages implies a decreased effect of stress on the kinetics of crystallization. Therefore, a realistic model of stress-induced crystallization should also consider the effect of stress relaxation to test the above hypothesis. The following assumptions are made:

(1) Polymer melts are incompressible fluids.

(2) The viscosity of polymer melt is very high. The gravity force and acceleration force are very small compared with the viscous force, and will be neglected.

(3) At every time instant, the flow is thought of as steady flow. The flow region for the next time step is obtained from the velocity field of last time step.

(4) The stress developed during the flow has significant effect on the crystallization process.

(5) During the post filling stage, the stress relaxation phenomenon follows a prescribed model.

6.2 Governing Equations

Most injection molded plastics products are of thin thickness. The shear rate and shear stress during injection molding process change dramatically across the thickness, resulting in multi-layer morphologies in the final product, especially for the semi-crystalline polymers. Consequently, a simple geometry slit cavity with half thickness of h (Fig. 6.1) is considered in this study.

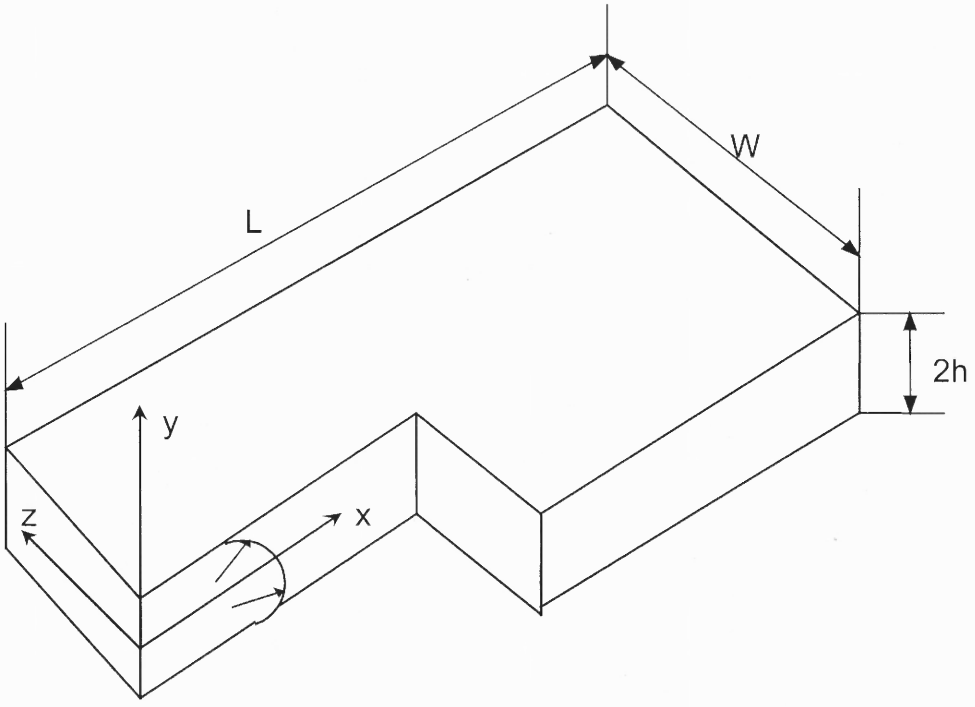

Figure 6.1 Mold cavity dimensions

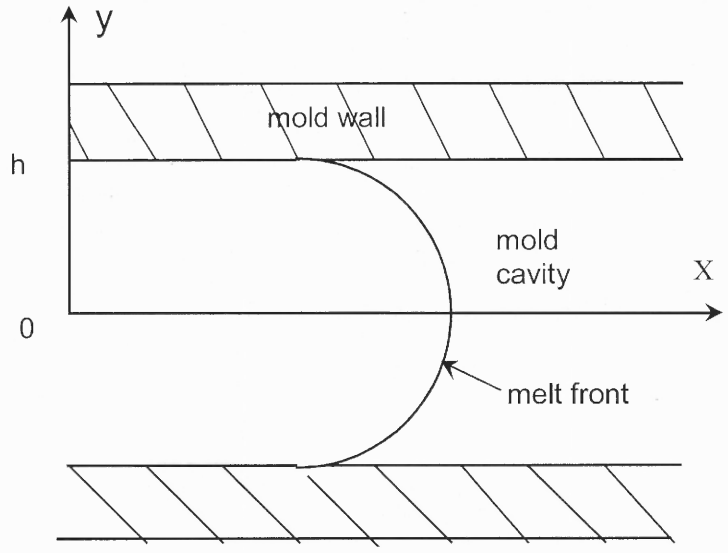

Figure 6.2 Calculation domain

Assuming that the width of the cavity is much larger than its thickness, transverse flow across the width (z direction in figure 6.1) can be neglected. The fountain flow phenomenon during the injection molding process will be considered, because it will influence the material transportation and temperature distribution, as well as shear stress and, the crystallinity distribution.

In general, the governing equations for a fluid flow problem are expressed by the conservation equations of momentum (known as Stokes equations), mass and energy. For the problem specified above, the governing equations can be simplified as follows:

Momentum Equation:

$$\frac{\partial}{\partial x}\left(2\eta\frac{\partial u}{\partial x}\right)+\frac{\partial}{\partial y}\left[\eta\left(\frac{\partial u}{\partial y}+\frac{\partial v}{\partial x}\right)\right]=-\frac{\partial P}{\partial x} \qquad (6.1a)$$

$$\frac{\partial}{\partial y}\left(2\eta\frac{\partial v}{\partial y}\right)+\frac{\partial}{\partial x}\left[\eta\left(\frac{\partial u}{\partial y}+\frac{\partial v}{\partial x}\right)\right]=-\frac{\partial P}{\partial y} \tag{6.1b}$$

Continuity Equation:

$$\frac{\partial u}{\partial x}+\frac{\partial v}{\partial y}=0 \tag{6.2}$$

where x and y represent the flow direction and thickness direction, respectively. u and v are the velocities in x and y directions. P is pressure, η apparent shear viscosity.

The flow in the mold cavity during the injection molding process is a transient process in the sense that both the flow velocity and flow region change with time. Time derivatives should, therefore, be included in the governing equations. This will certainly increase the complexity of the problem. For such a problem, an efficient method is using a quasi-steady treatment: At any instant, the flow region is considered to be constant, and the flow is assumed to be a steady state flow at this instant. The are computed according to the steady state boundary conditions, and the flow field for next time step is calculated according to the velocity results of the present time.

Since the dimensions in transverse and flow directions are much greater than the thickness, the heat conduction in the thickness is much more important than in the other two directions. Therefore, for the energy equation, only the heat conduction in thickness direction is considered. The energy equation was simplified as:

$$\rho C_P\left(\frac{\partial T}{\partial t}+u\frac{\partial T}{\partial x}+v\frac{\partial T}{\partial y}\right)=K_h\frac{\partial^2 T}{\partial y^2}+\boldsymbol{\tau}:\nabla V+\rho C_c\dot{\theta}\chi_\infty \tag{6.3}$$

where ρ, C_P, K_h and C_C are density, heat capacity, thermal conductivity, and heat of crystallization, respectively, $\dot{\theta}$ the rate of relative crystallization during the flow. $\boldsymbol{\tau}$ is the shear rate tensor and shear stress tensor, ∇V the velocity gradient of the flow field. $(\boldsymbol{\tau}:\nabla V)$ represents the viscous dissipation rate during the flow with $\boldsymbol{\tau}=\eta\dot{\boldsymbol{\gamma}}$. $\dot{\boldsymbol{\gamma}}$ is the shear rate tensor of the flow field:

$$\dot{\gamma}=\begin{pmatrix} 2\dfrac{\partial u}{\partial x} & \dfrac{\partial u}{\partial y}+\dfrac{\partial v}{\partial x} \\ \dfrac{\partial u}{\partial y}+\dfrac{\partial v}{\partial x} & 2\dfrac{\partial v}{\partial y} \end{pmatrix} \tag{6.3a}$$

and

$$\nabla V=\begin{bmatrix} \dfrac{\partial u}{\partial x} & \dfrac{\partial u}{\partial y} \\ \dfrac{\partial v}{\partial x} & \dfrac{\partial v}{\partial y} \end{bmatrix} \tag{6.3b}$$

The viscous dissipation term in Eq. (6.3) can be further simplified by assuming that the velocity gradient and shear rate along the thickness direction is a dominant factor for viscous dissipation compared with other components, that is:

$$\frac{\partial}{\partial y}>>\frac{\partial}{\partial x} \tag{6.3c}$$

Therefore,

$$\boldsymbol{\tau}:\nabla V=\eta\dot{\gamma}^2 \tag{6.3d}$$

with

$$\dot{\gamma}=\frac{\partial u}{\partial y}+\frac{\partial v}{\partial x}\cong\frac{\partial u}{\partial y} \tag{6.3e}$$

On the basis that some crystallinity is generated during the injection process, the heat released by the crystallization process should be included in the formulation - as expressed by the last term in the energy equation.

6.3 Initial and Boundary Conditions

At the mold inlet, it is assumed that the melt enters the mold with a constant temperature, T_0, and a fully developed velocity profile for a power law fluid:

$$T(0,y,t) = T_0 \tag{6.4}$$

$$u(0,y,t) = \left(\frac{s+2}{s+1}\right)\left(\frac{Q}{2wh}\right)\left[1-\left(\frac{y}{h}\right)^{s+1}\right] \tag{6.5a}$$

$$v(0,y,t) = 0 \tag{6.5b}$$

where $s = 1/\tilde{n}$, $\tilde{n}$ is the power law index. w and h are the width and thickness of the mold cavity.

If the melt comes in contact with the wall of the mold, non-slip condition applies:

$$u(x,h,t) = 0 \tag{6.6a}$$

$$v(x,h,t) = 0 \tag{6.6b}$$

It is generally assumed that once the melt contacts the mold wall, it will maintain the mold temperature. However, the contact can never be perfect and heat resistance inevitably exists between the mold wall and polymers melt. According to the recent study by Sridhar (1998), the thermal contact resistance (TCR) between PET and the mold metal is in the range of $10^{-5} - 10^{-3}\ m^2 \cdot K/W$. Therefore, the boundary condition for the energy equation at the mold wall should have the form:

$$K_h \frac{\partial T}{\partial y}\bigg|_+ = \frac{1}{R_h}(T - T_w) \tag{6.7}$$

where R_h is the heat resistance between the melt and mold wall, T_w the wall temperature, K_h the thermal conductivity of the polymer melt.

At the central line of the mold cavity, symmetric conditions are used:

$$\frac{\partial u}{\partial y}(x,0,t) = 0 \tag{6.8a}$$

$$\frac{\partial v}{\partial y}(x,0,t) = 0 \tag{6.8b}$$

$$\frac{\partial T}{\partial y}(x,0,t) = 0 \tag{6.9}$$

As stated in Chapter 5, the unfilled region in the mold cavity is represented by pseudo-fluid. The boundary conditions on the pseudo-fluid should be chosen in such a

way that they have little effect on the progress of the filled region. On the wall, there is no restriction for the pseudo-fluid to move. On the other end of the mold, the pseudo-fluid is free to leave for the melt to fill the mold cavity. The boundary conditions are illustrated in figure 6.3.

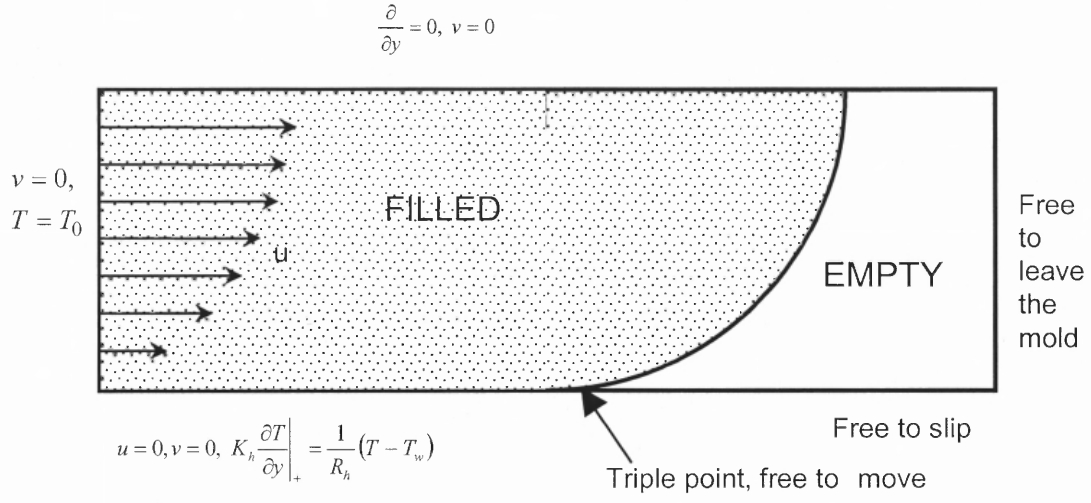

Figure 6.3 Boundary conditions for the mold flow analysis using pseudo-concentration technique

6.4 The Rheological Model

Polymer viscosity is the most important property used in flow simulations. Most polymers exhibit two regimes of flow behavior, Newtonian and shear-thinning. Newtonian behavior occurs at low shear rates. With increasing the shear rate, the viscosity tends to decrease in what is termed a shear-thinning behavior.

To incorporate the dependence of melt viscosity on shear rate, temperature and pressure, the following five constant $(\tilde{n}, \tau^*, \mathrm{B}, \mathrm{T}_b, \beta)$, Cross-exponential model is adequate for simulating the filling stage in injection molding:

$$\eta = \frac{\eta_0(T,P)}{1+\left[\frac{\eta_0\dot{\gamma}}{\tau^*}\right]^{1-\tilde{n}}} \tag{6.10a}$$

where

$$\eta_0(T,P) = B\exp(T_b/T)\exp(\beta P) \tag{6.10b}$$

where η_0 is the zero shear rate viscosity at a reference temperature T_0, $\tilde{n}$ the power law index, T_b the material constants, which represent the effect of temperature on viscosity, and $\dot{\gamma}$ the shear rate; τ^* is the shear stress at which shear thinning begins; β is the factor that accounts for the effect of pressure on the melt viscosity. All the parameters involved in the model can be obtained by either experiment or from the literature.

The Cross-exponential model treats polymer viscosity as a function of temperature and shear rate. It handles both the Newtonian and the shear-thinning flow regimes found in polymer rheology. Unlike many other models in present use, the constants of the Cross-exponential model do have a physical significance. The transition between the two regimes is characterized by τ^*, while the slope of the shear-thinning curve is characterized by $(1-\tilde{n})$.

Crystallization during the filling stage may lead to an increase in viscosity of the polymer melt and influence the mold filling process. To consider the effect of crystallinity on the rheological properties of the polymer melt, the model proposed by Titomanlio et al (1997) is adopted to describe the effect of crystallinity upon viscosity:

$$\eta_\chi = \frac{\eta(T,\dot{\gamma},\chi)}{\eta(T,\dot{\gamma},\chi=0)} = 1 + f\exp(-h/\chi^m) \tag{6.11}$$

where η_χ is the viscosity enhancement factor, $\eta(T,\dot{\gamma},\chi=0)$ is the viscosity with no crystallinity as expressed by Eq. (6.10a), *f, h, m* are material constants that can be estimated from experimental data.

6.5 Transport Equations of Induction Time Index and Crystallinity

If some crystals are formed during the filling stage, then it is inevitably that the crystals formed would be transported with the flow field. Similarly, the accumulated induction time index would be transported with the flow field. Therefore, two extra equations governing the transportation of the induction time index and crystallinity should be included.

From Eq. (4.6), the term inside the integral can be thought of as the accumulation rate of induction time index. Therefore, the transportation model of the induction time index in a flow field takes the form:

$$\frac{\partial \bar{t}}{\partial t} + u\frac{\partial \bar{t}}{\partial x} + v\frac{\partial \bar{t}}{\partial y} = \frac{1}{t_i(T,\tau)} \tag{6.12}$$

where $t_i(T,\tau)$ is the non-isothermal induction time at stressed state as expressed in Eq. (4.19).

The transportation equation of the crystallinity in a flow field takes the form:

$$\frac{\partial \theta}{\partial t} + u\frac{\partial \theta}{\partial x} + v\frac{\partial \theta}{\partial y} = nK(T)(1-\theta)[-\ln(1-\theta)]^{(n-1)/n} \tag{6.13}$$

The right hand of Eq. (6.13) is the relative crystallization rate as expressed in Eq. (4.7)

6.6 Governing Equations for Post Filling Stage

In the post filling stage, the mold cavity is completely filled and the melt flow ceases. The problem is reduced to a pure heat transfer problem and the governing energy equation is reduced to the following energy equation:

$$\rho C_P \frac{\partial T}{\partial t} = K_h \frac{\partial^2 T}{\partial y^2} + \rho C_c \dot{\theta}\chi \tag{6.13}$$

The initial conditions for the energy equation of the post filling stage are the temperature distribution at the end of filling stage.

6.7 Stress Relaxation Model

During the cooling stage, both stress and molecular orientation undergo a relaxation process. The stresses developed during the filling stage decrease with time and eventually vanish. Therefore, the effect of stress on the crystallization process in the mold cavity does not last for the whole cycle time. In the regions that the polymeric material is still in the molten state after filling, the stresses may vanish as long as the flow stops, since the stress relaxation time for molten polymer is in the order of $10^{-2} - 10^{-3}$ seconds. However, in the skin layer, the stress may be frozen-in by the fast cooling of the cold mold wall. To

consider the effect of stress on the crystallization kinetics in injection molding, the stress relaxation process should be included.

The stress relaxation behavior of polymers can be expressed by a simple Maxwell model:

$$\tau = \tau_0 \exp(-\frac{t}{\lambda}) \tag{6. 14}$$

where τ_0 is the initial stress, λ is the relaxation time. In the case of injection molding, the stresses at the end of filling can be taken as the initial shear stresses for Eq. (6.14).

The stress relaxation time λ is a material constant that is strongly temperature dependent. The well-known William-Landel-Ferry (WLF) (Ferry, 1980) shift model was used to model the relationship between the relaxation time and temperature:

$$\log\left(\frac{\lambda}{\lambda_0}\right) = -\frac{B_1(T - T_s)}{B_2 + (T - T_s)} \tag{6.15}$$

where B_1 and B_2 are material constants; T_s the reference temperature, and λ_0 the relaxation time at the reference temperature.

The WFL model is valid only in the temperature range $T_g < T < T_g + 100^0 C$. The polymer temperature in injection molding process is outside this range. The relaxation information of most materials is generally not available near the processing temperatures. To demonstrate the effect of stress relaxation on the crystallization kinetics, a set of trial value of the constants in the WFL model is used, based on the fact that most amorphous thermoplastics have similar relaxation behavior (Osswald, 1995).

CHAPTER 7

FINITE ELEMENT EQUATION FORMULATION

7.1 Introduction

The finite element method solution of Stokes equations and continuity equation requires the solution of a large number of linear equations. There are several methods to reduce the number of equations involved in the computation. The most used method is penalty function method. In the penalty function method, a small perturbation related to pressure is introduced into the continuity equation. By substituting the pressure in the Navier-Stokes equations with the pressure from the perturbed continuity equation, the pressure in the Navier-Stokes equation is eliminated. The penalty function method may reduce equations of the system by the number of pressure nodes. For a large system, this reduction can save considerable computation time.

Penalty function method is usually combined with discontinuous pressure elements (Crouzeix-Raviart elements) (Cuvelier,1986). Figure 7.1 shows two kind of Crouzeix-Raviart elements used in the simulation. The 7-node triangular element is called extended quadratic element. There is only one pressure node in the element, which is located in the centroid of the element. The pressure in the element is linear and the interpolation function of the pressure includes two derivatives:

$$P = P_c \phi_1^p + \frac{\partial P}{\partial x} \phi_2^p + \frac{\partial P}{\partial y} \phi_3^p \tag{7.1}$$

where, the pressure interpolation functions are:

$$\phi_1^P = 1 \tag{7.2a}$$

$$\phi_2^P = x - x_c \tag{7.2b}$$

$$\phi_3^P = y - y_c \tag{7.2c}$$

Although it seems that the Crouzeix-Raviart elements have more velocity nodes than the ordinary quadratic elements, however, by appropriate manipulation of the resultant finite element equation, the velocities and pressure derivatives in the centroid can be eliminated. By further employing the penalty formulation, the pressure is also eliminated. The resultant finite element equations are reduced by four.

The finite element mode for the temperature, pseudo concentration, induction time index, and crystallinity is linear element, as illustrated in figure 7.1 (triangular element with three nodes and rectangular element with four nodes).

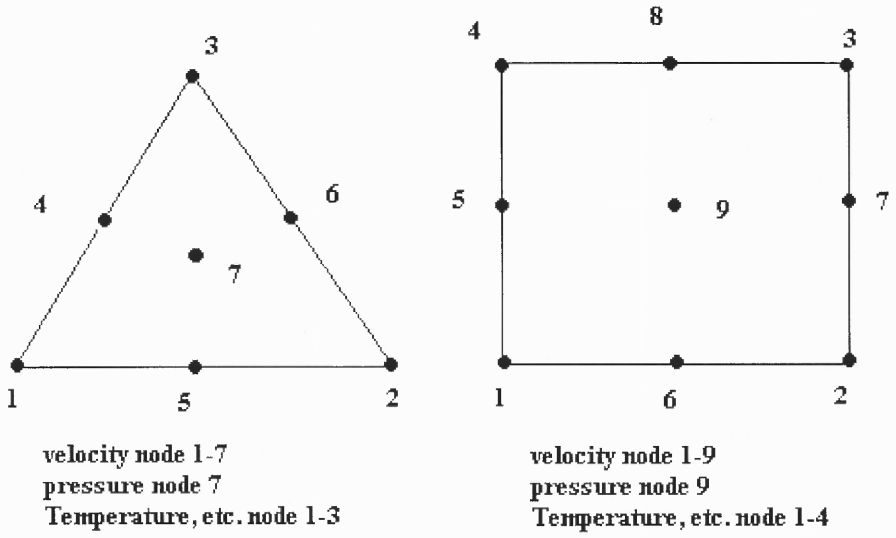

Figure 7.1 Finite element model

The variables in the element can be expressed by the interpolation function for each node:

$$u = \sum_i \phi_i^v u_i \tag{7.3a}$$

$$v = \sum_i \phi_i^v v_i \tag{7.3b}$$

$$P = \sum_i \phi_i^P P_i \tag{7.3c}$$

$$F = \sum_i \phi_i^F F_i \tag{7.4}$$

$$T = \sum_i \phi_i^T T_i \tag{7.5}$$

$$\theta = \sum_i \phi_i^\theta \theta_i \tag{7.6}$$

$$\bar{t} = \sum_i \phi_i^t \bar{t}_i \tag{7.7}$$

where the subscript i denotes the variable value in node i, and symbol ϕ represents the interpolation functions for each variable.

7.2 Finite Element Equations

7.2.1 Finite Element Equations for Velocities and Pressure

The Galerkin method is used to discretize the Navier-Stokes equations, in which a test function, usually the interpolation function, is used to multiply the whole equation and integrate across the whole element.

$$\int_\Omega \phi_i^v \left\{ \frac{\partial}{\partial x}\left(2\eta \frac{\partial u}{\partial x}\right) + \frac{\partial}{\partial y}\left[\eta\left(\frac{\partial u}{\partial y} + \frac{\partial v}{\partial x}\right)\right] + \frac{\partial P}{\partial x} \right\} d\Omega = 0 \tag{7.8a}$$

$$\int_\Omega \phi_i^v \left\{ \frac{\partial}{\partial y}\left(2\eta \frac{\partial v}{\partial y}\right) + \frac{\partial}{\partial x}\left[\eta\left(\frac{\partial u}{\partial y} + \frac{\partial v}{\partial x}\right)\right] + \frac{\partial P}{\partial y} \right\} d\Omega = 0 \tag{7.8b}$$

$$\int_\Omega \phi_i^P \left[\frac{\partial u}{\partial x} + \frac{\partial v}{\partial y} \right] d\Omega = 0 \tag{7.8c}$$

where Ω represents the element.

Integrating the above equations by parts and substituting u, v, P with equation (7.3), the following finite element equations are obtained:

$$\left[\mathbf{K}^{11}\right]\{\mathbf{u}\}+\left[\mathbf{K}^{12}\right]\{\mathbf{v}\}+\left[\mathbf{K}^{13}\right]\{\mathbf{P}\}=\{\mathbf{t}_x\} \tag{7.9a}$$

$$\left[\mathbf{K}^{21}\right]\{\mathbf{u}\}+\left[\mathbf{K}^{22}\right]\{\mathbf{v}\}+\left[\mathbf{K}^{23}\right]\{\mathbf{P}\}=\{\mathbf{t}_y\} \tag{7.9b}$$

$$\left[\mathbf{K}^{31}\right]\{\mathbf{u}\}+\left[\mathbf{K}^{32}\right]\{\mathbf{v}\}=\mathbf{0} \tag{7.9c}$$

The components of the matrix involved in the element equations are as follows:

$$K_{ij}^{11}=\int_{\Omega}\eta\left[\frac{\partial\phi_i^v}{\partial x}\frac{\partial\phi_j^v}{\partial x}+\frac{\partial\phi_i^v}{\partial y}\frac{\partial\phi_i^j}{\partial y}\right]d\Omega \tag{7.10a}$$

$$K_{ij}^{22}=\int_{\Omega}\eta\left[\frac{\partial\phi_i^v}{\partial x}\frac{\partial\phi_j^v}{\partial x}+2\frac{\partial\phi_i^v}{\partial y}\frac{\partial\phi_j^v}{\partial y}\right]d\Omega \tag{7.10b}$$

$$K_{ij}^{12}=\int_{\Omega}\eta\left[\frac{\partial\phi_i^v}{\partial y}\frac{\partial\phi_j^v}{\partial x}\right]d\Omega \tag{7.10c}$$

$$K_{ij}^{13}=\int_{\Omega}\frac{\partial\phi_i^v}{\partial x}\phi_j^p\,d\Omega \tag{7.10d}$$

$$K_{ij}^{21}=\int_{\Omega}\eta\left[\frac{\partial\phi_i^v}{\partial x}\frac{\partial\phi_j^v}{\partial y}\right]d\Omega \tag{7.10e}$$

$$K_{ij}^{23} = \int_{\Omega} \eta \frac{\partial \phi_i^v}{\partial y} \phi_j^p d\Omega \tag{7.10f}$$

$$\left[K^{31}\right] = \left[K^{13}\right]^T \tag{7.10g}$$

$$\left[K^{32}\right] = \left[K^{23}\right]^T \tag{7.10h}$$

$$t_{xi} = \int_{\Gamma} \left[2\eta \frac{\partial u}{\partial x} n_x + \eta \left(\frac{\partial u}{\partial y} + \frac{\partial v}{\partial x} \right) n_y - P n_x \right] \phi_i^v ds \tag{7.10a}$$

$$t_{y_i} = \int_{\Gamma} \left[2\eta \frac{\partial v}{\partial y} n_y + \eta \left(\frac{\partial u}{\partial y} + \frac{\partial v}{\partial x} \right) n_x - P n_y \right] \phi_i^v ds \tag{7.10b}$$

Where Ω is the area of the element, Γ represents the boundary of the elements, n_x and n_y represent the outward normal direction cosines of the boundary. Eq. (7.10) is the second type boundary condition.

A large number of equations are involved in Eq. (7.9). It takes a lot of computing time and computer memory to get the numerical solutions. To reduce the number of equations and reduce the computation time, penalty method is used in this work. In the penalty method, the continuity equation is perturbed with a small parameter times the pressure. Then the pressure is eliminated from the momentum equations, thus uncoupling the momentum equations and the continuity equation. Introducing a small perturbation of

pressure into the continuity equation (6.3) and following the same integration procedure above, we have:

$$[\mathbf{K}^{31}]\{\mathbf{u}\}+[\mathbf{K}^{32}]\{\mathbf{v}\}=\delta[\mathbf{D}]\{\mathbf{P}\} \tag{7.11a}$$

or

$$\{\mathbf{P}\}=\frac{1}{\delta}[\mathbf{D}]^{-1}([\mathbf{K}^{31}]\{\mathbf{u}\}+[\mathbf{K}^{32}]\{\mathbf{v}\}) \tag{7.11b}$$

where

$$D_{ij}=\int_{\Omega}\phi_i^P\phi_j^P d\Omega \tag{7.11c}$$

δ is a very small number usually in the range of $10^{-8}-10^{-13}$. Large values of δ may cause significant errors in the solution, and too small values may cause the singularity of the coefficient matrix of the equations.

Substituting into Eqs. (7.9a-b), the pressure term in the momentum equation is thus eliminated:

$$[\mathbf{K}^{11}]\{\mathbf{u}\}+[\mathbf{K}^{12}]\{\mathbf{v}\}+[\mathbf{K}^{13}][\mathbf{D}]^{-1}([\mathbf{K}^{31}]\{\mathbf{u}\}+[\mathbf{K}^{32}]\{\mathbf{v}\})\frac{1}{\delta}=\{\mathbf{t}_x\} \tag{7.12a}$$

$$[\mathbf{K}^{21}]\{\mathbf{u}\}+[\mathbf{K}^{22}]\{\mathbf{v}\}+[\mathbf{K}^{23}][\mathbf{D}]^{-1}\left([\mathbf{K}^{31}]\{\mathbf{u}\}+[\mathbf{K}^{32}]\{\mathbf{v}\}\right)\frac{1}{\delta}=\{\mathbf{t}_x\} \tag{7.12b}$$

The penalty method involves the calculation of matrix D and its inverse. To take the advantages of penalty method, matrix D should have the simplest form.

7.2.2 Finite Element Equation Formulation for Pseudo-Fluid, Temperature, Crystallinity and Induction Time Index

The transport equations for these parameters are dominated by the advection of the flow. If the conventional Galerkin method is used for this problem, severe oscillations are generated. This can be improved by applying the Taylor-Galerkin method to the transport equations. The procedure for the formulation is well documented in the literature (Usmani, et al. 1992). The following is the resultant finite element equations:

(a) Energy Equation

$$\left(\frac{\mathbf{M}}{\Delta t}+\frac{\mathbf{K}_d}{2}\right)\{\mathbf{T}_{n+1}\}=\left(\frac{\mathbf{M}}{\Delta t}-\frac{\mathbf{K}_d}{2}-\rho c(\mathbf{K}_a+\mathbf{K}_{bd})\right)\{\mathbf{T}_n\}+\mathbf{Q} \tag{7.13}$$

(b) Pseudo-fluid transport equation:

$$\left(\frac{\mathbf{M}_F}{\Delta t}\right)\{\mathbf{F}_{n+1}\}=\left(\frac{\mathbf{M}_F}{\Delta t}-\mathbf{K}_a-\mathbf{K}_{bd}\right)\{\mathbf{F}_n\} \tag{7.14}$$

(c) Transport of Crystallinity

$$\left(\frac{\mathbf{M}_{\theta}}{\Delta t}\right)\{\boldsymbol{\theta}_{n+1}\} = \left(\frac{\mathbf{M}}{\Delta t} - (\mathbf{K}_a + \mathbf{K}_{bd})\right)\{\boldsymbol{\theta}_n\} + \mathbf{Q}_{\theta} \tag{7.15}$$

(d) Transport of induction time index

$$\left(\frac{\mathbf{M}_{\bar{t}}}{\Delta t}\right)\{\bar{\mathbf{t}}_{n+1}\} = \left(\frac{\mathbf{M}_{\bar{t}}}{\Delta t} - (\mathbf{K}_a + \mathbf{K}_{bd})\right)\{\bar{\mathbf{t}}_n\} + \dot{\bar{\mathbf{t}}} \tag{7.16}$$

Since the transport equations for the pseudo-fluid, crystallinity and induction time index are almost purely advective, only initial conditions were applied to these equations. For the pseudo-fluid, a pre-assumed distributed F value is used as the initial value with the cut-off value F_c indicating the initial front position. For the crystallinity, since the differential form of crystallization kinetics equation is used, a sufficiently small value such as 10^{-15} is used as the initial value. For the induction time index, the initial value is zero.

7.3 Computation Procedure

The computation procedure includes the computation of the velocity distribution, advancement of the melt front by solving the pseudo-fluid transport equation, temperature calculation, induction time index computation, as well as the crystallinity generation if the induction time index exceeds unity. Figure 7.2 shows a flow chart of the computation procedure.

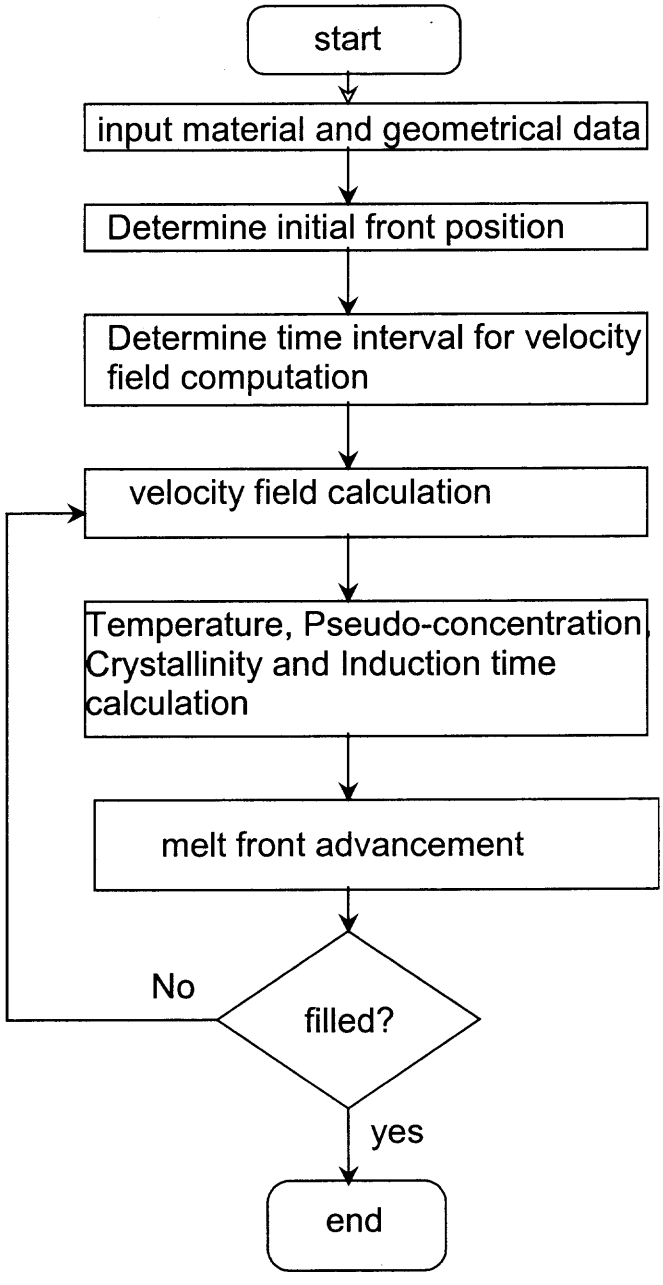

Figure 7.2 Flow chart of computation procedure

7.4 Computation Time Saving Consideration

The pseudo concentration technique treats the whole mold cavity as a complete flow field, which is filled with polymer melt in the filled region and pseudo fluid in the empty region. The main disadvantage is the unnecessary computation of the unfilled region

during the early stage of mold filling, at which most of the mold cavity is empty. Since a very small flow and thermal properties are assigned to the pseudo fluid, it has little influence on the solution of the real flow field. The empty region that is far from the melt front has no effect on the result of the computation. Therefore, it is reasonable to narrow the computation region from the whole mold cavity to the filled region and a small region near the melt front in the empty region, as illustrated in Figure 7.3. This treatment will save a lot of computation time and not lose the accuracy of the computation.

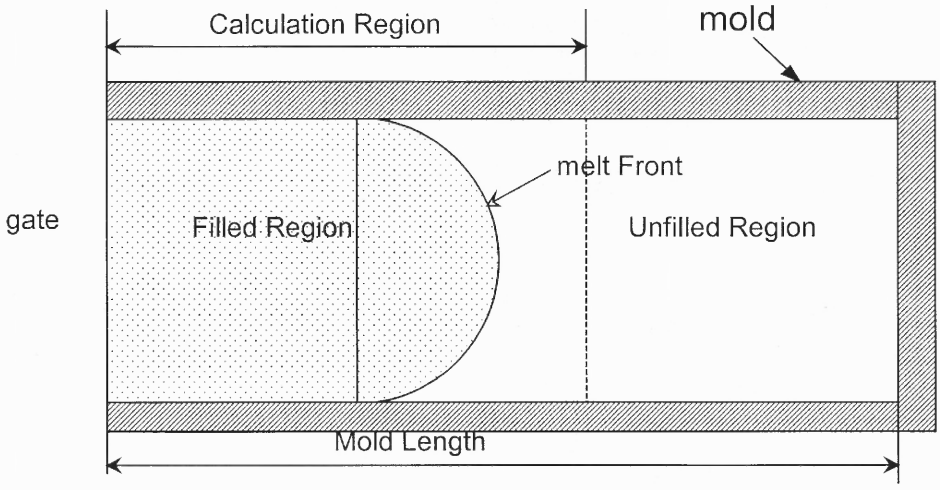

Figure 7.3 Computation region during the filling process

CHAPTER 8

SIMULATION RESULTS AND DISCUSSION

8.1 Simulation of Injection Molding of PET

PET is an engineering thermoplastic material that has been widely used in the production of fibers, beverage bottles, transparent films for many years. Recently, more interest has risen for the application of PET in engineering applications such as auto parts, gears and cams. PET has higher strength and service temperature than commodity plastics like PE and PP and it can compete with nylon and acetals in mechanical properties. PET may be amorphous or semicrystalline, the latter can reach about 50% crystallinity in the bulk material. Semicrystalline PET is a slow crystalline thermoplastic. The microstructure of injection molded semicrystalline PET parts can be significantly affected by the injection molding conditions. In this study, the injection molding of PET is simulated using the proposed method and crystallization model.

8.1.1 Parameters Used in the Simulation

The input data for the numerical simulation of injection molding process includes the rheological properties, thermal properties, and the constants involved in the kinetics of crystallization equations. For most plastic materials, the material properties are temperature dependent. To simplify the calculations, thermal conductivity K_h, material density ρ, and heat capacity C_p were assumed to be of the same values in the crystalline state and molten state. It is further assumed that K_h, ρ and C_p are constants that are independent of temperature.

The literature values of thermal conductivity K_h vary from 0.14 to 0.23 J/(s-m-K). In the work of Sridhar (1999), the experimental results showed an average of heat conduction for PET is of about 0.17 J/(s-m-K), and this value is used in the present simulations. The other important parameter is the thermal contact resistance (TCR) between the plastic material and mold wall. During the filling stage, the molten polymer melt enters the mold cavity with high speed and high pressure. The contact between the two surfaces is almost perfect because of the deformation of the molten or soft polymer material under high pressures. Hence the TCR at this stage is very small. However, in the post filling stage, the polymer material cools down and the pressure in the mold decreases rapidly. The TCR increases with the decrease of the cavity pressure. Furthermore, the shrinkage of the plastic material during the cooling causes a small gap between the material surface and mold wall. The gap increases with cooling time, and, therefore, the TCR becomes greater as the molding cools down. According to the simulation result of Sridhar (1999), the TCR during an injection molding cycle for the PET material is in the range of 10^{-5} - 10^{-3} m-K/W, with the former value occurring in the early stage of cooling, and the latter value at the end of cooling. In this study, an average value of TCR is used for the calculation for cooling stage. A very small or zero TCR is used for the simulation of filling stage. The effect of TCR on the crystallinity distribution was simulated to address the importance of selection of the appropriate value for TCR.

The parameters and material constants used in the simulation are listed below:

(a) Constants in the Cross-exponential rheological model (Narh et al.1995a):

$$B = 8.467 \times 10^{-5} \text{ Pa} \cdot \text{s}$$

$$T_b = 8574 \text{ K}$$

$$\tau^* = 4.903 \times 10^5 \text{ Pa}$$

$$\tilde{n} = 0.2193$$

(b) Parameters in the quiescent state crystallization kinetics (from Chapter 4):

$$\left(\frac{1}{t_{1/2}}\right)_0 = 4.25 \times 10^4 \text{ s}^{-1}$$

$$K_g = 3.66 \times 10^5 \text{ K}^2$$

(c) Parameters for induction time in quiescent state (Chan and Isayev, 1992):

$$t_m = 4.68 \times 10^{13} \text{ s} \cdot \text{K}^a$$

a=6.4

$$T_m^0 = 280 \text{ °C}$$

$$T_g = 73 \text{ °C}$$

(d) Thermal properties:

Heat capacity: $C_P = 1.8 \times 10^3$ J/Kg · K

Thermal conductivity: $K_h = 0.17$ J/s · m · K

Heat of fusion of 100% crystals: $C_c = 1.25 \times 10^5$ J/Kg

(e) Dimensions of mold cavity for simulation:

Length: L=20 cm, Thickness: H=3 mm, Width=1 cm

8.1.2 Crystallinity at the End of Filling Stage

During the filling stage, the polymer melt is injected into the mold cavity with high speed. The polymer melt experiences high shear stresses and pressure. The effect of the

shear stress on the crystallization kinetics can also be memorized by the melt and this memory will follow the polymer melt where it flows.

Figure 8.1 shows the induction time index distribution at the end of filling with different injection rates (Q) and mold temperatures (T_w). All other processing parameters were kept constant. The induction time index is a parameter used to determine the onset of the crystallization. When the accumulated induction time index reaches unit, it indicates that the crystallization begins. It can be seen for Fig 8.1 that in some areas in the mold cavity, especially near the wall area, the induction time index has reached unity. This means that in these areas, the crystallization has already begun before or at the time the mold cavity is filled. Near the entrance of the mold cavity, the crystallization area is thicker than the crystallization area at the end of the mold cavity. This phenomenon may be explained by the fountain flow during the injection stage: Near the entrance of the mold cavity, the polymer melt absorbs on to the cavity wall first, and a thin skin layer is formed at the early stage of the filling. In this area, the material has the longest residence time and experiences the longest thermal and shearing history. Away from the entrance, the polymer melt flows from the high temperature core area towards the wall area. Its residence time is shorter than that of the materials in the skin layers near the entrance of the mold cavity.

The effect of injection rate on the onset of crystallization in the filling stage is clear: Although higher injection speed generates higher shear rate and shear stress, the

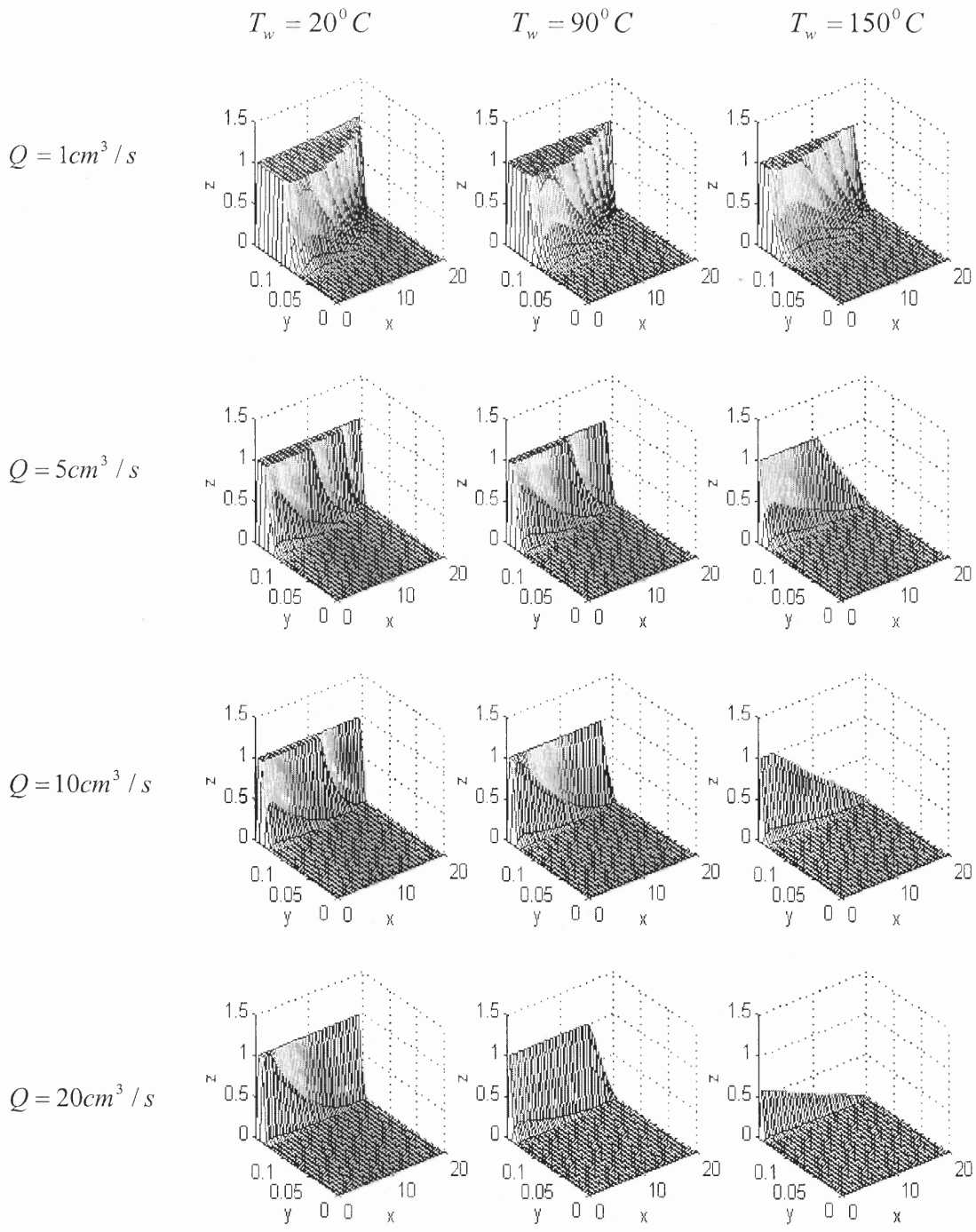

Figure 8.1 Induction time index distribution at the end of filling stage

filling stage is shorter and the residence time at the crystallization temperature is also decreased. The crystallizing area, thus, decreases with increasing injection rate and mold temperature.

Figure 8.2 shows the crystallinity distribution with the same conditions used in Figure 8.1. It can be seen that in some areas in the mold cavity, crystallization has already begun during the filling stage. However, there is no significant amount of crystallinity generated at the end of filling, either under high injection speed or low injection speed. At very low injection rate, the maximum crystallinity is about 1%, and this is in the skin layer near the entrance. The main reason for this is that PET is a very slow crystallizing plastic. Its crystallization rate is very slow at the early stage of crystallization. Because there is little amount of crystallinity generated in the filling stage, it is acceptable to neglect the effect of crystallinity on the viscosity of the melt for slow crystallizing plastics.

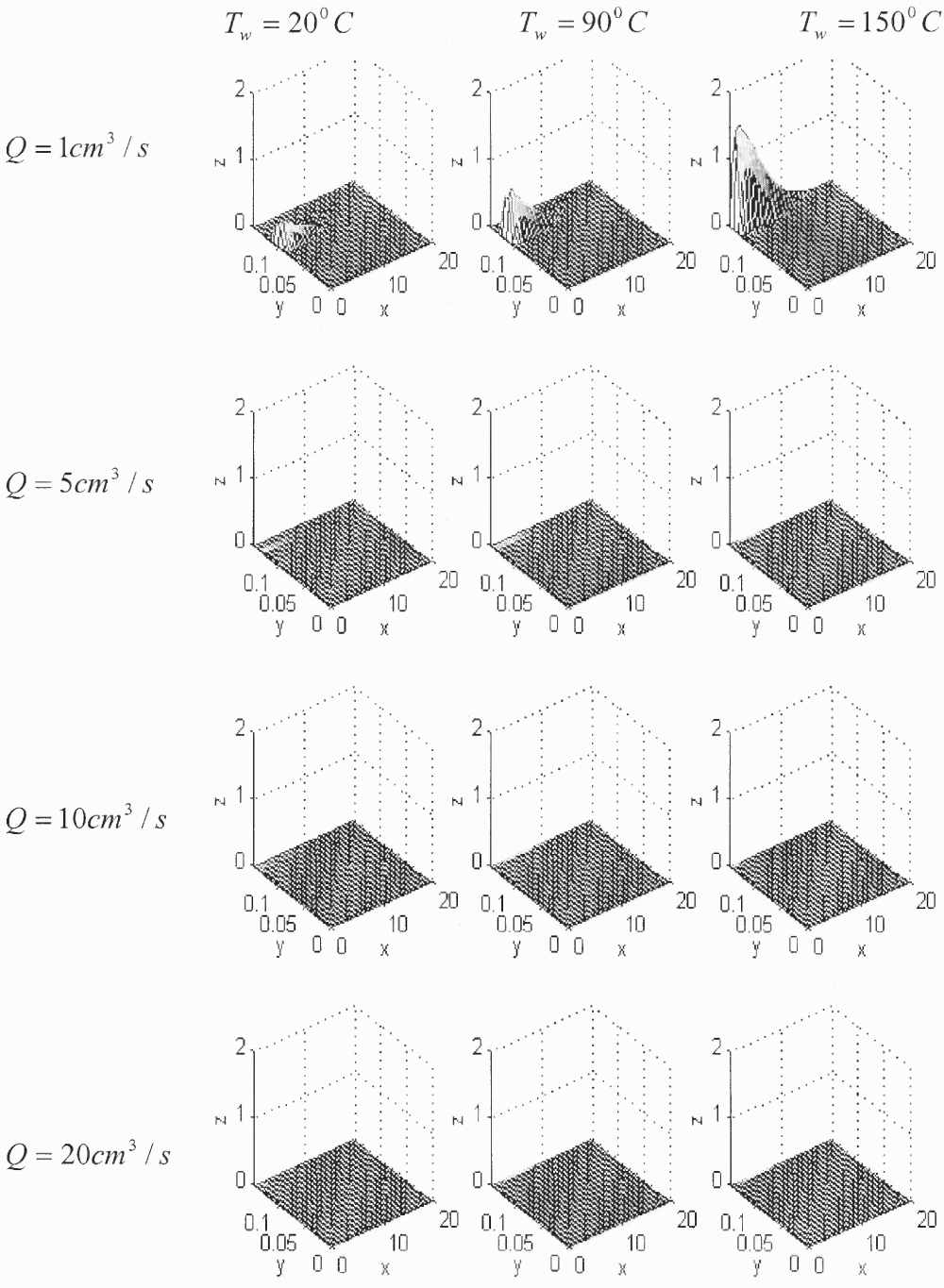

Figure 8.2 Crystallinity distribution at the end of filling stage with different injection rates

8.1.3 The Effect of Stress Relaxation on the Development of Crystallinity

During the cooling stage, the shear stress developed during the injection stage will decrease due to the molecular relaxation of the polymers. Since the relaxation behavior of polymer is not available in the wide temperature range, stress relaxation parameters in the stress relaxation model are selected by trial-and-error to show the effect of stress on crystallinity distribution in injection molded plastics. Figure 8.3 shows the results of four different stress relaxation models. In plot A, the stress relaxation was not considered. The result shows a wide range of stress induced crystallization. In plot B, it was assumed that the stress is completely relaxed once the mold is completely filled. The stress effect in the cooling stage was not considered. The result shows that no stress-induced crystallization occurs. In plot C, the stress was supposed to be completely relaxed if the material is still in the molten state once the mold cavity is filled. However, in the skin layer, no stress relaxation is considered. The result shows that in the skin layer away from the wall surface, there is a stress-induced crystallization layer. In plot D, a stress relaxation model was introduced in which following parameters are used in Eq. 6.15:

$$\lambda_0 = 10^5 \text{ seconds}, \; B_1 = 8.86^0 C, \; B_2 = 101.6^0 C \text{ and } T_s = T_g = 73^0 C$$

The above parameters were chosen in such a way that the stress in the molten material relaxes rapidly. B_1 and B_2 are the values for most amorphous polymers (Osswald, 1995). The results showed a stress-induced crystallization layer that is smaller than in plot C.

Figure 8.4 shows the effect of selection of stress relaxation parameters on the calculated crystallinity result. If too small value of λ_0 is used, as for example $\lambda_0 = 10^4$ seconds, the result shows no difference from quiescent state crystallization. However, if

too large value is used, the stress-induced crystallization area will extend from skin to the core area. For the present simulation of the injection molding process of semicrystalline plastics, the stress relaxation parameters are chosen in such a way that the stress effect is kept inside the skin layer. For PET, $\lambda_0 = 10^5 \sim 5 \times 10^5$.

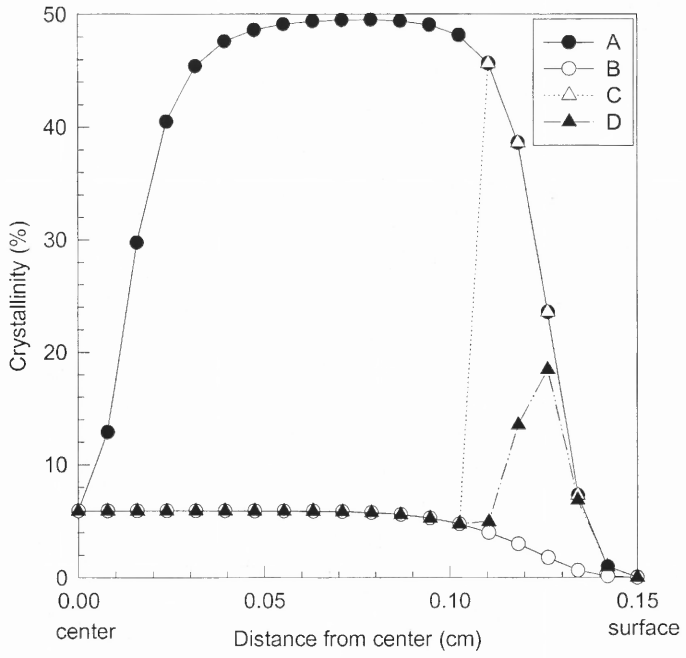

Figure 8.3 Comparison of different stress relaxation models:
A: No stress relaxation is considered; B: Stress effect is not considered in cooling stage;
C: Stress remains constant in the skin layer, but relaxed completely outside skin layer;
D: Stress relaxation follows the WFL model
Injection rate: Q=5 cm^3/s; Mold temperature: 90°C

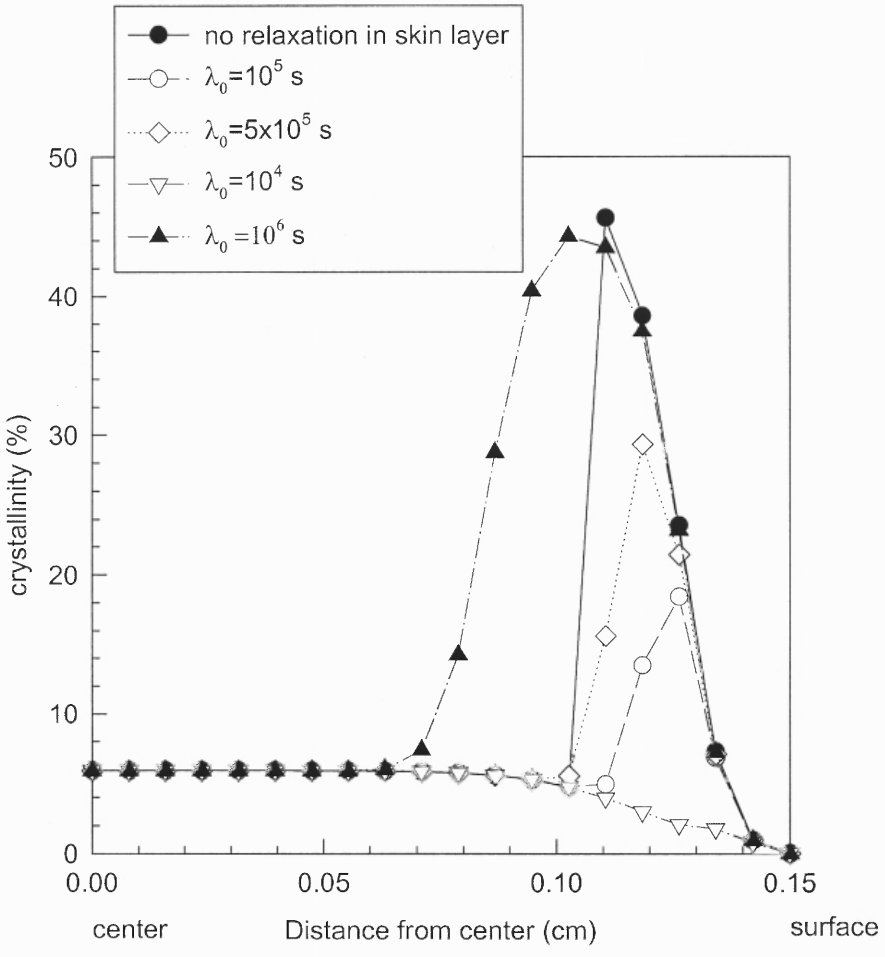

Figure 8.4 Comparison of different parameter selections for stress relaxation
Injection rate Q=5 cm^3 / s ; Mold temperature 90°C

8.1.4 Effect of Injection Speed

Injection speed is a very important processing parameter. High injection speed favors higher production rate and lower cost of the part. However, the properties of the injection molded plastic parts are strongly affected by the injection speed. Figure 8.5 shows the final crystallinity distribution across the thickness at the geometrical center of the moldings. At low injection speed, the prolonged shear time produces higher crystallinity near the surface region. Although high injection speed generates high shear stresses, the effect on the crystallinity is offset by the short injection time. Since the polymer melt has high temperature at the end of filling compared with the low injection speed, the shear stress relaxes faster under high injection speed than in low injection speed. The stress effect at high injection speed is not so pronounced compared with that at low injection speed.

Figure 8.6 shows the skin layer build-up at the end of filling stage with different injection speeds. The high heat convection in the flow direction at high injection speed prevents the formation of thick skin layer. Comparing Fig. 8.6 and Fig. 8.1, one can find that the crystallization areas in the mold cavity during the injection process are located inside the skin layer. Outside the skin layer, the polymer is in the molten stage and at a temperature higher than the crystallization temperature, and no crystal forms.

Figure 8.7 shows the pressure profile along the flow direction in the mold cavity at the end of filling for different injection speeds. High mold pressure corresponds to high injection speed. However, at extremely low injection speed, such as 0.5 cm^3/s, the pressure at the entrance of the mold is very high, exceeding the pressure for high injection speed. This is because a very thick skin layer forms due to the very low heat

convection at low injection rate. And the prolonged filling time causes the polymer melt to cool down and further increase the melt viscosity. The flow channel becomes so narrow that very high injection pressure is needed to fill the remaining region of the mold cavity. Once the pressure exceeds the maximum injection pressure of the injection molding machine, the mold cavity cannot be completely filled and short shot occurs. Since little amount of crystallinity is formed during the filling stage for very slow crystallizing plastics, such as PET, the injection pressure is not affected by the crystalline behavior of the plastics. Simulations to incorporate the effect of crystallinity on the flow behavior were carried out using the model proposed by Titomanlio et al. (1997). However, no difference was observed in the final result.

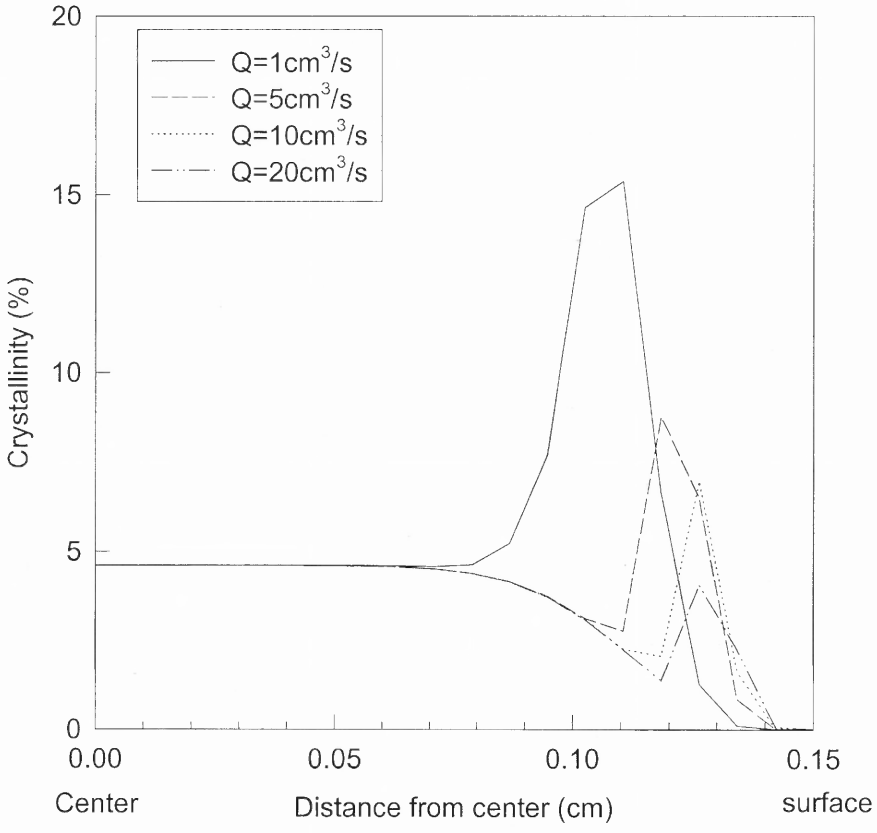

Figure 8.5 Effect of injection speed on the final crystallinity distribution across the part thickness
Material PET; Melt temperature 270°C; Mold temperature 90°C

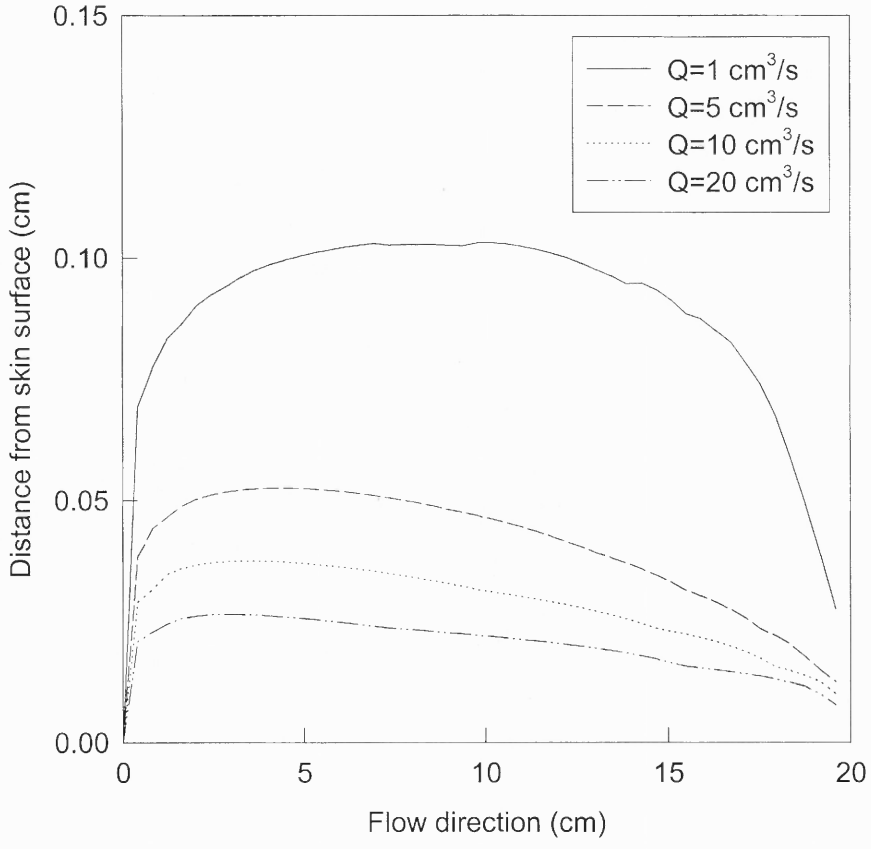

Figure 8.6 Skin layer thickness at the end of filling for different injection speed
PET: Melt temperature 270 °C; Mold temperature 90 °C

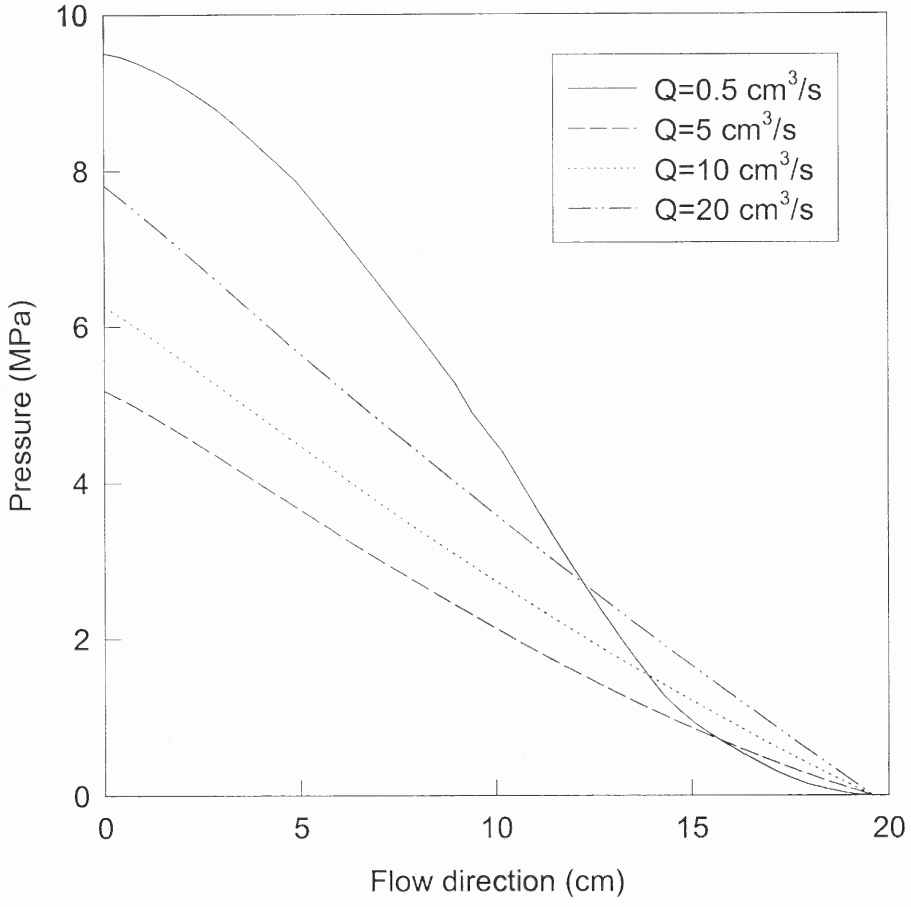

Figure 8.7 Cavity pressure at the end of filling for different injection speeds
Material: PET; Melt temperature 270 °C; Mold temperature 90 °C

8.1.5 Effect of Mold Temperature

The mold temperature is another very important processing parameter that determines the quality of the moldings, production rate and the morphology of the final part. In the slow crystallizing polymers, because their crystallization half times are of the same order of magnitude as the normal cooling times encountered in a typical injection molding process, they can exhibit unique structural gradients across the thickness direction and along the flow direction. Figure 8.8 shows the calculated crystallinity distribution results for different injection speeds after one minute holding time. Four different mold temperatures ranging from below glass transition temperature T_g, near T_g, and above T_g to crystallization temperature were used. Other parameters were kept constant.

At very low mold temperatures below the glass transition temperature T_g, the polymer melt in the mold cavity is subjected to a fast cooling and its temperature decreases so rapidly that no significant crystallinity forms in the final parts. In this case, a transparent amorphous or nearly amorphous part is obtained.

In the mold temperature range well above the glass transition temperature (for PET, T_g=73°C), there is generally a stress-induced crystallization layer, which has the highest degree of crystallinity across the thickness. In the core area, since the stress relaxes rapidly due to the high melt temperature at the end of filling stage, the crystallinity formed in this region is thermal dominated crystallization.

The degree of crystallinity in the moldings is very sensitive to the mold temperatures. Higher degree of crystallinity can be obtained with higher mold temperature. However, for a mold temperature as high as in the crystallization

temperature range, the thermal crystallization process is dominant and a uniformly crystallized part is obtained.

Figure 8.9 shows the skin layer build-up at the end of filling. Figure 8.10 shows the pressure distribution along the flow direction at the end of filling. As expected, low mold temperature causes thick skin layer and high injection pressure.

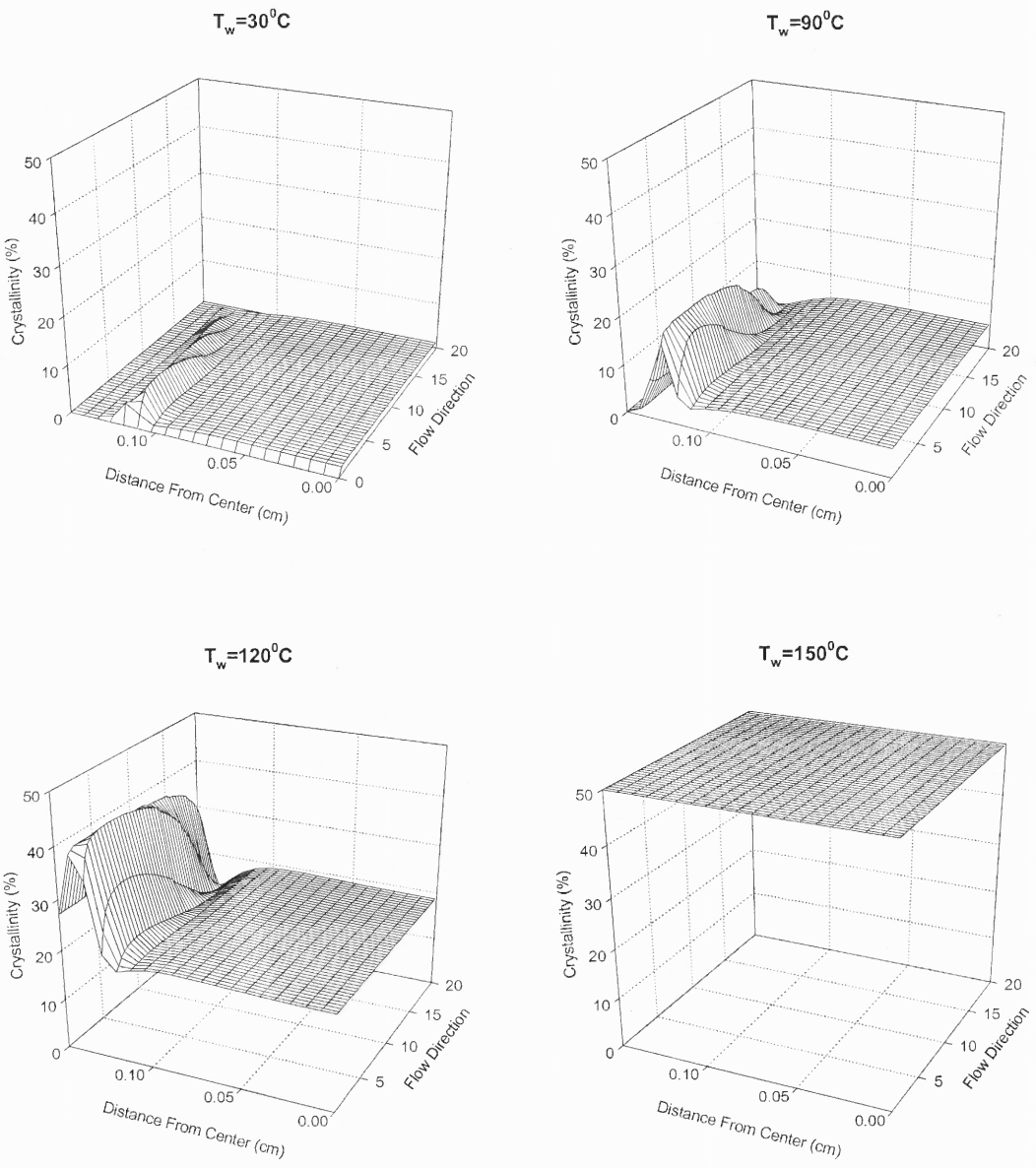

Figure 8.8 Effect of mold temperature on the final distribution of crystallinity
Material: PET; Injection rate: Q=5 cm^3 / s

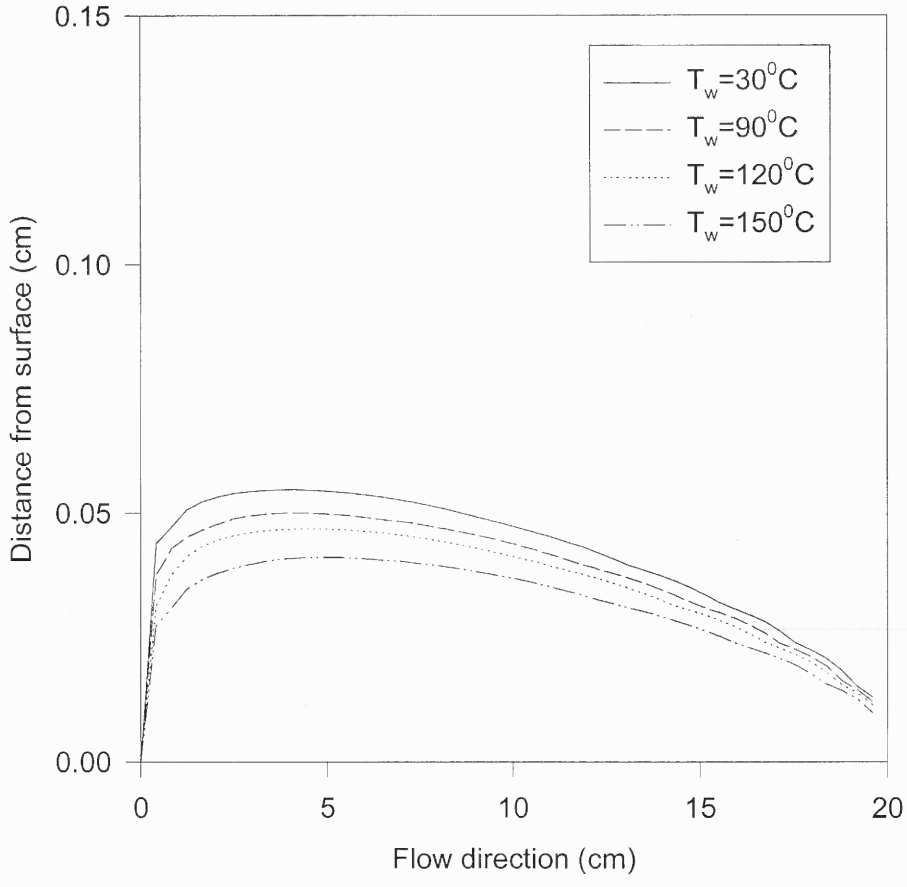

Figure 8.9 Effect of mold temperature on the build-up of skin layer at the end of filling stage
Material: PET; Injection rate: Q=5 cm^3 / s

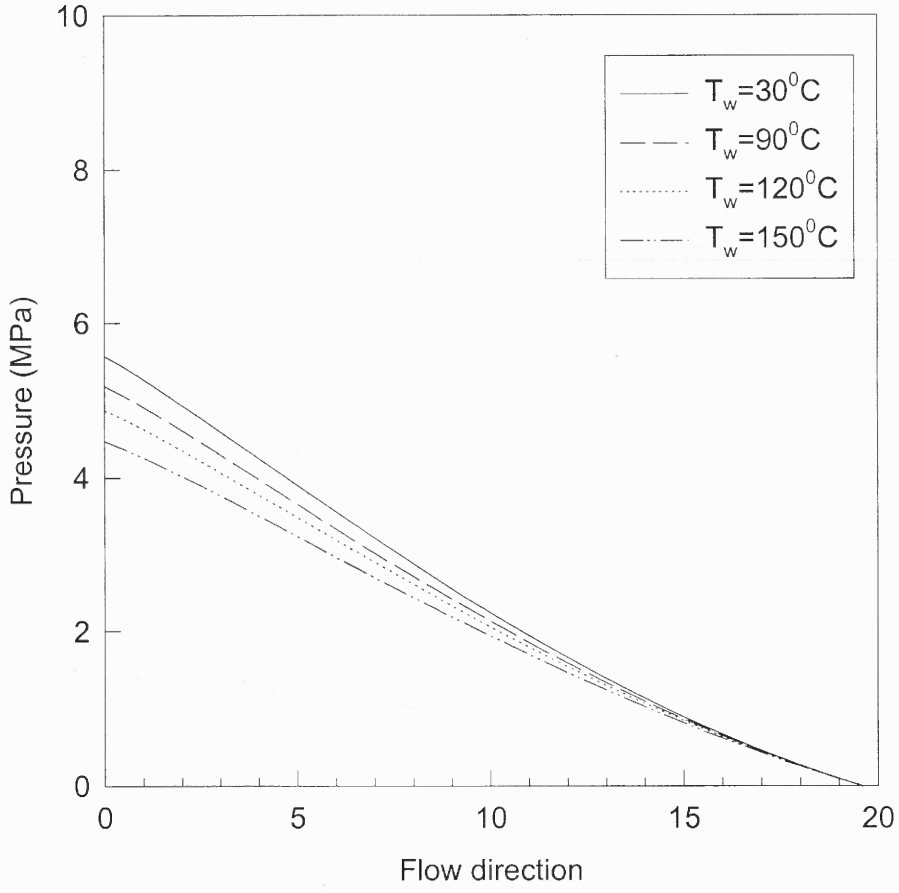

Figure 8.10 Pressure in the mold cavity under various mold temperature

Material: PET; Injection rate: Q=5 cm^3 / s

8.1.6 Effect of Holding Time

The holding time in the injection molding process is defined as the period between the end of filling and the ejection of the part from the mold. In general, longer holding time ensures dimensional stability, and low warpage of the final part. However, long holding time increases the production cycle time, and, therefore, reduces the production rate. The holding time is usually chosen in such a way that the molding's temperature is low enough to ensure that no further deformation happens after demolding. The demolding temperature is usually below the crystallization temperature. For this reason, if the other processing parameters are not changed, the prolonged holding time will not lead to further crystallization in the part.

The post filling is divided into two stages: the packing stage and cooling stage. In the packing stage, high pressure is maintained to pack in some melt to compensate for the contraction of the polymer when it cools down. The thermal contact resistance in the packing stage is very small due to the high pressure. However, in the cooling stage, the pressure is released and the contact between the skin of the molding and the mold wall becomes loose, and the thermal contact resistance (TCR) rises. The change of TCR from low to high can influence the temperature evolution in the cavity. Longer packing time ensures sufficient heat transfer from the melt to the cold mold, and short residence time at the crystallization temperatures. In this case, a lower degree of crystallinity part is obtained. Figure 8.11 shows the calculated results for different packing times with sufficient post filling times. A very small thermal contact resistance (10^{-5} $m^2 - K/W$) or a perfect contact between the polymer and the mold wall was used in the calculation. A

relatively large heat resistance value (10^{-3} $m^2 - K/W$) was used for the cooling stage. The result shows differences of crystallinity in the final part for various packing times.

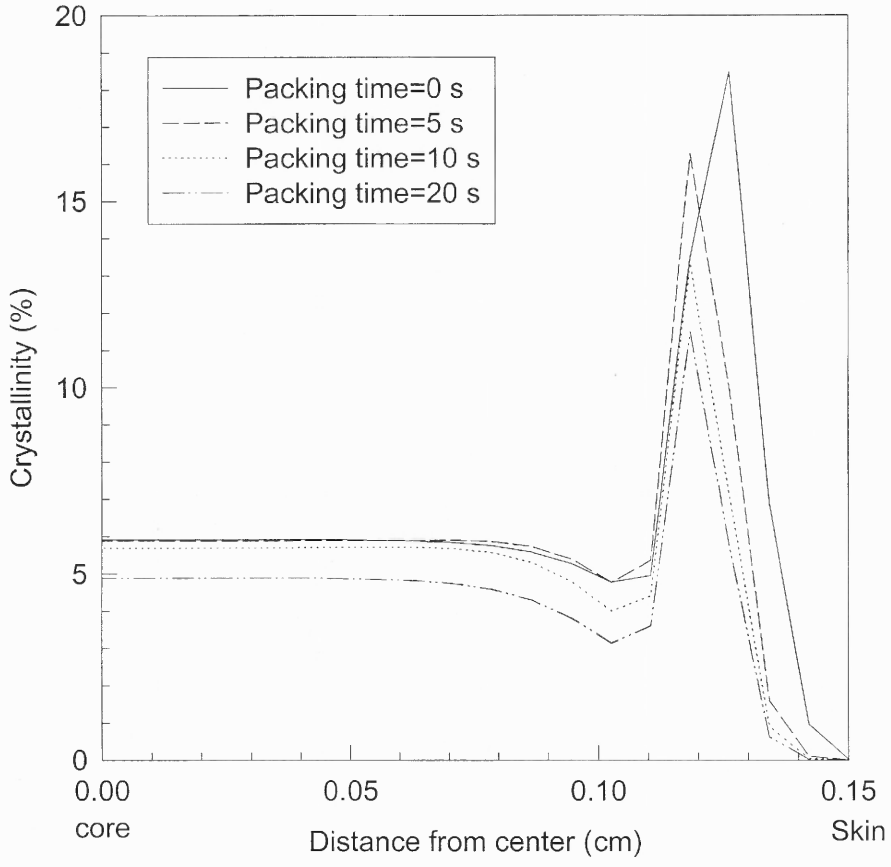

Figure 8. 11 Effect of packing time on the crystallinity distribution across the part thickness at geometrical center of the molding
Injection rate: 5 cm^3/s, Melt temperature: 270°C, Mold temperature: 90°C
TCR in packing stage: 1×10^{-5} $m^2 - K/W$; TCR in cooling stage: 1×10^{-3} $m^2 - K/W$

8.1.7 Effect of Melt Temperature

The injection temperature is the temperature at which the polymer melt is injected into the mold cavity. The melt temperature is usually in the range 30-40°C above the melting point of the polymer. The higher the melt temperature, the larger the shrinkage and warpage of the injection molded part. However, high melt temperature lowers the melt viscosity, and therefore increases the moldability of the polymer. Large and complex shaped moldings can be easily injection molded at high melt temperatures. The melt temperature also has some effect on the crystallinity in the final parts. Figure 8.12 shows the crystallinity distribution across the thickness for various melt temperatures. At high melt temperatures, since the polymer melt has high temperature at the end of filling, the shear stress relaxes rapidly and the stress induced crystallization is not so pronounced as in the case of low melt temperature. However, the simulation also showed that the melt temperature has no significant effect on the crystallinity in the core area.

Figure 8.13 shows the skin layer build-up at the end of filling for different melt temperature. As expected, the higher the melt temperature, the thinner the skin layer and the lower the injection pressure (Figure 8. 14)

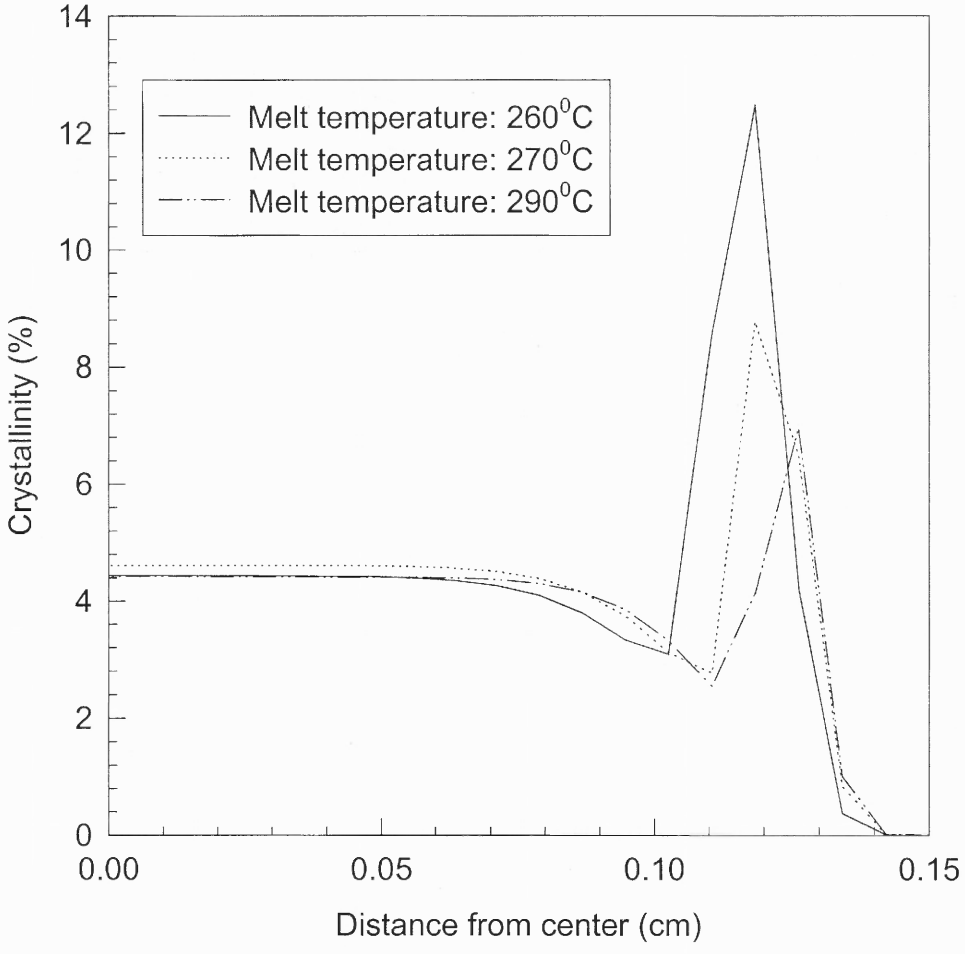

Figure 8.12 Effect of melt temperature on the final crystallinity distribution in the final part
Injection rate: $5\,cm^3/s$; Mold temperature: 90°C

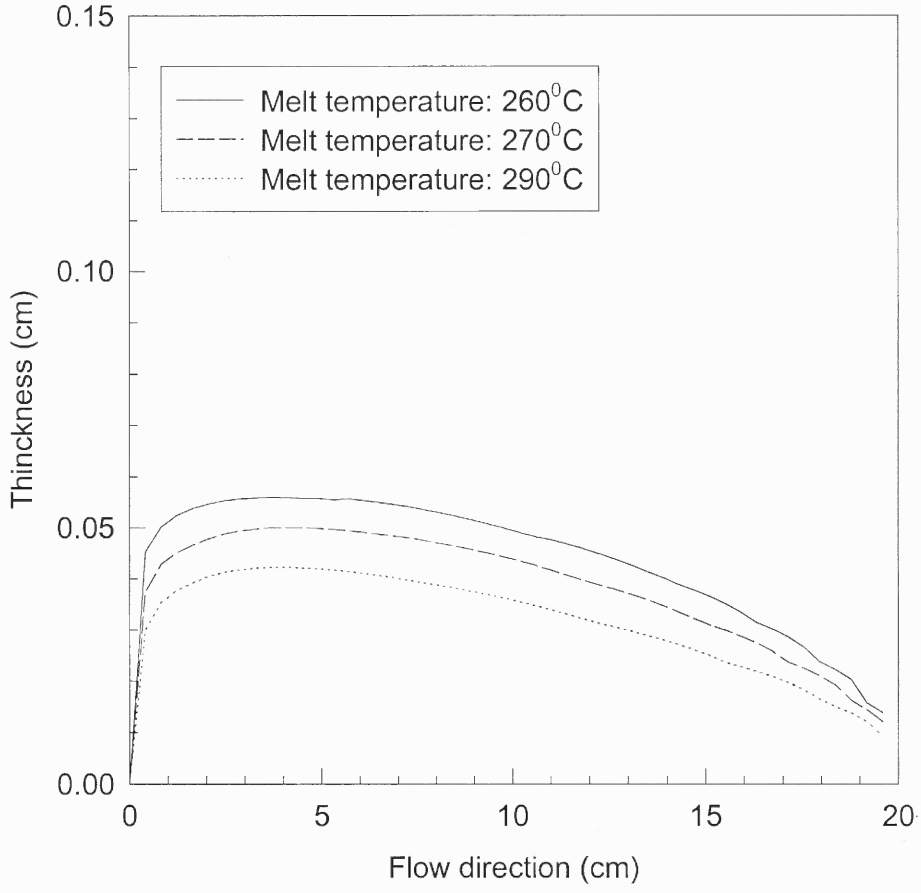

Figure 8. 13 Effect of melt temperature on the skin layer build-up at the end of filling

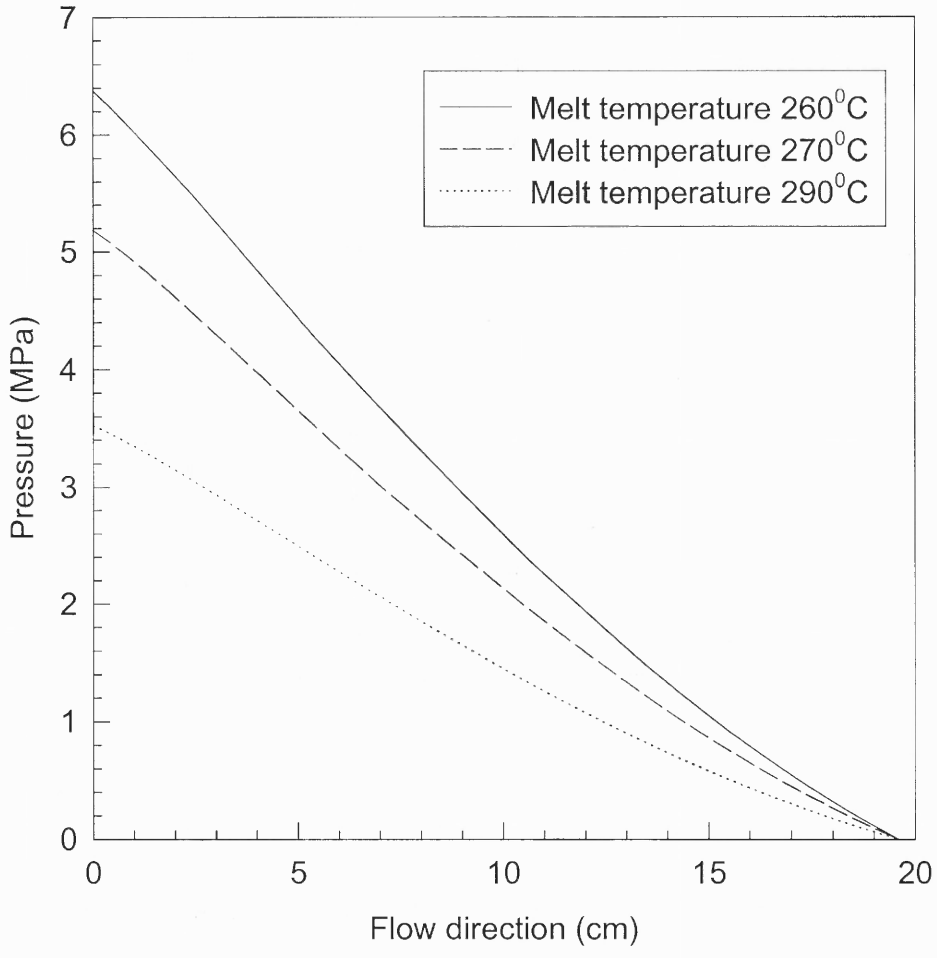

Figure 8. 14 Pressure in the mold cavity at different melt temperatures

8.1.8 The Effect of TCR

Thermal contact resistance (TCR) is the heat resistance between two contact surfaces. In the micro vision, the material surface can never be perfect and some gap or vacant areas exists between the contacted surfaces. This is the source of thermal resistance. In the injection molding process, the TCR between the polymer melt and the mold wall is not constant during the whole process. During the filling and the packing stage, high pressure forces the melt closely contact with the wall, TCR in this stage is very small. However, in the cooling stage, the interface gap between the molding and the mold wall increases as the material shrinks with its temperature cools down. The TCR is a few orders larger than the packing stage (Sridhar, 1999). The thermal resistance has significant effect on the temperature evolution inside the mold cavity and, therefore, has influence on the final crystallinity distribution. However, the thermal resistance is very difficult to measure, and TCR's evolution during the injection molding process is almost impossible to monitor. In this study, some different values are used in the simulation to show the sensitivity of the semicrystalline plastics to TCR. The selected values are in the range suggested by Sridhar (1999).

Figure 8.15 illustrates the effect of TCR on the final crystallinity distribution of the injection molded part in the thickness direction. Large TCR reduces the heat transfer rate from the material to the mold, and therefore, increases the material residence time in the crystallization range.

The result shows that TCR is a very important factor in the simulation of microstructure development in the injection molding parts. To accurately simulate the injection molding process, sufficient and reliable TCR information should be used.

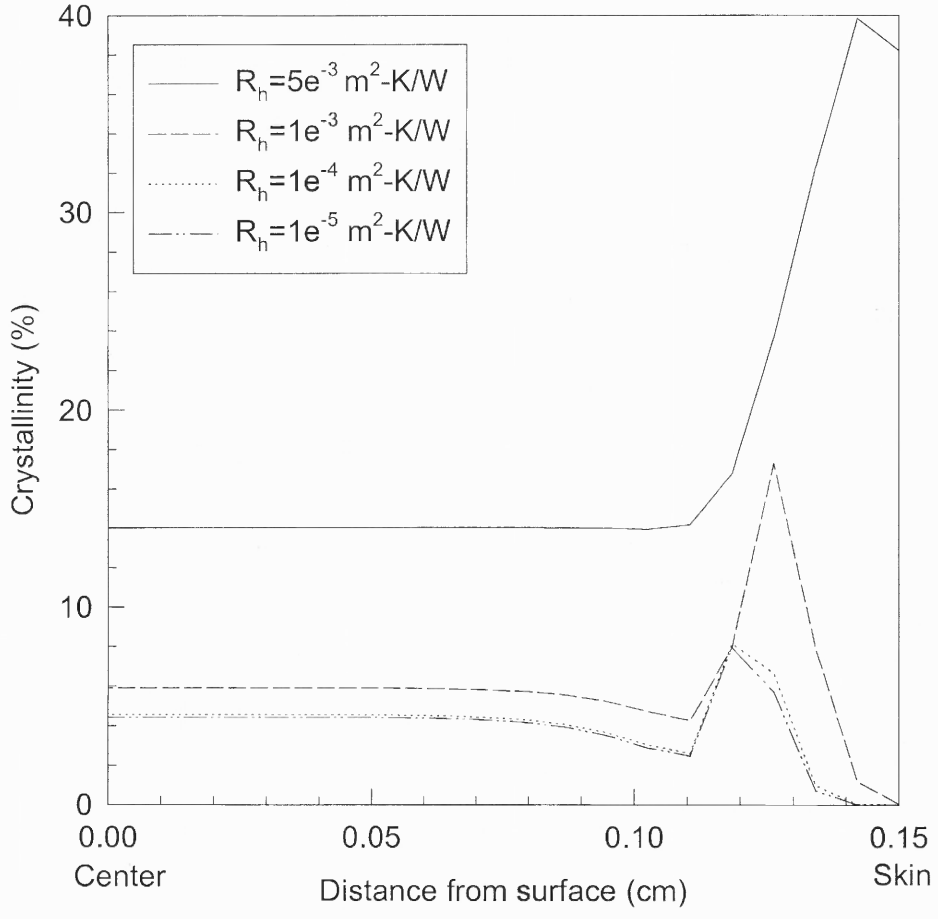

Figure 8.15 Effect of TCR on the crystallinity distribution
Injection rate: 5 cm^3 / s ; Melt temperature: 270°C; Mold temperature: 90°C

8.2 Simulation of Stress Induced Crystallization in Injection Molded Polypropylene

Polypropylene (PP) is a light-weight, moderately high melting temperature plastic that finds use in the manufacture of pipe, sheet, blown-molded containers and molded parts. It is stiffer, harder and of higher strength than many grades of polyethylene. It has excellent fatigue resistance, and it is often used for molded parts that contain an integral hinge. PP is a semicrystalline plastic that can reach about maximum of 50% crystallinity. PP is a fast crystallization plastic. Figure 8.16 shows a comparison of crystallization rate constants of PP (Titomanlio et al. 1997) and PET (Narh et al. 1995a) under quiescent state. The crystallization rate of PP is about ten times faster than that of the PET. The crystallinity of the injection molded PP parts is almost independent of processing conditions. For this reason, some previous simulation works on injection molding of PP did not consider the stress effect on the crystallization process of PP. As a result of its fast crystallization behavior, some crystals may form during the filling stage. The formed crystals may have significance effect on the viscosity of the melt, and hence influence the injection molding process. Titomanlio et al. (1997) considered the effect of crystallinity on the rheological behavior of PP for their simulations. In the packing stage, since considerable amount of crystallinity may form at this stage, the solidification of the melts may be significantly accelerated.

In this simulation, the focus was on the crystallization kinetics of PP in injection molding process.

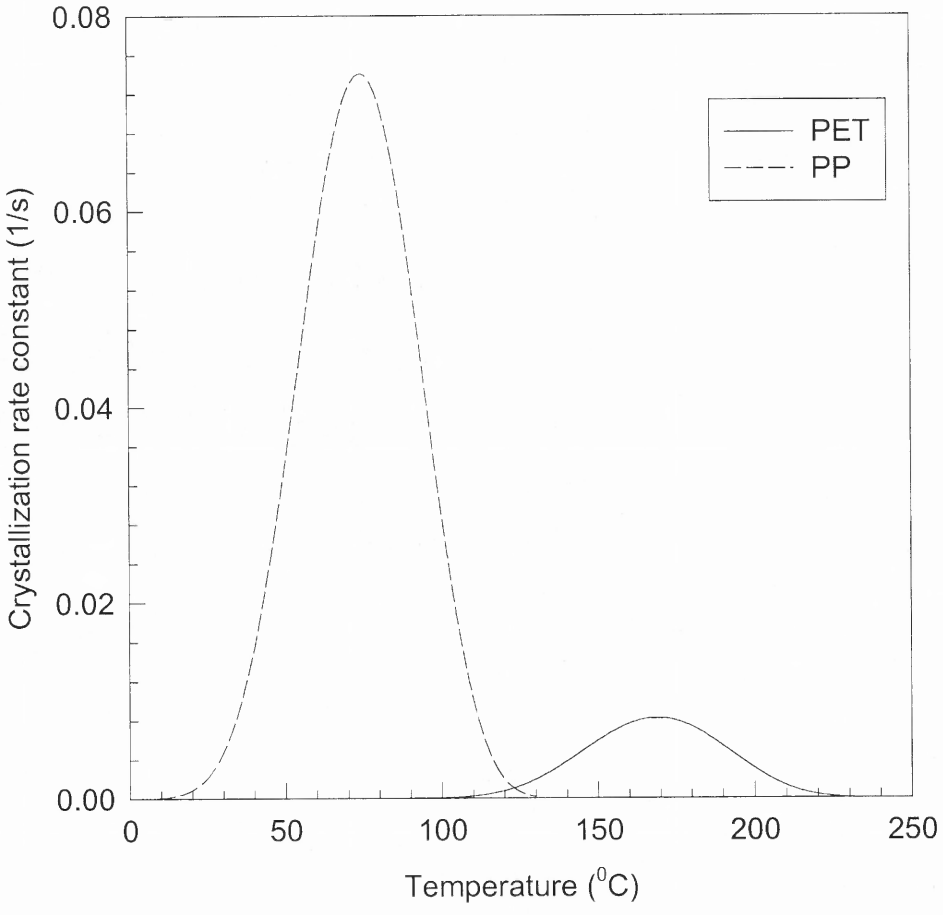

Figure 8.16 Comparison of crystallization rate of PP and PET

8.2.1 The Material Properties of PP

The material properties used in the simulation include the rheological and thermal properties required by the momentum and energy equations. The material constants for the rheological properties and quiescent state crystallization kinetics are chosen from literature (Isayev et al. 1995, Chan and Isayev 1992) and are listed as follows:

(a) Constants in the Cross-exponential rheology model:

$$B = 0.2\ \text{Pa}\cdot\text{s}$$

$$T_b = 5066.5\ \text{K}$$

$$\tau^* = 1.2\times10^4\ \text{Pa}$$

$$\tilde{n} = 0.34$$

(b) Parameters in the quiescent state crystallization kinetics:

$$\left(\frac{1}{t_{1/2}}\right)_0 = 2.07\times10^6\ \text{s}^{-1}$$

$$K_g = 2.99\times10^5\ \text{K}^2$$

(c) Parameters for induction time in quiescent state

$$t_m = 5.99\times10^{18}\ \text{s}\cdot\text{K}^a$$

$$a=10$$

$$T_m^0 = 172\ ^\circ\text{C}$$

$$T_g = -10\ ^\circ\text{C}$$

(d) Thermal properties

Thermal conductivity: $K_h = 0.193\ \text{W/m}\cdot\text{K}$

Specific heat capacity: $C_p = 2140\ \text{J/Kg}\cdot\text{K}$

Heat of fusion of 100% crystals: $C_c = 2.09 \times 10^5$ J/Kg

Density: $\rho = 920$ kg/m^3

(c) Parameters in the stress-induced crystallization kinetics

The constants in the stress-induced crystallization model are derived from the experimental results of Titomanlio et al. (1997) in Figure 1.9. The approximate induction times under different shear rates/shear stresses are listed in table 8.1

Table 8.1 Induction times and equilibrium melting point shifts of PP

Shear rate (1/s)	Viscosity (Pa.s)	Shear stress (Pa)	Induction time (s)	T_{shift} (°C)
0.6	16666	10000	320	5.38
0.3	18750	5625	500	3.536
0.1	25000	2500	800	1.675

The equilibrium melting point shifts are calculated from equation (4.22). The results are also listed in table 8.1. The relation of equilibrium temperature shift and the shear stress can be obtained by fitting the data in Table 8.1 to Eq. (4.20), and the resulting constants are: C_1=10 °C, C_2=5500 Pa. Figure 8.17 shows the equilibrium melting point shift with shear stress of PP. Figure 8.18 shows the effect of stress on the crystallization kinetics of PP.

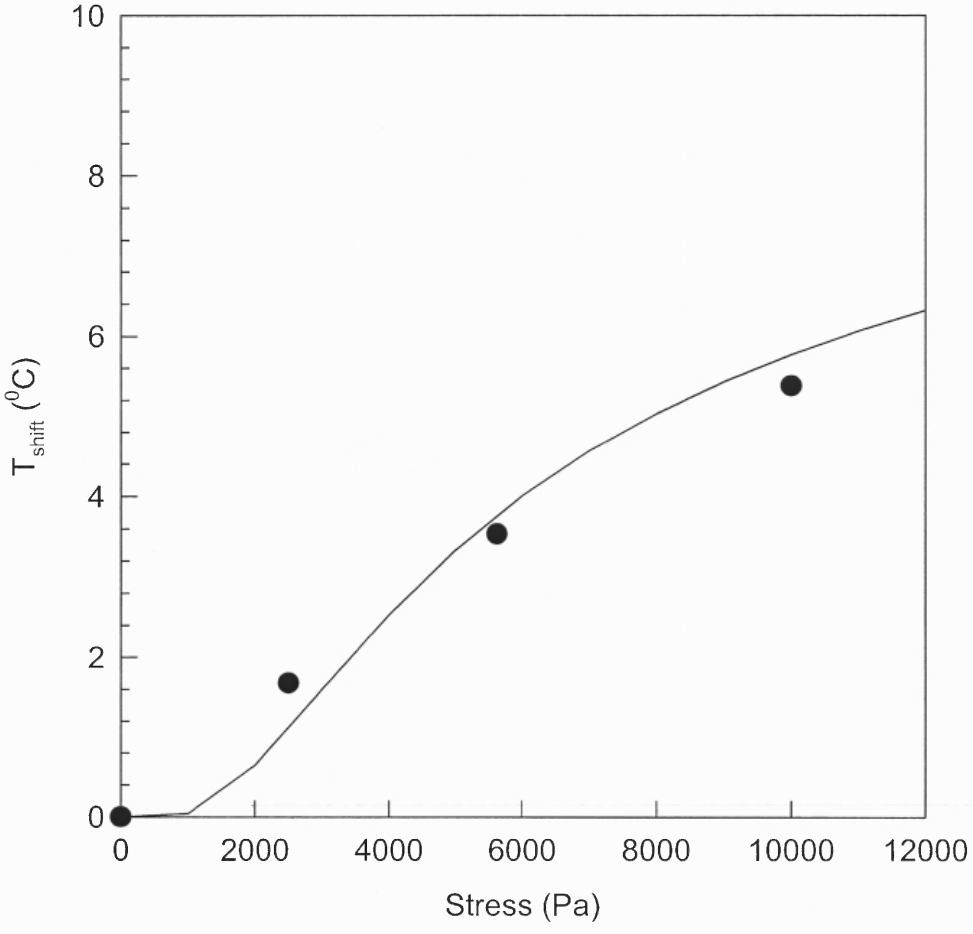

Figure 8.17 Equilibrium melting temperature shift for PP as a function of shear stress

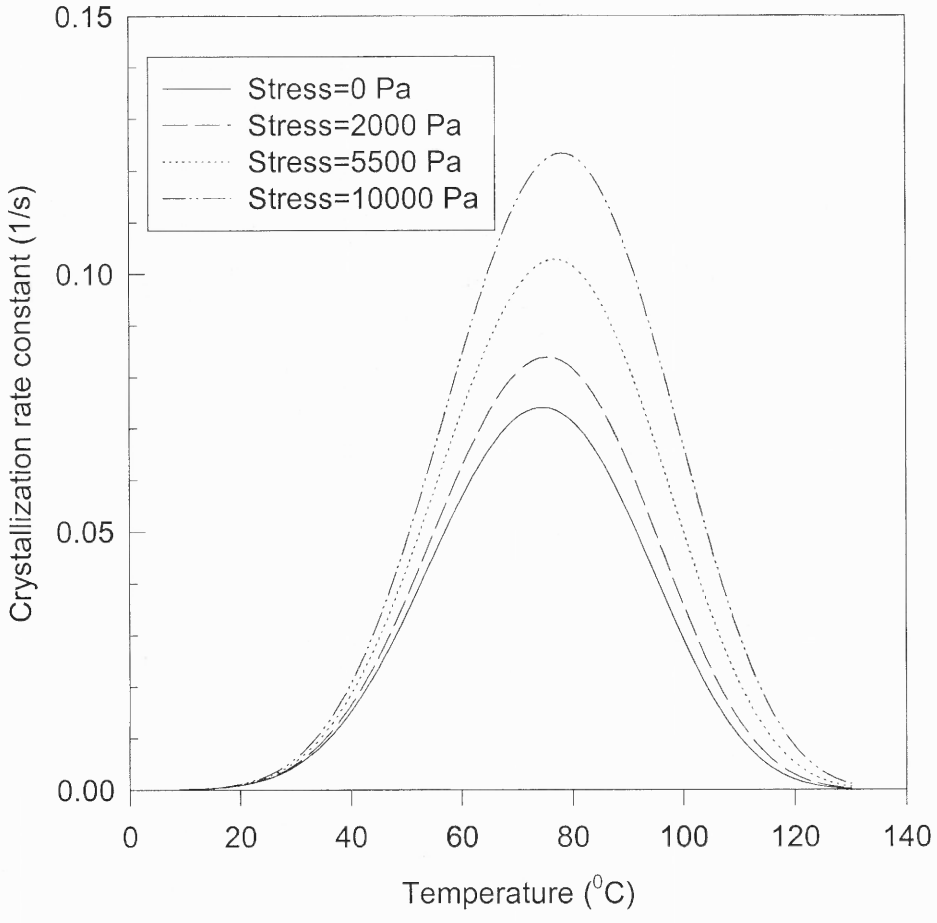

Figure 8.18 The effect of stress on the crystallization rate of iPP

8.2.2 Filling Stage

Figure 8.19 shows the induction time index distribution at the end of filling for iPP under various processing conditions. As we can see, the result is similar to that of PET described in previous sections. The crystallizing layer is thicker in low injection rate and low mold temperature, and thinner in high injection rate and high mold temperature.

Since iPP is a high crystallization rate plastic, there is considerable amount of crystallinity generated at the end of the filling stage for low injection rate and low mold temperatures (Fig. 8.20). As much as 5% crystallinity is formed near the entrance area. In this case, the crystallinity may have a significant effect on the filling stage. In the present simulation, these values are chosen from the work of Titomanlio et al. (1997), in which f=10000, h=1.5, m=0.4. These values give rise to an increase of viscosity by a factor of 2 when crystallinity is only about 1%. Calculations were carried out to account for the effect of crystallinity on the viscosity for the injection molding process. However, no significant influence was found in the final result. The reason is that the crystallizing areas are in the skin layer where the melt flow stops to form a solid layer. The rheological properties of the polymers in these areas have no influence on the main flow field in the mold cavity. However, they may affect the solidification process of the material, which is not considered in the present simulations.

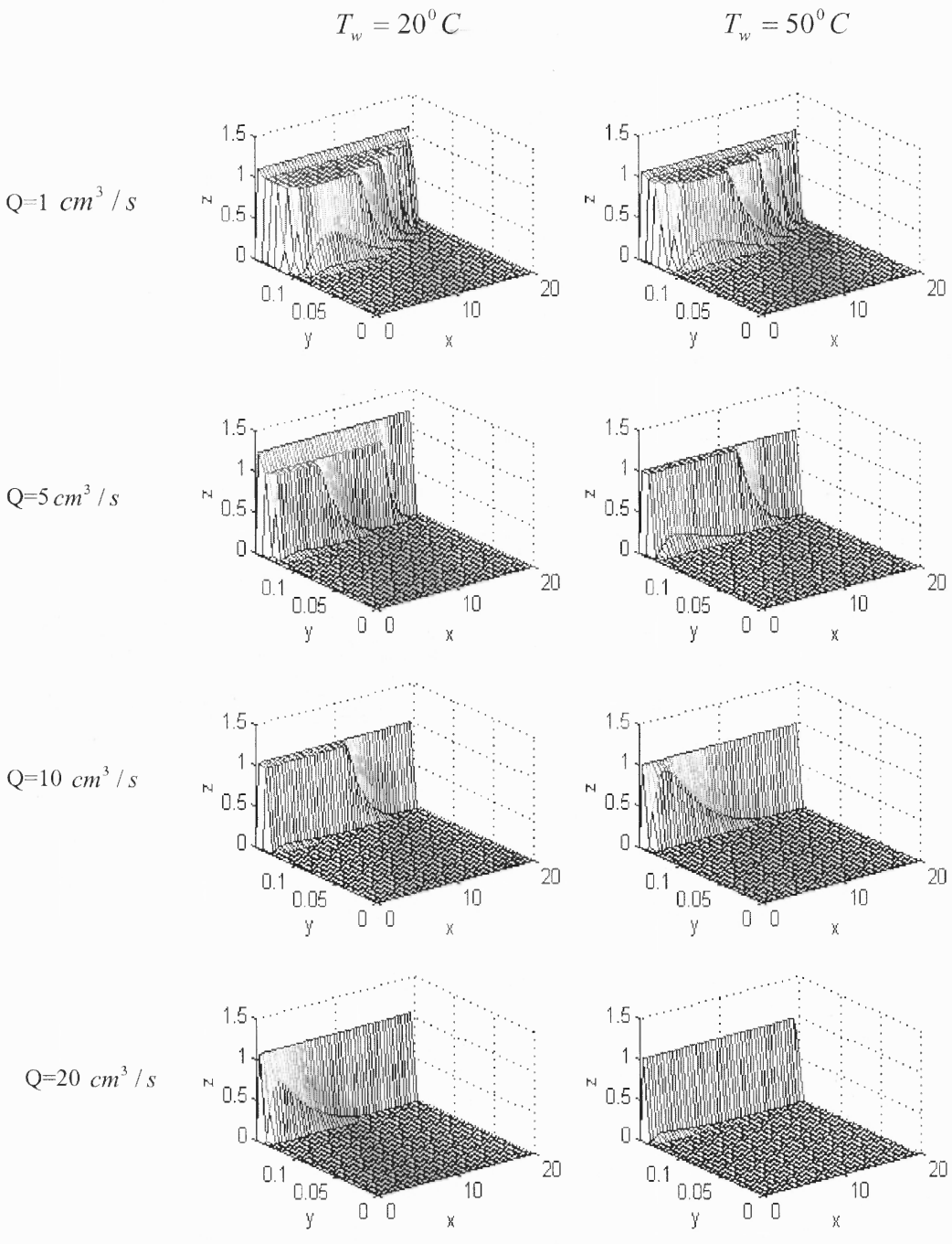

Figure 8.19 Induction time index at the end of filling stage
x--flow direction, y--distance to the center, z--induction time index

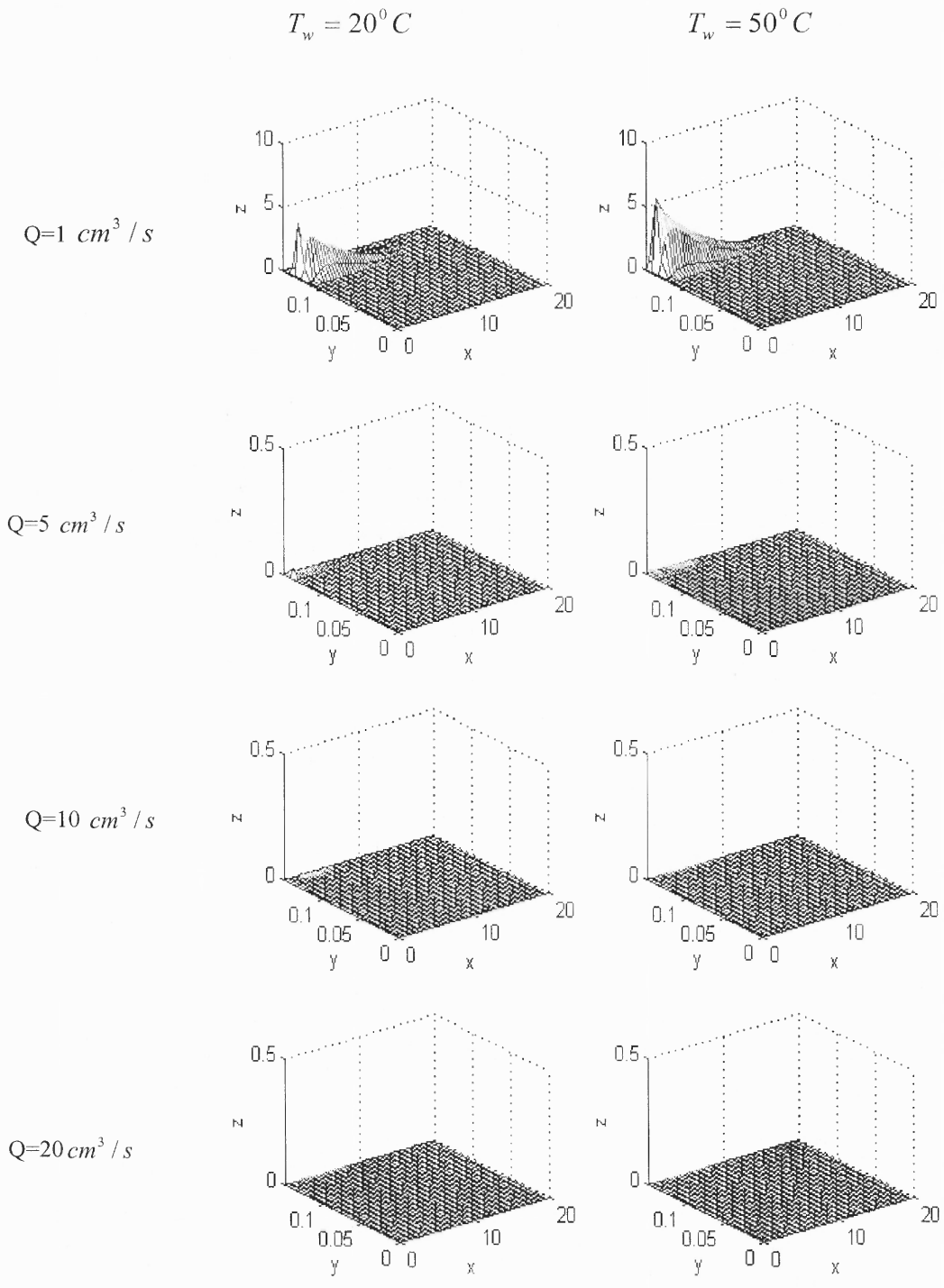

Figure 8.20 Crystallinity of iPP at the end of filling stage
x—flow direction, y—distance from the center, z—crystallinity (%)

8.2.3 Crystallinity in the Final iPP Part

Figure 8. 21 shows the final crystallinity distribution under various processing conditions. The following conclusions can be drawn from the simulation results:

(1) At low injection speed and low mold temperatures, there is a layer between the skin and core layers, where the crystallinity is the highest across the thickness. This layer can be attributed to the stress induced crystallization.

(2) At high injection speed, there is no clear difference between the crystallinity layers across the thickness. The high shear stress during the injection period relaxes rapidly because of the high melt temperature at the end of filling.

(3) At high mold temperatures, a uniformly crystallized part is obtained. Thermal crystallization plays a dominant role, and stress-induced crystallization only serves as the accelerating factor of the crystallization processes.

(4) For a fast crystallizing material, it is almost impossible to obtain an amorphous product. Even at very low mold temperatures, iPP can reach as high as 20% crystallinity in the final part.

(5) In the core region, crystallinity is thermally generated. The injection rate has no effect on the crystallinity in the core region.

(6) Mold temperature is the most important parameter on the degree of crystallinity in the molded iPP part.

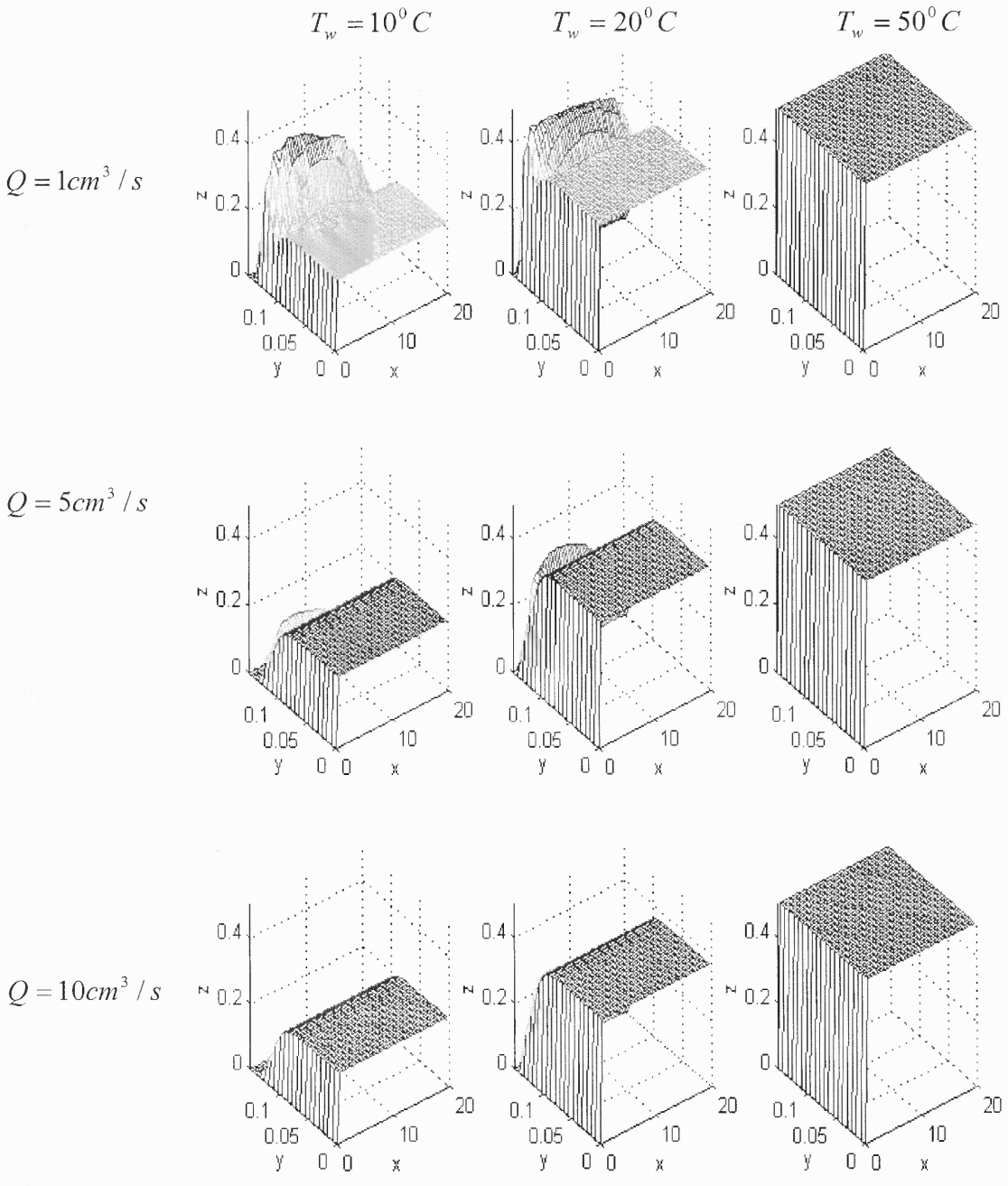

Figure 8. 21 Final crystallinity of injection molded PP at different processing conditions x-flow direction, y-distance from center; z-crystallinity

8.2.4 Crystallization Evolution during the Injection Molding Process of iPP

Since iPP is a fast crystallization thermoplastic, once the crystallization process starts, it takes a very short time for it to reach its ultimate crystallinity if the condition permits. It is generally impossible to get totally amorphous parts from fast crystallization plastics such as iPP. The crystallinity evolution in the injection molding process of PP has been simulated in the present studies. Figure 8.22 shows the predicted crystallinity profile in the thickness direction as a function of time at the geometrical center of the mold cavity. The effect of stress on the crystallization was included in Fig. 8. 22. Figure 8.23 shows the crystallinity evolution without considering the effect of stress. In both cases, the crystallization process near the wall surface is much faster than that in the core region, since the material near the wall area reaches crystallization temperature earlier than the material in the core area. The presence of shear stress only accelerates the crystallization process near the wall area, where the stress can not relax immediately. The core area is the last to complete the crystallization process. Although the crystallization process across the thickness is much different at different positions, the final crystallinity along the thickness does not vary significantly for fast crystallization plastics at ordinary processing conditions. It is seen that after sufficient time, the part becomes a uniform crystalline part. It can be concluded that for fast crystallization plastics, the stress only influences the initial crystallization process, and, it has no significant effect on the final crystallization distribution.

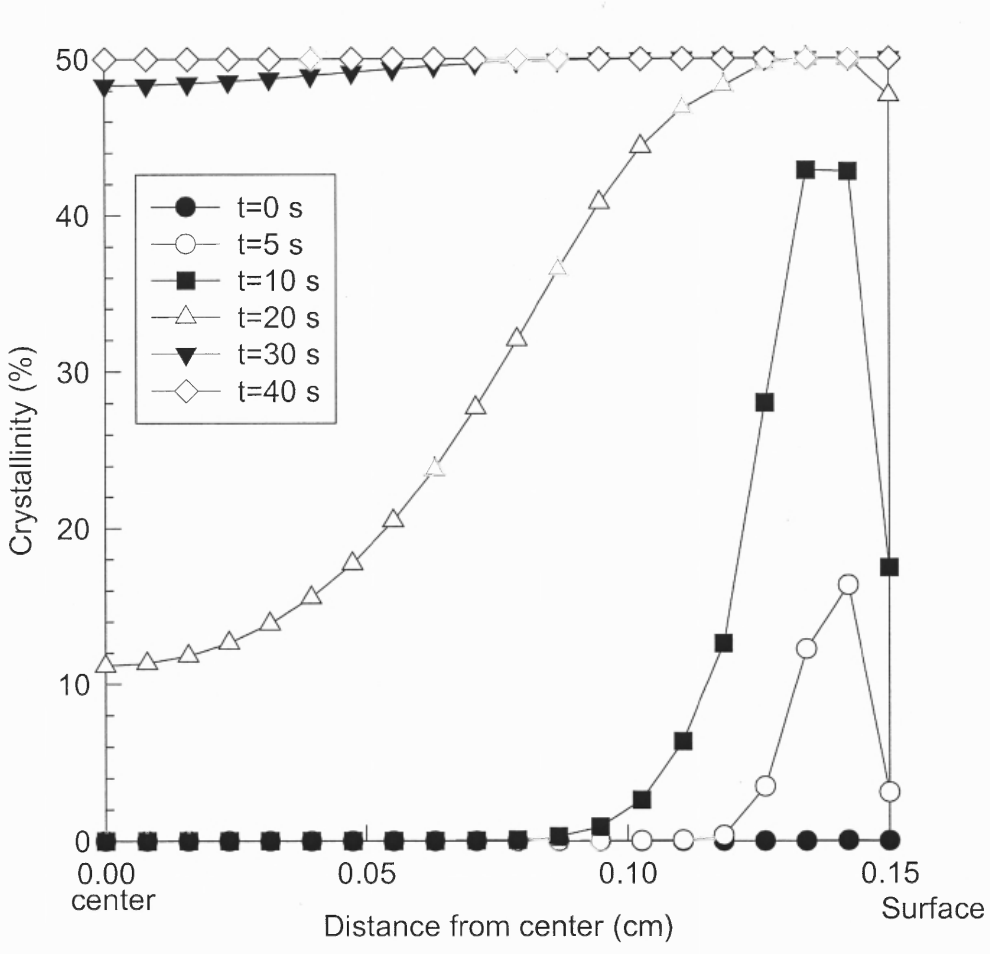

Figure 8.22 Crystallinity evolution during the post filling stage with the consideration of shear stress

Injection rate Q=5 cm^3/s ; Mold temperature T=50°C

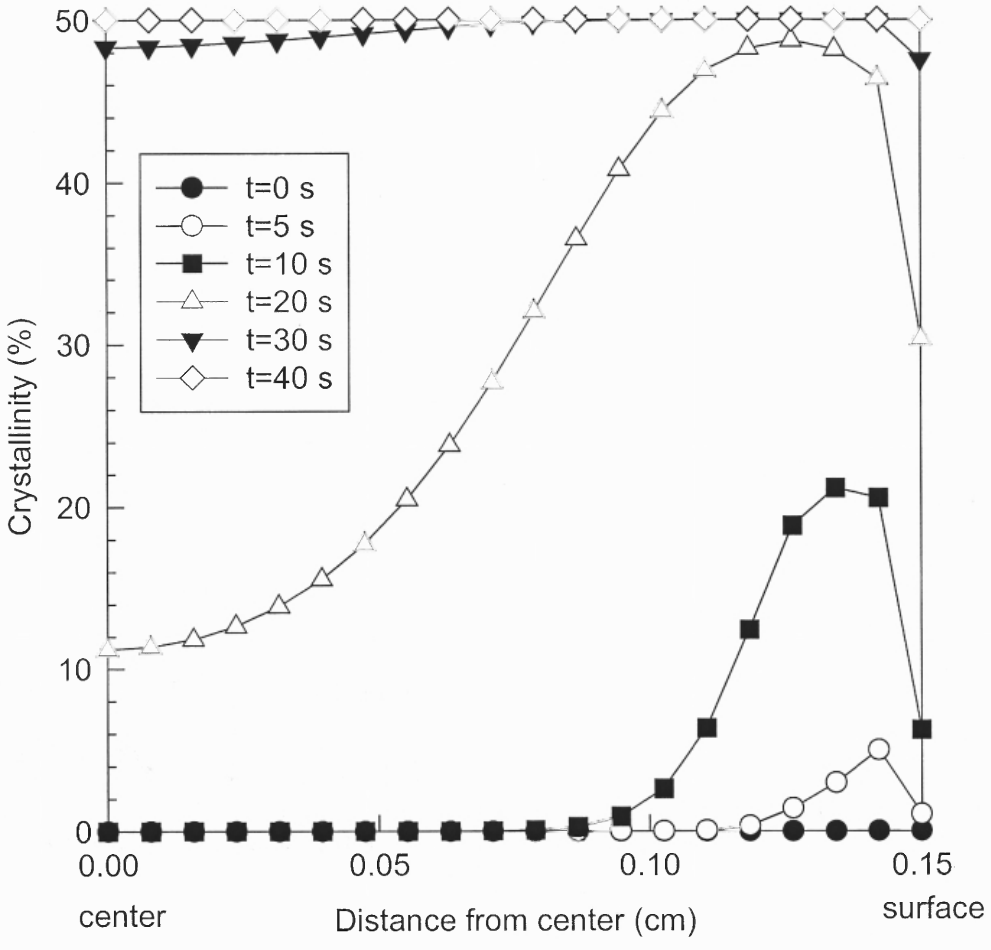

Figure 8.23 Crystallinity evolution in the post-filling stage without considering the effect of shear stress
Injection rate Q=5 cm^3 / s ; Mold temperature 50°C

CHAPTER 9

CONCLUSIONS AND FUTURE WORK

9.1 Conclusions

A stress-induced crystallization model was developed to predict the crystallization behavior of semicrystalline thermoplastics. The model is based on the theory that shear stresses related to shear flow cause chain or molecular orientation in the polymer melt. The entropy of the polymer melt flow in shear is decreased in the oriented state, and as a result, the melting point of the polymer shifts to high temperatures. The shifted melting point under stressed state increases the supercooling which is the driving force for crystallization. The model predicts that the crystallization rate increases with the increase of shear stress; the temperature at which the polymer crystallizes at its highest rate shifts to higher temperatures with the effect of shear stress; the crystallization temperatures are also broadened. Because it was assumed that the effect of shear stress on the kinetics of crystallization is only by increasing the supercooling, the basic equation of quiescent state crystallization does not change, and can be directly applied to model stress-induced crystallization by simply shifting the equilibrium melting point to higher temperatures. A previously developed relationship between the temperature shift and the shear stress was used in the model. The equilibrium melting point shift can be determined by simple experiment such as rotational plate rheometric measurements. The sudden increase in the stress-time plot can be interpreted as the induction time under stressed state.

The model developed and utilized does not consider the entropy reduction due to extensional flow orientations, due to lack of experimental evidence. Thus the fountain effect on the crystallization kinetics is neglected. The model can qualitatively, at least, describe the

stress-induced crystallization process in polymers. The quantitative model that can predict the stress induced crystallization behavior of the polymers may be obtained by assuming that other parameters involved in the quiescent state model have functional relationship with stress.

The model was used to predict the crystallinity distribution in the injection molded semicrystalline plastics with the consideration of shear stress relaxation. The results reproduced most of the features that were obtained by experiment in the literature (Hsiung, 1993). In general, a three-layer microstructure across the thickness can be obtained with low injection rate and moderate mold temperatures: a thin amorphous skin layer, a stress-induced crystallization layer which has the highest crystallinity, and a core layer, either amorphous or with thermally induced crystallinity. For slow-crystallizing thermoplastics such as PET, a completely amorphous part can be obtained at high injection rates and low mold temperatures. However, for fast crystallization plastics such as iPP, it is very difficult to get a completely amorphous part. The simulation results showed that at high mold temperatures, e. g., in the range of crystallization temperature, the crystallization process in injection molding was mainly thermal crystallization. In this case, other processing parameters, such as injection rate, melt temperature, have little effect on the final crystallinity distribution.

The simulation results on the filling stage, showed that at the end of filling stage, in some areas, mainly near the wall, the crystallization process has already started before the mold is filled. At low injection rate and low mold temperatures, the amount of crystallinity formed in slow crystallizing plastics such as PET can reach 1%. For fast crystallization plastics such as PP, the crystallinity at the end of the filling stage can reach as high as 5%. The effect of crystallinity on the viscosity of the plastic melt was considered using the model

proposed by Titomanlio (1997). However, no significant effect was observed in the final results. The main reason for this is that the crystallized area is located in skin layer, where the melt becomes solidified.

The simulation results also showed that the crystallinity of injection molded semicrystalline plastics is very sensitive to the thermal contact resistance (TCR) between the plastics and mold wall. Higher TCR increases the residence time in the crystallization temperature resulting in high crystallinity in the part. Consequently, it is very important that the actual value of TCR is determined in order to obtain accurate simulation results for injection molding of semicrystalline plastics.

The melt temperature showed little effect on the crystallinity distribution. However, a high melt temperature lowers the viscosity of the melt and reduces the formation of skin layer. This requires low injection pressure to fill the mold. Complex shaped and thin wall parts can be easily injection molded with high melt temperatures.

The formation of skin layer was also simulated under different processing conditions. The skin layer thickness decreases with the increase of injection rate and mold temperature. The injection pressure increases with the increase of injection rate. However, at very low injection rate and low mold temperature, the injection pressure may be higher than in the high injection rate because of the increased thickness of skin layer. Eventually, the injection pressure may exceed the available injection pressure from the hydraulic system leading to short shot.

The crystallization process of iPP in the cooling stage was simulated with and without consideration of the effect of stress. The results showed that the shear stress only influences the progress of crystallization, but no significant effect was obtained on the final crystallinity.

9.2 Recommended Future Work

The proposed stress-induced crystallization model was based on the equilibrium melting point shift assumption. Although it can predict most of the behaviors of stress-induced crystallization, experimental work needs to be carried out to validate the model. An accurate model may be obtained by assuming that the parameters in the quiescent state model (Hoffman, 1964) are also functions of shear stress. Therefore, more experimental work needs to be conducted to get the relationship between the parameters and the shear stress. Future work should also include the following:

1. Extensive experimental study on the crystallinity distribution in the injection molded semicrystalline plastic parts.
2. Study on the relaxation behavior of plastics at elevated temperature near their melting point. Stress relaxation in the cooling stage has major influence on the crystallinity distribution. Accurate model of stress relaxation will result in accurate simulation of injection molding of semicrystalline plastics.
3. Investigation of TCR evolution in the cooling stage. Since the crystallinity is sensitive to TCR, accurate information on TCR in the injection molding process is very important.
4. Investigation of boundary conditions in the triple point as well as in the melt wall contact area. The simulation showed that the boundary conditions at the triple point should be free to slip. However, the length of slippage has influence on the shape of front curve. The non-slip boundary condition in the melt contact area is also not realistic since it causes the skin layer in the gate area to be the thickest in the flow direction.

APPENDIX A

TAYLOR-GALERKIN METHOD FOR THE HYPERBOLIC EQUATIONS

In this section the finite element equations were formulated for both the pure advection (pseudo-concentration) and the advection-diffusion (energy equation, induction time and crystallinity distribution equations), using the Talor-Galerkin method of Donea and the Zienkiewicz and coworkers.

The pseudo-concentration equation is a hyperbolic or pure advection equation. If the pseudo-concentration function is advected using conventional Galerkin finite element method, severe oscillations are generated. This can be improved by applying the Taylor-Galerkin method.

For the incompressible or divergence free ($\nabla \cdot \mathbf{v} = 0$), Eq. (5.1) can be rewritten:

$$\mathbf{F}' + (\mathbf{v} \cdot \nabla)\mathbf{F} = 0 \tag{A.1}$$

Using a forward time Taylor series, we can write:

$$\frac{\mathbf{F}_{n+1} - \mathbf{F}_n}{\Delta t} = \mathbf{F}'_n + \frac{\Delta t}{2}\mathbf{F}''_n + O(\Delta t)^2 \tag{A.2}$$

From equation (A.1) we have:

$$\mathbf{F}'_n = -(\mathbf{v}_n \cdot \nabla)\mathbf{F} \tag{A.3}$$

Differentiating (A.3) to the second order, we have:

$$\mathbf{F}_n'' = -(\mathbf{v}_n \cdot \nabla)\mathbf{F}_n' - (\mathbf{v}_n' \cdot \nabla)\mathbf{F}$$

$$= (\mathbf{v}_n \cdot \nabla)(\mathbf{v}_n \cdot \nabla)\mathbf{F}_n - (\mathbf{v}_n' \cdot \nabla)\mathbf{F}_n \qquad \text{(A.4)}$$

Substituting equations (A.3) and (A.4) into equation (A.2), we obtain the final temporally discretized form as

$$\frac{\mathbf{F}_{n+1} - \mathbf{F}_n}{\Delta t} = \left[-(\mathbf{v}_n \cdot \nabla) - \frac{\Delta t}{2}(\mathbf{v}_n' \cdot \nabla) + \frac{\Delta t}{2}(\mathbf{v}_n \cdot \nabla)^2 \right]\mathbf{F}_n \qquad \text{(A.5)}$$

Equation (A.5) can be simplified approximating v_n as $(v_{n+1} - v_n)/\Delta t$, which gives:

$$\frac{\mathbf{F}_{n+1} - \mathbf{F}_n}{\Delta t} = \left[-\left(\mathbf{v}_{n+\frac{1}{2}} \cdot \nabla \right) + \frac{\Delta t}{2}(\mathbf{v}_n \cdot \nabla)^2 \right]\mathbf{F}_n \qquad \text{(A.5)}$$

Where $\mathbf{v}_{n+\frac{1}{2}}$ represents $(\mathbf{v}_{n+1} + \mathbf{v}_n)/2$. The conventional GFEM can now be used to spatially discretize equation (A.5). Using interpolation function N_i to approximate $\mathbf{F}$ and the same function N_j as weighting functions, we can write, for an element e, an equation of the form:

$$\mathbf{M}_F \frac{\mathbf{F}_{n+1} - \mathbf{F}_n}{\Delta t} + \mathbf{K}_F \mathbf{F}_n = 0 \qquad \text{(A.6)}$$

which can be written in the more familiar form of:

$$\left(\frac{\mathbf{M}_F}{\Delta t}\right)(\mathbf{F}_{n+1}) = \left(\frac{\mathbf{M}_F}{\Delta t} + \mathbf{K}_F\right)\mathbf{F}_n \tag{A.7}$$

where:

$$\mathbf{M}_F = \int_\Omega N_i N_j d\Omega \tag{A.8}$$

K_F is the sum of an advection part $\mathbf{K}_a$ and a balancing diffusion type part $\mathbf{K}_{bd}$ which are defined as follows:

$$\mathbf{K}_a = \int_\Omega -\left(N_i \left(u_{n+\frac{1}{2}} \right) \frac{\partial N_j}{\partial x} + N_i \left(v_{n+\frac{1}{2}} \right) \frac{\partial N_j}{\partial y} \right) d\Omega \tag{A.9}$$

and

$$\mathbf{K}_{bd} = \frac{\Delta t}{2} \int_\Omega \left[N_i (u^2) \frac{\partial^2 N_i}{\partial x^2} + N_i (v^2) \frac{\partial^2 N_j}{\partial y^2} + N_i (uv) \frac{\partial^2 N_j}{\partial x \partial y} + N_i (vu) \frac{\partial^2 N_j}{\partial y \partial x} \right] d\Omega \tag{A.10}$$

Here all the velocities are at time level n. The second order derivatives in the equation (A.10) can be eliminated by using Green's theorem:

$$\mathbf{K}_{bd} = -\frac{\Delta t}{2} \int_\Omega \left[(u^2) \frac{\partial N_i}{\partial x} \frac{\partial N_j}{\partial x} + (v^2) \frac{\partial N_i}{\partial y} \frac{\partial N_j}{\partial y} + (uv) \frac{\partial N_i}{\partial y} \frac{\partial N_j}{\partial x} + (vu) \frac{\partial N_i}{\partial x} \frac{\partial N_j}{\partial y} \right] d\Omega \tag{A.11}$$

APPENDIX B

TAYLOR-GALERKIN METHOD FOR ENERGY EQUATION, INDUCTION TIME INDEX AND CRYSTALLINITY DISTRIBUTION EQUATIONS

In this section, the Taylor-Galerkin method is applied to the energy equation, as well as the induction time index and crystallinity distribution equation. Writing the energy conservation equation (6.3) with the heat generation term $\dot{\mathbf{Q}}$:

$$\rho C_p\left(\mathbf{T}' + \mathbf{v}\cdot\nabla\mathbf{T}\right) = \nabla\cdot k\nabla\mathbf{T} + \dot{\mathbf{Q}} \tag{B.1}$$

where $\mathbf{T}'$ represents the first derivative with respect of time and $\dot{\mathbf{Q}}$ represents the last two terms in Eq. (6.3). Using forward time Taylor series as in Appendix A:

$$\frac{\mathbf{T}_{n+1} - \mathbf{T}_n}{\Delta t} = \mathbf{T}_n' + \frac{\Delta t}{2}\mathbf{T}_n'' + O(\Delta t)^2 \tag{B.2}$$

From equation (B.1), we obtain:

$$\rho C_p \mathbf{T}_n' = -\rho C_P\left(\mathbf{v}_n\cdot\nabla\right)\mathbf{T}_n + \nabla\cdot k\nabla\mathbf{T}_n + \dot{\mathbf{Q}}_n \tag{B.3}$$

and

$$\rho C_P \mathrm{T}_n'' = -\rho C_P\left[\left(\mathbf{v}_n\cdot\nabla\right)\mathbf{T}_n' + \left(\mathbf{v}_n'\cdot\nabla\right)\mathbf{T}_n + \nabla\cdot k\nabla\mathbf{T}_n' + \ddot{\mathbf{Q}}\right] \tag{B.4}$$

Substituting equations (B.2) and (B.3) into equation (B.4), after approximating $\mathbf{v}'_n$ with $(\mathbf{v}_{n+1} - \mathbf{v}_n)/\Delta t$ we obtain:

$$\rho C_P \frac{\mathbf{T}_{n+1} - \mathbf{T}_n}{\Delta t} = -\rho C_P[(\mathbf{v}_{n+1} \cdot \nabla)\mathbf{T}_n + \nabla \cdot k\nabla \mathbf{T}'_n + \dot{\mathbf{Q}}_n$$

$$+ \frac{\Delta t}{2}\left(-\rho C_P(\mathbf{v}_n \cdot \nabla)\mathbf{T}'_n + \nabla \cdot k\nabla \mathbf{T}'_n + \ddot{\mathbf{Q}}_n\right) \tag{B.5}$$

The $\mathbf{T}'_n$ in the fourth term can be approximated by equation (B.3); however, the remaining $\mathbf{T}'_n$ in the fifth term is simply approximated by $(\mathbf{T}_{n+1} - \mathbf{T}_n)/\Delta t$ to avoid third order derivatives. Thus, we can rewrite equation (B.5) as:

$$\left(\frac{\rho C_P}{\Delta t} - \frac{\nabla \cdot k\nabla}{2}\right)\mathbf{T}_{n+1} = \left[\frac{\rho C_P}{\Delta t} - \frac{\nabla \cdot k\nabla}{2} + \rho C_P\left(\left(\mathbf{v}_{n+\frac{1}{2}} \cdot \nabla\right) + \frac{\Delta t}{2}(\mathbf{v}_n \cdot \nabla)^2\right)\right]\mathbf{T}_n$$

$$+ \left(1 - \frac{\Delta t}{2}(\mathbf{v}_n \cdot \nabla)\dot{\mathbf{Q}}_n\right) + \frac{\Delta t}{2}\ddot{\mathbf{Q}}_n \tag{B.6}$$

By discretizing (B.6) in space by conventional GFEM as usual, after using Green's theorem on the second order terms, the fully discretized equations can be written as:

$$\left(\frac{\mathbf{M}}{\Delta t} + \frac{\mathbf{K}_d}{2}\right)\mathbf{T}_{n+1} = \left(\frac{\mathbf{M}}{\Delta t} + \frac{\mathbf{K}_d}{2} - \rho C(\mathbf{K}_a + \mathbf{K}_{bd})\right)\mathbf{T}_n + \mathbf{Q} \tag{B.7}$$

where $\mathbf{M}$ is the mass matrix:

$$\mathbf{M} = \rho C_P \int_\Omega N_i N_j d\Omega \tag{B.8}$$

$$\mathbf{K}_d = \int_\Omega k\left(\frac{\partial N_i}{\partial x}\frac{\partial N_j}{\partial x} + \frac{\partial N_i}{\partial y}\frac{\partial N_j}{\partial y}\right)d\Omega + \int_\Gamma h\left(N_i N_j\right)d\Gamma \tag{B.9}$$

$\mathbf{K}_a$ and $\mathbf{K}_{bd}$ are the same as defined in equations (A.) and (A.)

The heat generation vector is:

$$\mathbf{Q} = \int_\Omega \left(N_i N_j \left(\dot{\mathbf{Q}}_n + \frac{\Delta t}{2}\ddot{\mathbf{Q}}_n \right) - \frac{\Delta t}{2}\left(N_i u_n \frac{\partial N_j}{\partial x} + N_i v_n \frac{\partial N_j}{\partial y} \right)\dot{\mathbf{Q}}_n \right) d\Omega \tag{B.10}$$

The above advection approximation includes an 'upwind' or 'balancing diffusion' type term.

APPENDIX C

COMPUTER PROGRAMS

The programs consist of two parts. The first program is used to simulate the filling stage. The velocity, temperature, induction time index and crystallinity distribution were calculated. The second program is used to calculate the temperature field and the final crystallinity after the injection molding cycle. Some symbols used in the program are list as follows:

Global: Global matrix for velocity field

Global_T: Global matrix for temperature field

Global_F: Global Matrix for pseudo-concentration

Global_I: Global Matrix for induction time index

Global_C: Global matrix for crystallinity

GF: right side matrix for finite element equations of velocity

GF_T: right side matrix for finite element equations of temperature

GF_F: right side matrix for finite element equations of pseudo-concentration

GF_I: right side matrix for finite element equations of induction time index

GE_C: right side matrix for finite element equations of crystallinity

UX, VX: velocities in x and y direction

T: Temperature field

F: Pseudo-concentration field

STRESS: stress field

SHEAR: shear rate field

INDUCT: Induction time index

CRYST: Crystallinity

X, Y: x and y coordinate of a node

XF: x coordinate of melt front

YF: y coordinate of melt front

Node: element node

Elemet_stiffness: sub-program to formulate the element stiffness of velocity

Element_stiffness_T: sub-program to formulate the element stiffness of Temperature, induction time index and crystallinity

Element_stiffness_F: sub-program to formulate the element stiffness of pseudo-concentration

Implement_boundary: sub-program to impose boundary condition to the finite element equations

Boudary_node: sub-program to determine the boundary node

Solve_equation: Finite equation solver for velocity solution

Solve_equation_F: finite equation solver for temperature, pseudo-concentration, induction time index and crystallinity

```
C PROGRAM TO SIMULATE THE FILLING STAGE

      MAIN PROGRAM
      DIMENSION NODE(5000,9),NODE_F(5000,4)
      DOUBLE PRECISION GLOBAL(10000,200),GF(10000),X(5000),
      Y(5000),UX(5000),UY(5000),F(5000),GLOBAL_F(5000,100),
     #GF_F(5000),VISCOS(5000),XF(100),YF(100),
     #GLOBAL_C(5000,100), GF_C(5000),
     #GLOBAL_I(5000,100),GF_I(5000),SHEAR(5000),
     #INDUCT(5000), CRYST(5000),
     #GLOBAL_T(5000,100),GF_T(5000),T(5000),STRESS(5000)
      COMMON/VISCO/VISCOS,T_B,TAO, RINDEX, B
      COMMON/SHEAR/SHEAR, STRESS
      COMMON/NXY/NX,NY/CO/X,Y/TIME/DT
      COMMON/TEM/T
      COMMON/VEL/UX,UY
      COMMON/BI/TW, TI
      COMMON/CRYST/T_HALF, FKG, T_M, A, TM0, T_G
      COMMON/HEAT/CP,HC,FKH
      COMMON/DENS/DENSITY
      COMMON/CC/INDUCT,CRYST
      Common/GT/Global_T,GF_T/IC/Global_I, GF_I/SC/
     #Global_C, GF_C/GV/Global, GF
      OPEN(8, FILE='INPUT.DAT',ACCESS='SEQUENCIAL',
     # STATUS='OLD')
      READ(8, 10)NX, NY
 10   FORMAT(2I4)
      READ(8,11)CAVITY_LENGTH, CAVITY_HALF_THICKNESS
 11   FORMAT(2F12.6)
      READ(8,12)TW, TI
 12   FROMAT(2F12.6)
      READ(8,13)U
 13   FORMAT(F12.6)
      READ(8,14)CP,HC,FKH
 14   FORMAT(3E12.6)
      READ(8,15)T_HALF,FKG,T_M,A,TM0,T_G
 15   FORMAT(5E12.6)
      READ(8,16)DENSITY
 16   FORMAT(E12.6)
      NDF=2
      FC=3.
      NODENUM=(2*NY-1)*(2*NX-1)
      LEMENT_NUM=(NX-1)*(NY-1)

C GENERATE THE COORDINATES OF ALL NODES AND GET NODES IN THE ELEMENT

      CALL COORDINATE(CAVITY_LENGTH,CAVITY_HALF_THICKNESS)
      CALL ELEMENT_NODE(NODE)
      CALL ELEMENT_NODE_F(NODE_F)
      OPEN(10,FILE='NODE.DAT',STATUS='OLD')
      WRITE(10,5) ((NODE(I,J),J=1,9),I=1,LEMENT_NUM)
  5   FORMAT(9I4)
      DISTANCE=Y(2)-Y(1)
      DX=RL/(NX-1)
```

```
      DT=DISTANCE/U

C   HALF BAND CALCULATION
      LHB=0
      DO 102 LE=1,LEMENT_NUM
      DO 101 I=1,9
      DO 101 J=I,9
      NW=(ABS(NODE(LE,I)-NODE(LE,J))+1)
      IF(LHB.LT.NW)THEN
      LHB=NW
      ENDIF
 101  CONTINUE
 102  CONTINUE

C     HALF BAND OF VELOCIY MATRIX
      LBAND=LHB
      LH1=LHB*NDF

C     HALF BAND OF PSEUDO-CONCENTRATION MATRIX
      LHB=0
      DO 110 LE=1,LEMENT_NUM
      DO 111 I=1,4
      DO 111 J=I,4
      NW=(ABS(NODE_F(LE,I)-NODE_F(LE,J))+1)
      IF(LHB.LT.NW)THEN
      LHB=NW
      ENDIF
  111 CONTINUE
  110 CONTINUE
      LHB_F=LHB

C     INITIAL VALUE OF VISCOSITY AND PSEUDO-COCENTRATION F
      DO 122 I=1,NODENUM
      VISCOS(I)=1000.
  122 F(I)=0
      N=0
      DO 112 I=1,2*NX-1
      DO 112 J=1,2*NY-1
      N=N+1
      F(N)=FC-X(N)
      IF(F(N).GE.1) NF=I
  112 CONTINUE
      WRITE(*,*) "****",NF

      DO 222 I=1,NODENUM
      VISCOS(I)=1.
      CRYST(I)=1E-15
      INDUCT(I)=0.
      IF(F(I).GE.1)THEN
      VISCOS(I)=1000.
      ENDIF
222   CONTINUE

C     INITIAL VELOCITY

      N=0
      DO 113 I=1,2*NX-1
```

```
      DO 113 J=1,2*NY-1
      N=N+1
      UX(N)=(2.*RINDEX+1.)/(RINDEX+1.)*U*(1.-
     #((ABS(CAVITY_HALF_THICKNESS-
     #Y(N)))/CAVITY_HALF_THICKNESS)
     #**(1./RINDEX+1.))
      UY(N)=0
      T(N)=TI
  113 CONTINUE

C CALCULATE INITIAL MELT FRONT POSITION
      DO 420 I=1,2*NY-1
      DO 420 J=1,2*NX-2
      N1=(J-1)*(2*NY-1)+I
      N2=J*(2*NY-1)+I
      IF(F(N1).GT.1.)THEN
      IF(F(N2).LE.1.)THEN
      XF(I)=X(N1)+(X(N1)-X(N2))*(1.-F(N1))/(F(N1)-F(N2))
      YF(I)=Y(N1)
      ENDIF
      ENDIF
  420 CONTINUE

      OPEN(4,FILE='FRONT.DAT',ACCESS='SEQUENTIAL',
     #FORM='FORMATTED',STATUS='NEW')
      LCYCLE=0
 2000 LCYCLE=LCYCLE+1
      WRITE(*,*) "CYCLE STEP=", LCYCLE

C  NXX, THE CALCULATION POSITION BEYOND THE MELT FRONT LINE
      DO 145 I=1,2*NX-1, 2
      NN=I*(2*NY-1)
      XL=XF(2*NY-1)+2*DX
      IF(X(NN).LT.XL) NXX=(I+5)/2
      IF(NXX.GE.NX) NXX=NX
  145 CONTINUE
      CALL SHEAR_RATE(NODE,F,NXX,NY)
      CALL GLOBAL_MATRIX(NODE,LH1,NDF,NXX,NY,F)
      CALL IMPLEMENT_BOUNDARY(LH1,NDF,F,
     #XF,NXX,NY, CAVITY_HALF_THICKNESS)
      NODENUM=(2*NXX-1)*(2*NY-1)
      LEMENT_NUM=(NXX-1)*(NY-1)
      NEQU=NODENUM*2
      CALL SOLVE_EQUATION(GLOBAL,GF,NEQU,LH1)
      DO 21 I=1,NODENUM
      UX(I)=GF(2*I-1)
      UY(I)=GF(2*I)
  21  CONTINUE
      CALL GLOBAL_MT(LHB_F,T,NODE_F,F,NXX,NY)
      CALL BOUNDARY_T(LHB_F,NXX,NY,NF)
      CALL SOLVE_EQUATION_F(GLOBAL_T,GF_T,NODENUM,LHB_F)
      CALL SOLVE_EQUATION_F(GLOBAL_I,GF_I,NODENUM,LHB_F)
      CALL SOLVE_EQUATION_F(GLOBAL_C,GF_C,NODENUM,LHB_F)
      DO 612 I=2,2*NY-1
  612 T(I)=TI
      DO 614 I=2,2*NXX-1
      NN=(I-1)*(2*NY-1)+1
```

```
  614 T(NN)=TW
      DO 600 I=1,NODENUM
      INDUCT(I)=GF_I(I)
      CRYST(I)=GF_C(I)
  600 T(I)=GF_T(I)
      DO 602 J=1,NF
      DO 602 I=2,2*NY-1
      NN=(J-1)*(2*NY-1)+I
  602 T(NN)=TI
      DO 604 I=NF+1,2*NXX-1
      NN=(I-1)*(2*NY-1)+1
  604 T(NN)=TW
      CALL GLOBAL_PSEUDO(NODE_F,LHB_F,F,GLOBAL_F,
     #GF_F,NXX,NY)
      CALL BOUNDARY_F(GLOBAL_F,GF_F,LHB_F,FC,NXX,NY)
      CALL SOLVE_EQUATION_F(GLOBAL_F,GF_F,NODENUM,LHB_F)

C      NEW FRONT POSITION
      DO 400 I=1,2*NY-1
      DO 400 J=1,2*NXX-2
      N1=(J-1)*(2*NY-1)+I
      N2=J*(2*NY-1)+I
      IF(GF_F(N1).GT.1.)THEN
      IF(GF_F(N2).LE.1.)THEN
      XF(I)=X(N1)+(X(N1)-X(N2))*(1.-GF_F(N1))/
     #(GF_F(N1)-GF_F(N2))
      YF(I)=Y(N1)
      ENDIF
      ENDIF
  400 CONTINUE
      IF(MOD(LCYCLE,5).EQ.0)THEN
      WRITE(4,502)(XF(I),YF(I),I=1,2*NY-1)
      ENDIF

C     UPDATE F VALUE
      DO 401 I=1,2*NY-1
      DO 401 J=1,NX*2-1
      N1=(J-1)*(2*NY-1)+I
      GF_F(N1)=1+XF(I)-X(N1)
  401 CONTINUE
      DO 402 I=1,(2*NX-1)*(2*NY-1)
      F(I)=GF_F(I)
  402 CONTINUE
      WRITE(*,*) "END OF CYCLE ", LCYCLE

C     JUDGE IF THE CAVITY IS FULL
      JUDGE=0
      DO 403 I=1,NODENUM
      IF(F(I).LT.1.)JUDGE=JUDGE+1
  403 CONTINUE
      WRITE(*,*)'NODE THAT EMPTY',JUDGE
      IF(JUDGE.LT.2*(2*NY-1)) GOTO 1001
      IF(F(NODENUM).GE.0.999) GOTO 1001
      GOTO 2000
 1001 CONTINUE
      WRITE(*,*)"TOTAL TIME=", DT*LCYCLE
      OPEN(5,FILE='FILE1.DAT',STATUS='NEW')
```

```
      WRITE(5,500) (X(I),Y(I),UX(I),UY(I),T(I),I=1,NODENUM)
 500  FORMAT(5(E12.6,4X))
      OPEN(6,FILE='FILE2.DAT',STATUS='NEW')
      WRITE(6, 501) (STRESS(I), INDUCT(I),
     # CRYST(I),   I=1,NODENUM)
 501  FORMAT(3(E12.6, 4X))
      STOP
      END

C     THIS IS THE SUB-PROGRAM TO GENERATE THE ELEMENT NODE

      SUBROUTINE ELEMENT_NODE(NODE)
      DIMENSION NODE(5000,9)
      COMMON/NXY/NX,NY
      NODENUM=(2*NY-1)*(2*NX-1)
      LEMENT=0
      DO 100 INX=1,2*NX-3,2
      DO 100 INY=1,2*NY-3,2
      LEMENT=LEMENT+1
      NYY=2*NY-1
      NODE(LEMENT,1)=NYY*(INX-1)+INY
      NODE(LEMENT,2)=NYY*(INX+1)+INY
      NODE(LEMENT,3)=NODE(LEMENT,2)+2
      NODE(LEMENT,4)=NODE(LEMENT,1)+2
      NODE(LEMENT,5)=NODE(LEMENT,1)+1
      NODE(LEMENT,6)=NYY*INX+INY
      NODE(LEMENT,7)=NODE(LEMENT,2)+1
      NODE(LEMENT,8)=NODE(LEMENT,6)+2
      NODE(LEMENT,9)=NODE(LEMENT,6)+1
  100 CONTINUE
      END

C SUB-PROGRAM TO GENERATE COORDINATES OF THE NODES

      SUBROUTINE COORDINATE(RLENGTH,THICKNESS)
      DOUBLE PRECISION X(5000),Y(5000),SUM(100),DLE(100)
      COMMON/NXY/NX,NY
      COMMON/CO/X,Y
      TOTAL=0.
      DO 10 I=1,NY-1
      TOTAL=TOTAL+1.5**(I-1.)
      SUM(I)=0.
  10  CONTINUE
      DY=THICKNESS/TOTAL
      WRITE(*,*) "DY===",DY
      DLE(1)=DY
      SUM(1)=0.
      DO 20 I=2,NY-1
      DLE(I)=DY*1.5**(I-1)
      SUM(I)=0.
      DO 30 J=2,I
  30  SUM(I)=SUM(I)+DLE(J-1)
  20  CONTINUE
      DO 1  I=1,2*NX-1
      LE=(I-1)*(2*NY-1)+1
      X(LE)=RLENGTH/(2.*NX-2.)*(I-1)
      Y(LE)=0.
```

```
      DO 1  J=1,NY-1
      DO 1 K=1,2
      LE=LE+1
      Y(LE)=SUM(J)+DLE(J)/2.*K
      X(LE)=RLENGTH/(2.*NX-2.)*(I-1)
1     CONTINUE
      END

      SUBROUTINE ELEMENT_STIFFNESS(IE,NODE,SK,RLF,AD,T,F)
      DIMENSION NODE(5000,9)
      DOUBLE PRECISION FAI(9), D1KC(9), D1AT(9),PFX(9),
     #PFY(9),RK11(9,9),RK22(9,9),RKPX(3,9),
     #RKPY(3,9), RL(2,2),
     # X(5000),Y(5000),RINVL(2,2)
      DOUBLE PRECISION D(3,3),RLP(2,2),SK(18,18),
     #RLF(3,18),AD(3,3),
     #RK12(9,9),T(5000),F(5000),VISCOS(5000)

      DOUBLE PRECISION  KC,AT,C, WI,WJ,XC,YC,DEL,
     #DETLP,DELTD1,DELTD2,DELTD,DUDY,
     #DUDX,DVDX,DVDY,SHEAR,VIS
      COMMON/NXY/NX,NY
      COMMON/CO/X,Y
      COMMON/VISCO/VISCOS,T_B,TAO,RINDEX,B
      DO 10 I=1,9
      DO 10 J=1,9
      RK11(I,J)=0.
      RK22(I,J)=0.
      RK12(I,J)=0.
 10   CONTINUE
      DO 20 I=1,3
      DO 20 J=1,9
      RKPX(I,J)=0.
 20   RKPY(I,J)=0.
      C=0.77459667
      DO 1000 M=1,9
      DO 100 N=1,9
      KC=-C
      DO 200 I=1,3
      AT=-C
      DO 201 J=1,3
      CALL INTE_FUNCTION(KC,AT,FAI,D1KC,D1AT)
      DO 101 K1=1,2
      DO 101 K2=1,2
101   RL(K1,K2)=0
      XC=0
      YC=0
      PSEUDO=0
      DO 102 KK=1,9
      RL(1,1)=RL(1,1)+D1KC(KK)*X(NODE(IE,KK))
      RL(2,2)=RL(2,2)+D1AT(KK)*Y(NODE(IE,KK))
      RL(1,2)=RL(1,2)+D1KC(KK)*Y(NODE(IE,KK))
      RL(2,1)=RL(2,1)+D1AT(KK)*X(NODE(IE,KK))
      XC=XC+FAI(KK)*X(NODE(IE,KK))
      YC=YC+FAI(KK)*Y(NODE(IE,KK))
      PSEUDO=PSEUDO+FAI(KK)*F(NODE(IE,KK))
102   CONTINUE
```

```
      DEL=RL(1,1)*RL(2,2)-RL(1,2)*RL(2,1)
      RINVL(1,1)=RL(2,2)/DEL
      RINVL(1,2)=-RL(1,2)/DEL
      RINVL(2,2)=RL(1,1)/DEL
      RINVL(2,1)=-RL(2,1)/DEL
      WI=0.5555555555
      IF(I.EQ.2) THEN
      WI=0.8888888889
      ENDIF
      WJ=0.5555555555
      IF(J.EQ.2) THEN
      WJ=0.8888888889
      ENDIF
      PFX(M)=(RINVL(1,1)*D1KC(M)+RINVL(1,2)*D1AT(M))
      PFX(N)=(RINVL(1,1)*D1KC(N)+RINVL(1,2)*D1AT(N))
      PFY(M)=RINVL(2,1)*D1KC(M)+RINVL(2,2)*D1AT(M)
      PFY(N)=RINVL(2,1)*D1KC(N)+RINVL(2,2)*D1AT(N)
      RK11(M,N)=RK11(M,N)+PFX(M)*PFX(N)
     #*DEL*WI*WJ
      RK22(M,N)=RK22(M,N)+PFY(M)*PFY(N)
     #*DEL*WI*WJ
      RK12(M,N)=RK12(M,N)+PFX(M)*PFY(N)*DEL*WI*WJ
      IF(M.EQ.1) THEN
      RKPX(M,N)=RKPX(M,N)-PFX(N)*DEL*WI*WJ
      RKPY(M,N)=RKPY(M,N)-PFY(N)*DEL*WI*WJ
      ENDIF
      IF(M.EQ.2)THEN
      RKPX(M,N)=RKPX(M,N)-PFX(N)*(XC-X(NODE(IE,9)))
     #*DEL*WI*WJ
      RKPY(M,N)=RKPY(M,N)-PFY(N)*(XC-X(NODE(IE,9)))
     #*DEL*WI*WJ
      ENDIF
      IF(M.EQ.3)THEN
      RKPX(M,N)=RKPX(M,N)-PFX(N)*(YC-Y(NODE(IE,9)))
     #*DEL*WI*WJ
      RKPY(M,N)=RKPY(M,N)-PFY(N)*(YC-Y(NODE(IE,9)))
     #*DEL*WI*WJ
      ENDIF
      AT=AT+C
201   CONTINUE
      KC=KC+C
200   CONTINUE
100   CONTINUE
1000  CONTINUE
      DO 300 I=1,3
      DO 300 J=1,3
 300  D(I,J)=0.
      C=0.57735207
      DO 301 I=1,2
      KC=C
      IF(I.EQ.1)THEN
      KC=-C
      ENDIF
      DO 302  J=1,2
      AT=C
      IF(J .EQ. 1)THEN
      AT=-C
```

```
      ENDIF
      CALL INTE_FUNCTION(KC,AT,FAI,D1KC,D1AT)
      DO 303 I1=1,2
      DO 303 J1=1,2
303   RLP(I1,J1)=0.
      XC=0
      YC=0
      DO 304 KK=1,9
      RLP(1,1)=RLP(1,1)+D1KC(KK)*X(NODE(IE,KK))
      RLP(1,2)=RLP(1,2)+D1KC(KK)*Y(NODE(IE,KK))
      RLP(2,1)=RLP(2,1)+D1AT(KK)*X(NODE(IE,KK))
      RLP(2,2)=RLP(2,2)+D1AT(KK)*Y(NODE(IE,KK))
      XC=XC+FAI(KK)*X(NODE(IE,KK))
      YC=YC+FAI(KK)*Y(NODE(IE,KK))
304   CONTINUE
      DETLP=RLP(1,1)*RLP(2,2)-RLP(1,2)*RLP(2,1)
      D(1,1)=D(1,1)+DETLP
      D(1,2)=D(1,2)+(XC-X(NODE(IE,9)))*DETLP
      D(1,3)=D(1,3)+(YC-Y(NODE(IE,9)))*DETLP
      D(2,2)=D(2,2)+(XC-X(NODE(IE,9)))**2*DETLP
      D(2,3)=D(2,3)+(XC-X(NODE(IE,9)))*(YC-Y(NODE(IE,9)))*DETLP
      D(3,3)=D(3,3)+(YC-Y(NODE(IE,9)))**2*DETLP
302   CONTINUE
301   CONTINUE
      DO 306 I=1,3
      DO 306 J=I,3
306   D(J,I)=D(I,J)
      AD(1,1)=D(3,3)*D(2,2)-D(2,3)*D(3,2)
      AD(2,1)=-(D(2,1)*D(3,3)-D(2,3)*D(3,1))
      AD(3,1)=D(2,1)*D(3,2)-D(2,2)*D(3,1)
      AD(1,2)=-(D(1,2)*D(3,3)-D(1,3)*D(3,2))
      AD(2,2)=D(1,1)*D(3,3)-D(1,3)*D(3,1)
      AD(3,2)=-(D(1,1)*D(3,2)-D(1,2)*D(3,1))
      AD(1,3)=D(1,2)*D(2,3)-D(1,3)*D(2,2)
      AD(2,3)=-(D(1,1)*D(2,3)-D(1,3)*D(2,1))
      AD(3,3)=D(1,1)*D(2,2)-D(1,2)*D(2,1)
      DELTD1=D(1,1)*D(2,2)*D(3,3)+D(1,2)*D(2,3)*D(3,1)
     #+D(2,1)*D(3,2)*D(1,3)
      DELTD2=-D(1,3)*D(2,2)*D(3,1)-D(2,3)*D(3,2)*D(1,1)
     #-D(1,2)*D(2,1)*D(3,3)
      DELTD=DELTD1+DELTD2
      DO 305 I=1,3
      DO 305 J=1,3
305   AD(I,J)=AD(I,J)/DELTD
      VIS=VISCOS(IE)
      DO 501 I=1,9
      DO 500 J=1,9
      SK(2*I-1,J*2-1)=(RK11(I,J)+RK22(I,J))*VIS
      SK(I*2,J*2)=(RK22(I,J)+RK11(I,J))*VIS
500   CONTINUE
501   CONTINUE
      DO 600 I=1,3
      DO 600 J=1,9
      RLF(I,2*J-1)=RKPX(I,J)
      RLF(I,2*J)=RKPY(I,J)
600   CONTINUE
      RETURN
```

```
      END

C INTERPOLATION FUNCTION AND ITS DERIVATIVES FOR VELOCITY

      SUBROUTINE INTE_FUNCTION(KC,AT,FAI,D1KC,D1AT)
      DOUBLE PRECISION FAI(9),D1KC(9),D1AT(9)
      DOUBLE PRECISION KC,AT
      FAI(1)=(KC**2-KC)*(AT**2-AT)/4.
      FAI(2)=(KC**2+KC)*(AT**2-AT)/4.
      FAI(3)=(KC**2+KC)*(AT**2+AT)/4.
      FAI(4)=(KC**2-KC)*(AT**2+AT)/4.
      FAI(5)=(KC**2-KC)*(1.-AT**2)/2.
      FAI(6)=(1.-KC**2)*(AT**2-AT)/2.
      FAI(7)=(KC**2+KC)*(1.-AT**2)/2.
      FAI(8)=(1.-KC**2)*(AT**2+AT)/2.
      FAI(9)=(1.-KC**2)*(1.-AT**2)

      D1KC(1)=(2.*KC-1.)*(AT*AT-AT)/4.
      D1KC(2)=(2.*KC+1.)*(AT*AT-AT)/4.
      D1KC(3)=(2.*KC+1.)*(AT*AT+AT)/4.
      D1KC(4)=(2.*KC-1.)*(AT*AT+AT)/4.
      D1KC(5)=(2.*KC-1.)*(1.-AT**2)/2.
      D1KC(6)=-KC*(AT**2-AT)
      D1KC(7)=(2.*KC+1.)*(1.-AT**2)/2.
      D1KC(8)=-KC*(AT**2+AT)
      D1KC(9)=-2.*KC*(1.-AT**2.)

      D1AT(1)=(2.*AT-1.)*(KC*KC-KC)/4.
      D1AT(2)=(2.*AT-1.)*(KC*KC+KC)/4.
      D1AT(3)=(2.*AT+1.)*(KC*KC+KC)/4.
      D1AT(4)=(2.*AT+1.)*(KC*KC-KC)/4.
      D1AT(5)=-(KC*KC-KC)*AT
      D1AT(6)=(2.*AT-1.)*(1.-KC*KC)/2.
      D1AT(7)=-AT*(KC**2+KC)
      D1AT(8)=(1.-KC**2)*(2.*AT+1.)/2.
      D1AT(9)=-2.*AT*(1.-KC**2.)
      RETURN
      END

C SUB-PROGRAM FOR CALCULATE VELOCITY MATRIX

      SUBROUTINE GLOBAL_MATRIX(NODE,LHB,NDF,F,NX,NY)
      DOUBLE PRECISION GLOBAL(10000,200), GF(10000),
     #S(18,18),RKPP(18,18),
     #RLFE(3,18),AD(3,3),FL(18,3),
     #TMPF(18,3),T(5000),F(5000)
      DIMENSION NODE(5000,9)
      DOUBLE PRECISION PENALTY
      COMMON/TEM/T
      COMMON/VISCO/VISCOS,T_B,TAO, RINDEX, B
      Common/GV/global, GF
      PENALTY=2E8
      NODENUM=(2*NX-1)*(2*NY-1)
      LEMENT_NUM=(NX-1)*(NY-1)
      DO 10 I=1,NODENUM*2
      GF(I)=0.
      DO 10 J=1,LHB
```

```
      GLOBAL(I,J)=0.
   10 CONTINUE
      KLM=0
      DO 123 KLM=1,LEMENT_NUM
      CALL ELEMENT_STIFFNESS(KLM,NODE,S,RLFE,AD,T,F)
      DO 13 I=1,18
      DO 13 J=1,18
      RKPP(I,J)=0.
   13 CONTINUE
      DO 121 I=1,3
      DO 121 J=1,18
      TMPF(J,I)=0.
      FL(J,I)=RLFE(I,J)
  121 CONTINUE
      DO 125 I=1,18
      DO 124 J=1,3
      DO 122 K=1,3
      TMPF(I,J)=TMPF(I,J)+FL(I,K)*AD(K,J)
  122 CONTINUE
  124 CONTINUE
  125 CONTINUE
      DO 17 I3=1,18
      DO 16 K3=1,18
      DO 12 K=1,3
      RKPP(I3,K3)=RKPP(I3,K3)+TMPF(I3,K)*RLFE(K,K3)
   12 CONTINUE
   16 CONTINUE
   17 CONTINUE
      DO 200 I=1,9
      NR=(NODE(KLM,I)-1)*NDF
      DO 203 II=1,NDF
      NR=NR+1
      LE=(I-1)*NDF+II
      DO 202 J=1,9
      NCL=(NODE(KLM,J)-1)*NDF
      DO 201 JJ=1,NDF
      ME=(J-1)*NDF+JJ
      NC=NCL+JJ+1-NR
      IF(NC.GT.0)THEN
      GLOBAL(NR,NC)=GLOBAL(NR,NC)+S(LE,ME)
     #+RKPP(LE,ME)*PENALTY
      ENDIF
  201 CONTINUE
  202 CONTINUE
  203 CONTINUE
  200 CONTINUE
  123 CONTINUE
      RETURN
      END

C
      SUBROUTINE GLOBAL_PSEUDO(NODE_F,LHB,F,GLOBAL_F,
     #GF_F, nx, ny)
      DIMENSION NODE_F(5000,4)
      DOUBLE PRECISION F(5000),RKFF(4,4),BF(4)
     #,GLOBAL_F(5000,100),GF_F(5000)
      COMMON/TIME/DT
```

```
      N_ELEMENT=(NX-1)*(NY-1)*4
      N_NODE=(2*NX-1)*(2*NY-1)
      DO 111 I=1,N_NODE
      GF_F(I)=0.
      DO 111 J=1,LHB
      GLOBAL_F(I,J)=0.
  111 CONTINUE
      DO 123 KLM=1,N_ELEMENT
      CALL ELEMENT_F(KLM,NODE_F,RKFF,BF,F)
      DO 250 I=1,4
      LR=NODE_F(KLM,I)
      GF_F(LR)=GF_F(LR)+BF(I)
      DO 250 J=1,4
      NCL=(NODE_F(KLM,J)-1)
      NC=NCL+2-LR
      IF(NC.GT.0)THEN
      GLOBAL_F(LR,NC)=GLOBAL_F(LR,NC)+RKFF(I,J)/DT
      ENDIF
  250 CONTINUE
  123 CONTINUE
      RETURN
      END

      SUBROUTINE ELEMENT_NODE_F(NODE_F)
      DIMENSION NODE_F(5000,4)
      COMMON/NXY/NX,NY
      LEMENT_F=0
      DO 10 I=1,2*NX-2
      DO 10 J=1,2*NY-2
      LEMENT_F=LEMENT_F+1
      NODE_F(LEMENT_F,1)=(I-1)*(2*NY-1)+J
      NODE_F(LEMENT_F,2)=I*(2*NY-1)+J
      NODE_F(LEMENT_F,3)=NODE_F(LEMENT_F,2)+1
      NODE_F(LEMENT_F,4)=NODE_F(LEMENT_F,1)+1
   10 CONTINUE
      RETURN
      END


      SUBROUTINE ELEMENT_F(IE,NODE_F,RKFF,BF,F)
      DIMENSION NODE_F(5000,4)
      DOUBLE PRECISION FAI(4), D1KC(4), D1AT(4),PFX(4),
     #PFY(4),RL(2,2),
     #X(5000),Y(5000),RINVL(2,2),
     #RKFF(4,4),RKA(4,4),RKBD(4,4),BF(4),
     #F(5000),B_C(4), B_I(4)
     #UX(5000),UY(5000)
      COMMON/CO/X,Y/NXY/NX,NY
      COMMON/VEL/UX,UY
      COMMON/TIME/DT
      DOUBLE PRECISION  KC,AT,C,DEL,XC,YC,U,V
      N_NODE=(2*NX-1)*(2*NY-1)
      N_ELEMENT=4*(NX-1)*(NY-1)
      DO 10 I=1,4
      BF(I)=0.
      B_C(I)=0.
      B_I(I)=0.
```

```
      DO 10 J=1,4
      RKFF(I,J)=0.
      RKA(I,J)=0.
      RKBD(I,J)=0.
   10 CONTINUE
      C=.5773502692
      DO 1000 M=1,4
      DO 100 N=1,4
      KC=-C
      DO 200 I=1,2
      AT=-C
      DO 201 J=1,2
      CALL INTE_FUNCTION_F(KC,AT,FAI,D1KC,D1AT)
      DO 101 K1=1,2
      DO 101 K2=1,2
  101 RL(K1,K2)=0
      XC=0
      YC=0
      U=0
      V=0
      DO 102 KK=1,4
      RL(1,1)=RL(1,1)+D1KC(KK)*X(NODE_F(IE,KK))
      RL(2,2)=RL(2,2)+D1AT(KK)*Y(NODE_F(IE,KK))
      RL(1,2)=RL(1,2)+D1KC(KK)*Y(NODE_F(IE,KK))
      RL(2,1)=RL(2,1)+D1AT(KK)*X(NODE_F(IE,KK))
      XC=XC+FAI(KK)*X(NODE_F(IE,KK))
      YC=YC+FAI(KK)*Y(NODE_F(IE,KK))
      U=U+FAI(KK)*UX(NODE_F(IE,KK))
      V=V+FAI(KK)*UY(NODE_F(IE,KK))
  102 CONTINUE

      DEL=RL(1,1)*RL(2,2)-RL(1,2)*RL(2,1)
      RINVL(1,1)=RL(2,2)/DEL
      RINVL(1,2)=-RL(1,2)/DEL
      RINVL(2,2)=RL(1,1)/DEL
      RINVL(2,1)=-RL(2,1)/DEL
      PFX(M)=(RINVL(1,1)*D1KC(M)+RINVL(1,2)*D1AT(M))
      PFX(N)=(RINVL(1,1)*D1KC(N)+RINVL(1,2)*D1AT(N))
      PFY(M)=RINVL(2,1)*D1KC(M)+RINVL(2,2)*D1AT(M)
      PFY(N)=RINVL(2,1)*D1KC(N)+RINVL(2,2)*D1AT(N)
      RKFF(M,N)=RKFF(M,N)+FAI(M)*FAI(N)*DEL
      RKA(M,N)=RKA(M,N)+(FAI(M)*PFX(N)*U+FAI(M)
     #*PFY(N)*V)*DEL
      RKBD(M,N)=RKBD(M,N)+(PFX(M)*PFX(N)*U*U+
     #PFY(M)*PFY(N)*V*V+PFX(M)*PFY(N)*U*V+
     #PFY(N)*PFX(M)*U*V)*DEL*DT/2.
      AT=AT+2.*C
  201 CONTINUE
      KC=KC+2.*C
  200 CONTINUE
  100 CONTINUE
 1000 CONTINUE
      DO 210 I=1,4
      DO 210 J=1,4
      BF(I)=BF(I)+(RKFF(I,J)/DT-RKA(I,J)-RKBD(I,J))*F(NODE_F(IE,J))
  210 CONTINUE
      RETURN
```

```
      END

      SUBROUTINE INTE_FUNCTION_F(KC,AT,FAI,D1KC,D1AT)
      DOUBLE PRECISION FAI(4),D1KC(4),D1AT(4),KC,AT
      FAI(1)=(1-AT)*(1-KC)/4.
      FAI(2)=(1-AT)*(1+KC)/4.
      FAI(3)=(1+AT)*(1+KC)/4.
      FAI(4)=(1+AT)*(1-KC)/4.

      D1KC(1)=-(1-AT)/4.
      D1KC(2)=(1-AT)/4.
      D1KC(3)=(1+AT)/4.
      D1KC(4)=-(1+AT)/4.
      D1AT(1)=-(1-KC)/4.
      D1AT(2)=-(1+KC)/4.
      D1AT(3)=(1+KC)/4.
      D1AT(4)=(1-KC)/4.
      RETURN
      END

      SUBROUTINE BOUNDARY_F(GLOBAL_F,GF_F,LHB,FC, nx, ny)
      DOUBLE PRECISION GLOBAL_F(5000,100),GF_F(5000)
      NODENUM=(2*NX-1)*(2*NY-1)
      DO 70  NB=1,2*NY-1
      IE=NB
      IT=LHB-1
      I=IE-LHB
      DO 71 II=1,IT
      I=I+1
      IF(I.GE.1)THEN
      J=IE-I+1
      GF_F(I)=GF_F(I)-GLOBAL_F(I,J)*FC
      GLOBAL_F(I,J)=0.
      ENDIF
71    CONTINUE
      GLOBAL_F(IE,1)=1.0
      GF_F(IE)=FC
      I=IE
      DO 72 II=2,LHB
      I=I+1
      IF(I.LE.NODENUM)THEN
      GF_F(I)=GF_F(I)-GLOBAL_F(IE,II)*FC
      GLOBAL_F(IE,II)=0.
      ENDIF
  72  CONTINUE
70    CONTINUE
      END



      SUBROUTINE BOUNDARY_NODE(NUM_VX0,NUM_VY0,nx,ny
     #,NODE_VX0,NODE_VY0,INLET_VX_NUM,INLET_VX,F,X,XF)
      DIMENSION NODE_VX0(1000),NODE_VY0(1000),INLET_VX(200)
      DOUBLE PRECISION F(5000),X(5000),XF(100),T(5000)
      COMMON/TEM/T
      NODENUM=(2*NX-1)*(2*NY-1)
      NUM_VX0=0
```

```
      NUM_VY0=0
      DO 100 I=1,2*NX-2
      N=(I-1)*(2*NY-1)+1
      IF((XF(1)-X(N)).GE.0.2)THEN
      NUM_VX0=NUM_VX0+1
      NODE_VX0(NUM_VX0)=(I-1)*(2*NY-1)+1
      ENDIF
      NUM_VY0=NUM_VY0+1
      NODE_VY0(NUM_VY0)=(I-1)*(2*NY-1)+1
      NUM_VY0=NUM_VY0+1
      NODE_VY0(NUM_VY0)=I*(2*NY-1)
100   CONTINUE
      N=(2*NX-2)*(2*NY-1)+1
      IF((XF(1)-X(N)).GE.0.2)THEN
      NUM_VX0=NUM_VX0+1
      NODE_VX0(NUM_VX0)=(2*NX-2)*(2*NY-1)+1
      ENDIF
      NUM_VY0=NUM_VY0+1
      NODE_VY0(NUM_VY0)=(2*NX-2)*(2*NY-1)+1
      NUM_VY0=NUM_VY0+1
      NODE_VY0(NUM_VY0)=(2*NX-1)*(2*NY-1)
      INLET_VX_NUM=0
      DO 200 I=1,2*NY-1
      INLET_VX_NUM=INLET_VX_NUM+1
      INLET_VX(INLET_VX_NUM)=INLET_VX_NUM
200   CONTINUE
      DO 300 I=1,2*NX-1
      DO 300 J=2,2*NY-1
      NUMBER=(I-1)*(2*NY-1)+J
      IF(F(NUMBER).GE.1) THEN
      IF(T(NUMBER).LE.120) THEN
      NUM_VX0=NUM_VX0+1
      NODE_VX0(NUM_VX0)=NUMBER
      NUM_VY0=NUM_VY0+1
      NODE_VY0(NUM_VY0)=NUMBER
      ENDIF
      ENDIF
300   CONTINUE
      DO 400 J=1,2*NY-1
      NUMBER=(2*NX-2)*(2*NY-1)+J
      IF(F(NUMBER).GE.0.999)THEN
      NUM_VX0=NUM_VX0+1
      NODE_VX0(NUM_VX0)=NUMBER
      ENDIF
400   CONTINUE
      RETURN
      END



      SUBROUTINE IMPLEMENT_BOUNDARY(LH1,NDF,F
     #,XF,NX,NY,CAVITY_HALF_THICKNESS)
      DOUBLE PRECISION GLOBAL(10000,200),GF(10000),
     #Y(5000),V(5000),F(5000),X(5000),XF(100),T(5000)
      DIMENSION NODE_VX0(1000),NODE_VY0(1000),INLET_VX(200)
      COMMON/CO/X,Y
```

```
      COMMON/TEM/T/GT/Global, GF
      CALL BOUNDARY_NODE(NUM_VX0,NUM_VY0,nx,ny
     #,NODE_VX0,NODE_VY0,INLET_VX_NUM,INLET_VX,F,X,XF)
      DO 10 I=1,INLET_VX_NUM
      V(I)=(2.*RINDEX+1.)/(RINDEX+1.)*U*
     #(1.-((ABS(H-Y(I)))/H)**(1./RINDEX+1.))
10    CONTINUE
      NODENUM=(2*NX-1)*(2*NY-1)
      LEMENT_NUM=(NX-1)*(NY-1)
      DO 30  NB=1,NUM_VX0
      IE=(NODE_VX0(NB)-1)*NDF+1
      IT=LHALF_BAND-1
      I=IE-LHALF_BAND
      DO 31 II=1,IT
      I=I+1
      IF(I.GE.1)THEN
      J=IE-I+1
      GLOBAL(I,J)=0.
      ENDIF
31    CONTINUE
      GLOBAL(IE,1)=1.0
      GF(IE)=0.
      I=IE
      DO 32 II=2,LHALF_BAND
      I=I+1
      IF(I.LT.NODENUM*NDF)THEN
      GLOBAL(IE,II)=0.
      ENDIF
32    CONTINUE
30    CONTINUE
      DO 40 NB=1,NUM_VY0
      IE=(NODE_VY0(NB))*NDF
      IT=LHALF_BAND-1
      I=IE-LHALF_BAND
      DO 41 II=1,IT
      I=I+1
      IF(I.GE.1)THEN
      J=IE-I+1
      GLOBAL(I,J)=0.
      ENDIF
41    CONTINUE
      GLOBAL(IE,1)=1.0
      GF(IE)=0.
      I=IE
      DO 40 II=2,LHALF_BAND
      I=I+1
      IF(I.LT.NODENUM*NDF)THEN
      GLOBAL(IE,II)=0.
      ENDIF
40    CONTINUE
      DO 70  NB=1,INLET_VX_NUM
      IE=(INLET_VX(NB)-1)*NDF+1
      IT=LHALF_BAND-1
      I=IE-LHALF_BAND
      DO 71 II=1,IT
      I=I+1
      IF(I.GE.1)THEN
```

```
      J=IE-I+1
      GF(I)=GF(I)-GLOBAL(I,J)*V(NB)
      GLOBAL(I,J)=0.
      ENDIF
71    CONTINUE
      GLOBAL(IE,1)=1.0
      GF(IE)=V(NB)
      I=IE
      DO 72 II=2,LHALF_BAND
      I=I+1
      IF(I.LT.NODENUM*2)THEN
      GF(I)=GF(I)-GLOBAL(IE,II)*V(NB)
      GLOBAL(IE,II)=0.
      ENDIF
72    CONTINUE
70    CONTINUE
      DO 80  NB=1,INLET_VX_NUM
      IE=(INLET_VX(NB))*NDF
      IT=LHALF_BAND-1
      I=IE-LHALF_BAND
      DO 81 II=1,IT
      I=I+1
      IF(I.GE.1)THEN
      J=IE-I+1
      GLOBAL(I,J)=0.
      ENDIF
81    CONTINUE
      GLOBAL(IE,1)=1.0
      GF(IE)=0
      I=IE
      DO 82 II=2,LHALF_BAND
      I=I+1
      IF(I.LT.NODENUM*2)THEN
      GLOBAL(IE,II)=0.
      ENDIF
82    CONTINUE
80    CONTINUE
      RETURN
      END



      SUBROUTINE SOLVE_EQUATION(GLOBAL,GF,N_NODE,
     #LHALF_BAND)
      DOUBLE PRECISION GLOBAL(10000,200),GF(10000),FACTOR
      NODENUM=N_NODE
      MEQNS=NODENUM-1
      DO 103 NPIV=1,MEQNS
      NPIVOT=NPIV+1
      LSTSUB=NPIV+LHALF_BAND-1
      IF(LSTSUB.GT.NODENUM)THEN
      LSTSUB=NODENUM
      ENDIF
      DO 102  NROW=NPIVOT,LSTSUB
      NCOL=NROW-NPIV+1
      FACTOR=GLOBAL(NPIV,NCOL)/GLOBAL(NPIV,1)
      DO 101 NCOL=NROW,LSTSUB
```

```
      ICOL=NCOL-NROW+1
      JCOL=NCOL-NPIV+1
      GLOBAL(NROW,ICOL)=GLOBAL(NROW,ICOL)-
     #FACTOR*GLOBAL(NPIV,JCOL)
101   CONTINUE
      GF(NROW)=GF(NROW)-FACTOR*GF(NPIV)
102   CONTINUE
103   CONTINUE
      DO 105 IJK=2,NODENUM
      NPIV=NODENUM-IJK+2
      GF(NPIV)=GF(NPIV)/GLOBAL(NPIV,1)
      LSTSUB=NPIV-LHALF_BAND+1
      IF(LSTSUB.LT.1)THEN
      LSTSUB=1
      ENDIF
      NPIVOT=NPIV-1
      DO 104 JKI=LSTSUB,NPIVOT
      NROW=NPIVOT-JKI+LSTSUB
      NCOL=NPIV-NROW+1
      FACTOR=GLOBAL(NROW,NCOL)
      GF(NROW)=GF(NROW)-FACTOR*GF(NPIV)
104   CONTINUE
105   CONTINUE
      GF(1)=GF(1)/GLOBAL(1,1)
      RETURN
      END


      SUBROUTINE SOLVE_EQUATION_F(GLOBAL,GF,N_NODE,
     #LHALF_BAND)
      DOUBLE PRECISION GLOBAL(5000,100),GF(5000),FACTOR
      NODENUM=N_NODE
      MEQNS=NODENUM-1
      DO 103 NPIV=1,MEQNS
      NPIVOT=NPIV+1
      LSTSUB=NPIV+LHALF_BAND-1
      IF(LSTSUB.GT.NODENUM)THEN
      LSTSUB=NODENUM
      ENDIF
      DO 102  NROW=NPIVOT,LSTSUB
      NCOL=NROW-NPIV+1
      FACTOR=GLOBAL(NPIV,NCOL)/GLOBAL(NPIV,1)
      DO 101 NCOL=NROW,LSTSUB
      ICOL=NCOL-NROW+1
      JCOL=NCOL-NPIV+1
      GLOBAL(NROW,ICOL)=GLOBAL(NROW,ICOL)-
     #FACTOR*GLOBAL(NPIV,JCOL)
101   CONTINUE
      GF(NROW)=GF(NROW)-FACTOR*GF(NPIV)
102   CONTINUE
103   CONTINUE
      DO 105 IJK=2,NODENUM
      NPIV=NODENUM-IJK+2
      GF(NPIV)=GF(NPIV)/GLOBAL(NPIV,1)
      LSTSUB=NPIV-LHALF_BAND+1
      IF(LSTSUB.LT.1)THEN
      LSTSUB=1
```

```
      ENDIF
      NPIVOT=NPIV-1
      DO 104 JKI=LSTSUB,NPIVOT
      NROW=NPIVOT-JKI+LSTSUB
      NCOL=NPIV-NROW+1
      FACTOR=GLOBAL(NROW,NCOL)
      GF(NROW)=GF(NROW)-FACTOR*GF(NPIV)
 104  CONTINUE
 105  CONTINUE
      GF(1)=GF(1)/GLOBAL(1,1)
      RETURN
      END


C SHEAR RATE AND STRESS

      SUBROUTINE SHEAR_RATE(NODE,F,NXX,NY)
      DIMENSION NODE(5000,9)
      DOUBLE PRECISION X(5000),Y(5000),UX(5000),UY(5000),
     #VISCOS(5000),SHEAR(5000),D1KC(9),D1AT(9),FAI(9),
     #RL(2,2),RINVL(2,2),F(5000),T(5000),STRESS(5000)
      COMMON/VISCO/VISCOS,T_B,TAO, RINDEX, B
      COMMON/CO/X,Y
      COMMON/TEM/T
      COMMON/VEL/UX,UY
      COMMON/SHEAR/SHEAR, STRESS
      TA=1E3
      T0=583
      LEMENT=(NX-1)*(NY-1)
      WRITE(*,*) LEMENT
      NODENUM=(2*NX-1)*(2*NY-1)
      CALL INTE_FUNCTION(0.,0.,FAI,D1KC,D1AT)
      DO 100 IE=1,LEMENT
      SHEAR(IE)=0.
      DO 10 I=1,2
      DO 10 J=1,2
  10  RL(I,J)=0.
      DO 102 KK=1,9
      RL(1,1)=RL(1,1)+D1KC(KK)*X(NODE(IE,KK))
      RL(2,2)=RL(2,2)+D1AT(KK)*Y(NODE(IE,KK))
      RL(1,2)=RL(1,2)+D1KC(KK)*Y(NODE(IE,KK))
      RL(2,1)=RL(2,1)+D1AT(KK)*X(NODE(IE,KK))
  102 CONTINUE
      DEL=RL(1,1)*RL(2,2)-RL(1,2)*RL(2,1)
      RINVL(1,1)=RL(2,2)/DEL
      RINVL(1,2)=-RL(1,2)/DEL
      RINVL(2,2)=RL(1,1)/DEL
      RINVL(2,1)=-RL(2,1)/DEL

      DO 103 KK=1,9
      SHEAR(IE)=SHEAR(IE)+(RINVL(2,1)*D1KC(KK)+
     #RINVL(2,2)*D1AT(KK))*UX(NODE(IE,KK))
     #+(RINVL(1,1)*D1KC(KK)
     #+RINVL(1,2)*D1AT(KK))*UY(NODE(IE,KK))
 103  CONTINUE
      IF(F(NODE(IE,9)).GE.1.)THEN
```

```
      TEM=T(NODE(IE,9))+273
      EXPT=B*EXP(T_B/TEM)
      VISCOS(IE)=EXPT/(1+(EXPT*SHEAR(IE)/TAO)**(1-RINDEX))
      STRESS(IE)=VISCOS(IE)*SHEAR(IE)
      ENDIF
      IF(T(NODE(IE,9)).LT.120.)VISCOS(IE)=1E20
      IF(F(NODE(IE,9)).LT.1.)VISCOS(IE)=1.
100   CONTINUE
      RETURN
      END


      SUBROUTINE ELEMENT_T(IE,NODE_F,F)
      DIMENSION NODE_F(5000,4)
      DOUBLE PRECISION FAI(4),D1KC(4),D1AT(4)
     #,PFX(4),PFY(4),
     # RL(2,2),X(5000),Y(5000),RINVL(2,2),BT(4),F(5000)
      DOUBLE PRECISION S(4,4),UX(5000),UY(5000),T(5000)
     #,KA(4,4),KBD(4,4),KD(4,4),MT(4,4), SHEAR(5000)
     #,STRESS(5000)
     #, BC(4), BI(4), SC(4,4),SI(4,4),
     #CRYST(5000), INDUCT(5000)
      COMMON/TCI/S,BT, SC, BC, SI, BI
      COMMON/VISCO/VISCOS,T_B,TAO, RINDEX, B
      COMMON/TEM/T
      COMMON/VEL/UX,UY
      COMMON/CRYST/T_HALF, FKG, T_M, A, TM0, T_G
      COMMON/HEAT/CP,HC,FKH
      COMMON/DENS/DENSITY
      COMMON/CC/INDUCT,CRYST
      COMMON/CO/X,Y
      COMMON/TIME/DTIME
      COMMON/SHEAR/SHEAR, STRESS
      DOUBLE PRECISION  KC,AT,C,XC,YC,DEL,U,V
      VISCOS_HEAT=SHEAR(IE)*STRESS(IE)
      DO 10 I=1,4
      BT(I)=0.
      NO(I)=NODE_F(IE,KK)
      DO 10 J=1,4
      KA(I,J)=0.
      KBD(I,J)=0.
      KD(I,J)=0.
      MT(I,J)=0.
   10 CONTINUE
      C=0.5773502692
      DO 1000 M=1,4
      DO 100 N=1,4
      KC=-C
      DO 200 I=1,2
      AT=-C
      DO 201 J=1,2
      CALL INTE_FUNCTION_F(KC,AT,FAI,D1KC,D1AT)
      DO 101 K1=1,2
      DO 101 K2=1,2
  101 RL(K1,K2)=0
      XC=0
      YC=0
```

```
      U=0.
      V=0.
      FF=0.
      STR=0.
      IND=0.
      DO 102 KK=1,4
      RL(1,1)=RL(1,1)+D1KC(KK)*X(NO(KK))
      RL(2,2)=RL(2,2)+D1AT(KK)*Y(NO(KK))
      RL(1,2)=RL(1,2)+D1KC(KK)*Y(NO(KK))
      RL(2,1)=RL(2,1)+D1AT(KK)*X(NO(KK))
      XC=XC+FAI(KK)*X(NO(KK))
      YC=YC+FAI(KK)*Y(NO(KK))
      U=U+FAI(KK)*UX(NO(KK))
      V=V+FAI(KK)*UY(NO(KK))
      FF=FF+FAI(KK)*F(NO(KK))
      STR=STR+STRESS(NO(KK))*FAI(KK)
      TEM=TEM+T(NO(KK))*FAI(KK)
      IND=IND+INDUCT(NO(KK))*FAI(KK)
  102 CONTINUE
      DEL=RL(1,1)*RL(2,2)-RL(1,2)*RL(2,1)
      RINVL(1,1)=RL(2,2)/DEL
      RINVL(1,2)=-RL(1,2)/DEL
      RINVL(2,2)=RL(1,1)/DEL
      RINVL(2,1)=-RL(2,1)/DEL
      PFX(M)=(RINVL(1,1)*D1KC(M)+RINVL(1,2)*D1AT(M))
      PFX(N)=(RINVL(1,1)*D1KC(N)+RINVL(1,2)*D1AT(N))
      PFY(M)=RINVL(2,1)*D1KC(M)+RINVL(2,2)*D1AT(M)
      PFY(N)=RINVL(2,1)*D1KC(N)+RINVL(2,2)*D1AT(N)
      IF(FF.LT.1.) THEN
      DENSITY=1
      CP=100
      ENDIF
      CONDUCT=FKH
      KBD(M,N)=KBD(M,N)+(U*U*PFX(M)*PFX(N)+
     #V*V*PFY(M)*PFY(N)+U*V*PFY(M)*PFX(N)+U*V*
     #PFX(M)*PFY(N))*DTIME/2.*DEL*DENS*CP
      KA(M,N)=KA(M,N)+FAI(M)*(U*PFX(N)+V*PFY(N))
      IF(FF.LT.1.) CONDUCT=0.0001
      KD(M,N)=KD(M,N)+CONDUCT*(PFY(M)*PFY(N))*DEL
      MT(M,N)=MT(M,N)+FAI(M)*FAI(N)*DEL
      BT(M)=BT(M)+VISCOS_HEAT*FAI(M)*DEL*DTIME
      T_SHIFT=C1*EXP(-C2/ABS(STR)
       TIME_INDUCT=TIMEM*(TM0-TEM+T_SHIFT)**(-A)
      BI(M)=BI(M)+1/TIME_INDUCT*FAI(M)*DEL*DTIME
      IF(INDUCT(IE).GE.1) THEN
      F0=2*(TEM+273)/(TEM+TM0+T_SHIFT+273*2)
      SUPERCOOL=TM0-TEM+T_SHIFT
       T_HALF=T_HALF0*EXP(-U_STAR/R/(TEM-T_ULT))*
     #EXP(-KG/SUPERCOOL/(TEM+273)/F0)
       CRYST_RATE=0.8325*T_HALF
      BC(M)=BC(F)+CRYST_RATE*AVRAMI*CRYST(IE)
     #**(1-1/AVRAMI)*DTIME%FAI(M)*DEL
      ENDIF
      AT=2.*C
  201 CONTINUE
      KC=2.*C
  200 CONTINUE
```

```
 100   CONTINUE
 1000 CONTINUE
      DO 210 I=1,4
      DO 210 J=1,4
      BT(I)=BT(I)+(MT(I,J)-(KA(I,J)*DENS*CP+
     #0.5*KD(I,J)+KBD(I,J)*DENS*CP
     #)*DTIME)*T(NODE_F(IE,J))
      BI(I)=BI(I)+(MT(I,J)-(KA(I,J)+
     #0.5*KD(I,J)+KBD(I,J)
      BT(I)=BT(I)+(MT(I,J)-(KA(I,J)+
     #0.5*KD(I,J)+KBD(I,J)
      S(I,J)=MT(I,J)*DENS*CP+0.5*KD(I,J)*DTIME
      SI(I,J)=MT(I,J)+0.5*KD(I,J)*DTIME
      SC(I,J)=SI(I,J)
  210 CONTINUE
      RETURN
      END
C
      SUBROUTINE GLOBAL_MT(GLOBAL_T,GF_T,LHB,NODE_F,F)
      DOUBLE PRECISION GLOBAL_T(5000,100), GF_T(5000),
     #S(4,4),BT(4),X(5000),Y(5000),F(5000),INDUCT(5000)
     #,CRYST(5000),BI(4),BC(4),SI(4,4),SC(4,4)
      DIMENSION NODE_F(5000,4)
      COMMON/CO/X,Y
      COMMON/TEM/T
      COMMON/CC/INDUCT, CRYST
      COMMON/IC/GLOBAL_I, GF_I
      COMMON/SC/GLOBAL_C, GF_C
      COMMON/NXY/NX,NY
      COMMON/TCI/S,BT,SC,BC,SI,BI
      COMMON/CC/CRYST, INDUCT
      NODENUM=(2*NX-1)*(2*NY-1)
      LEMENT_NUM=(NX-1)*(NY-1)*4
      DO 10 I=1,NODENUM
      GF_T(I)=0.
      DO 10 J=1,LHB
      GLOBAL_T(I,J)=0.
  10  CONTINUE
      DO 123 KLM=1,LEMENT_NUM
      CALL ELEMENT_T(KLM,NODE_F,F)
      DO 200 I=1,4
      NR=(NODE_F(KLM,I))
      GF_T(NR)=GF_T(NR)+BT(I)
      GF_I(NR)=GF_I(NR)+BI(I)
      GF_C(NR)=GF_C(NR)+BC(I)
      DO 200 J=1,4
      NCL=(NODE_F(KLM,J)-1)
      NC=NCL+2-NR
      IF(NC.GT.0)THEN
      GLOBAL_T(NR,NC)=GLOBAL_T(NR,NC)+S(I,J)
      GLOBAL_I(NR,NC)=GLOBAL_I(NR,NC)+SI(I,J)
      GLOBAL_C(NR,NC)=GLOBAL_C(NR,NC)+SC(I,J)
      ENDIF
 200  CONTINUE
 123  CONTINUE
      RETURN
      END
```

```
      SUBROUTINE BOUNDARY_T(LHB,NX,NY,NF)
      DOUBLE PRECISION GLOBAL_T(5000,100),GF_T(5000)
      Common/GT/Global_T, GF_T
      Common/BI/TW, TI
      NODENUM=(2*NX-1)*(2*NY-1)
      DO 70 NC=1,NF
      DO 70  NB=1,2*NY-1
      IE=(NC-1)*(2*NY-1)+NB
      IT=LHB-1
      I=IE-LHB
      DO 71 II=1,IT
      I=I+1
      IF(I.GE.1)THEN
      J=IE-I+1
      GF_T(I)=GF_T(I)-GLOBAL_T(I,J)*TI
      GLOBAL_T(I,J)=0.
      ENDIF
71    CONTINUE
      GLOBAL_T(IE,1)=1.0
      GF_T(IE)=TI
      I=IE
      DO 72 II=2,LHB
      I=I+1
      IF(I.LE.NODENUM)THEN
      GF_T(I)=GF_T(I)-GLOBAL_T(IE,II)*TI
      GLOBAL_T(IE,II)=0.
      ENDIF
72    CONTINUE
70    CONTINUE
      DO 80  NB=NF+1,2*NX-1
      IE=(NB-1)*(2*NY-1)+1
      IT=LHB-1
      I=IE-LHB
      DO 81 II=1,IT
      I=I+1
      IF(I.GE.1)THEN
      J=IE-I+1
      GF_T(I)=GF_T(I)-GLOBAL_T(I,J)*TW
      GLOBAL_T(I,J)=0.
      ENDIF
81    CONTINUE
      GLOBAL_T(IE,1)=1.0
      GF_T(IE)=TW
      I=IE
      DO 82 II=2,LHB
      I=I+1
      IF(I.LE.NODENUM)THEN
      GF_T(I)=GF_T(I)-GLOBAL_T(IE,II)*TW
      GLOBAL_T(IE,II)=0.
      ENDIF
82    CONTINUE
80    CONTINUE
      END
```

```
C****THIS IS A PROGRAM TO CALCULATE THE CRYSTALLIZATION
C****AFTER FILLING.

      DOUBLE PRECISION T(400,1000),CRYSTALL(400,1000),
     #STRESS(400,1000),DF(400,1000)
     #,INDUCT(400,1000),K(400,1000),BT(2),DC(400,1000),
     #GLOBAL_T(400,10),F1(400),ELEMENT_P(2,2),
     #X(400,1000),Y(400,1000),C_R(400,1000)
      DOUBLE PRECISION STRESS,TIME_INDUCT
      HOLD_TIME=50
      DT=0.01
C     PARAMETERS FOR INDUCTION TIME
      A=6.4
      TIMEM=4.68E13
C     MATERIAL PROPERTIES
      CONDUCT=1.9E4
      HEAT_CAPACITY=1.5E7
      DENSITY=1.356
      CRYST_CAPACITY=1.25E9
      ALFA=CONDUCT/DENSITY/HEAT_CAPACITY
      HEAT_RESISTANCE=5E-6

C     PARAMETRS FOR K

      T_HALF0=4.25E4
      KG=3.83E5
      U_STAR=6284
      R=8.31
      TM0=280
      TG=73
      T_ULT=TG-30
      AVRAMI=2
      LHALF=2
C READ FROM FILE THE ELEMENT NUMBER AND GRID NUMBER IN
C GAPWISE
      TM=250
      OPEN(9, FILE='FILE2.DAT',STATUS='OLD')
       READ(9,101) LEMENT,NY,TW

 101 FORMAT(I4,2X,I4,2X,F12.5)

C*****READ TEMPERATURE,CORDINATES FROM FILE

       OPEN(7,FILE='FILE1.DAT',STATUS='OLD')
       READ(7,102)((X(I,J),Y(I,J),T(I,J),
      #STRESS(I,J),J=1,NY),I=1,LEMENT)
 102   FORMAT(4(E12.5,4X))

C****READ CRYSTALLIZATION DATA AT THE END OF FILLING STAGE

      OPEN(10, FILE='FILE2.DAT',STATUS='OLD')
      READ(10,103)((DF(I,J),INDUCT(I,J),J=1,NY),
     #I=1,LEMENT)
 103 FORMAT(2(E12.5,4X))

      DY=Y(1,2)-Y(1,1)
      DO 11 I=1,LEMENT
```

```
      DO 11 J=1,NY
      K(I,J)=0
      DC(I,J)=0
      IF(DF(I,J).EQ.0) DF(I,J)=1E-15
 11   CONTINUE
      N=0
 200  N=N+1
      TIME=DT*N
      WRITE(*,*) TIME
      IF(TIME.GT.HOLD_TIME) GOTO 3000
      DO 9 I=1,LEMENT
      DO 9 J=1,NY
 9    C_R(I,J)=DC(I,J)
      DO 10 I=1,LEMENT
      DO 10 J=1,NY

C****STRESS RELAXATION

      AR=-(8.86*(T(I,J)-250))/(101.6+T(I,J)-250)
      RELAX=8*10**AR
      IF(AR.GT.5) GOTO 91
      IF(RELAX.LT.1E-4) THEN
      GOTO 91
      ENDIF
      STRESS(I,J)=STRESS(I,J)*EXP(-DT/RELAX)
  91  CONTINUE
      T_SHIFT=37.3*EXP(-40000/ABS(STRESS(I,J)))
      IF(INDUCT(I,J).GE.1)GOTO 201
      TIME_INDUCT=TIMEM*(TM0-T(LET,J)+T_SHIFT)**(-A)
      INDUCT(I,J)=INDUCT(I,J)+DT/TIME_INDUCT

C****CRYSTALLIZATION USING INTEGRAL EQUATION

 201  IF(INDUCT(I,J).GE.1) THEN
      TEM=T(I,J)
      F0=2*(TEM+273)/(TEM+TM0+T_SHIFT+273*2)
      SUPERCOOL=TM0-TEM+T_SHIFT
      T_HALF=T_HALF0*EXP(-U_STAR/R/(TEM-T_ULT))*
     #EXP(-KG/SUPERCOOL/(TEM+273)/F0)
      CRYST_RATE=0.8325*T_HALF
      DF(I,J)=DF(I,J)+CRYST_RATE*AVRAMI*DF(I,J)
      ***(1-1/AVRAMI)*DT
      DC(I,J)=1-EXP(-DF(I,J))
      ENDIF
 10    CONTINUE
      DO 240 LET=2,LEMENT
      DO 509 I=1,NY
      F1(I)=0
      DO 509 J=1,2
 509  GLOBAL_T(I,J)=0
      DO 510 J=1,NY-1
      ELEMENT_P(1,1)=DY/3.+ALFA/DY*DT
      ELEMENT_P(1,2)=DY/6.-ALFA/DY*DT
      ELEMENT_P(2,1)=DY/6.-ALFA/DY*DT
      ELEMENT_P(2,2)=DY/3.+ALFA/DY*DT
      BT(1)=DY/3.*T(LET,J)+DY/6.*T(LET,J+1)
     #+0.5*(DC(LET,J)C_R(LET,J))*CRYST_CAPACITY*DY/2/
```

```
     #HEAT_CAPACITY
      BT(2)=DY/6.*T(LET,J)+DY/3.*T(LET,J+1)
     #+0.5*(DC(LET,J)-C_R(LET,J))*CRYST_CAPACITY*DY/2/
     #HEAT_CAPACITY
      DO 611 K1=1,2
      LR=(J-1)+K1
      F1(LR)=F1(LR)+BT(K1)
      DO 611 K2=1,2
      NCL=J-1+K2-1
      NC=NCL+2-LR
      IF(NC.GT.0) THEN
      GLOBAL_T(LR,NC)=GLOBAL_T(LR,NC)+ELEMENT_P(K1,K2)
      ENDIF
  611 CONTINUE
  510 CONTINUE
      F1(NY)=TW
      IE=NY
      IT=LHALF-1
      I=IE-LHALF
      I=I+1
      IF(I.GE.1)THEN
      J=IE-I+1
      F1(I)=F1(I)-GLOBAL_T(I,J)*TW
      GLOBAL_T(I,J)=0.
      ENDIF
      GLOBAL_T(IE,1)=1.0
      F1(IE)=TW
      I=IE
      I=I+1
      IF(I.LE.NY)THEN
      F1(I)=F1(I)-GLOBAL_T(IE,2)*TW
      GLOBAL_T(IE,2)=0.
      ENDIF
      CALL SOLVE(GLOBAL_T,F1,NY,2)
      DO 280 J=1,NY
  280 T(LET,J)=F1(J)
  240 CONTINUE
      GOTO 200
 3000 CONTINUE
      OPEN(8, FILE='CRYSTALL.DAT',STATUS='OLD')
      WRITE(8,104) ((DC(I,J),T(I,J),STRESS(I,J),J=1,NY),
     #I=1,LEMENT)
  104 FORMAT(3(F12.5,4X))
      OPEN(10, FILE='1DIM.DAT',STATUS='OLD')
      WRITE(10,105)(Y(24,J),DC(24,J),J=1,NY)
  105 FORMAT(2F12.5)
      STOP
      END


      SUBROUTINE SOLVE(GLOBAL,GF,N_NODE,LHALF_BAND)
      DOUBLE PRECISION GLOBAL(400,10),
     #GF(400),FACTOR
      NODENUM=N_NODE
      MEQNS=NODENUM-1
      DO 103 NPIV=1,MEQNS
      NPIVOT=NPIV+1
```

```
      LSTSUB=NPIV+LHALF_BAND-1
      IF(LSTSUB.GT.NODENUM)THEN
      LSTSUB=NODENUM
      ENDIF
      DO 102  NROW=NPIVOT,LSTSUB
      NCOL=NROW-NPIV+1
      FACTOR=GLOBAL(NPIV,NCOL)/GLOBAL(NPIV,1)
      DO 101 NCOL=NROW,LSTSUB
      ICOL=NCOL-NROW+1
      JCOL=NCOL-NPIV+1
      GLOBAL(NROW,ICOL)=GLOBAL(NROW,ICOL)-
     #FACTOR*GLOBAL(NPIV,JCOL)
  101 CONTINUE
      GF(NROW)=GF(NROW)-FACTOR*GF(NPIV)
  102 CONTINUE
  103 CONTINUE
      DO 105 IJK=2,NODENUM
      NPIV=NODENUM-IJK+2
      GF(NPIV)=GF(NPIV)/GLOBAL(NPIV,1)
      LSTSUB=NPIV-LHALF_BAND+1
      IF(LSTSUB.LT.1)THEN
      LSTSUB=1
      ENDIF
      NPIVOT=NPIV-1
      DO 104 JKI=LSTSUB,NPIVOT
      NROW=NPIVOT-JKI+LSTSUB
      NCOL=NPIV-NROW+1
      FACTOR=GLOBAL(NROW,NCOL)
      GF(NROW)=GF(NROW)-FACTOR*GF(NPIV)
  104 CONTINUE
  105 CONTINUE
      GF(1)=GF(1)/GLOBAL(1,1)
      RETURN
      END
```

REFERENCES

1. J. H. Argyris, and T. J. R. Hughes, "Special Issue on Oil Reservoir Simulation," *Computer Methods in Applied Mechanics and Engineering,* vol. 47, 1984.

2. M. Avrami, "Kinetics of Phase Change, I. General Theory," *Journal of Chemistry Physics,* vol 7, pp1103-12, 1939.

3. M. Avrami, M, "Kinetics of Phase Change, II. Transformation-time Relations for Random Distribution of Nuclei," *Journal of Chemistry Physics*, vol. 8, pp212-224, 1940.

4. M. Avrami, "Granulation, Phase Change and Microstructure: kinetics of Phase Change," *Journal of Chemistry and. Phys*ics, vol. 9, pp177-184, 1941.

5. E. Baer and A. Moet, *High Performance Polymers: Structure, Properties, Composites, Fibers,* Oxford University Press, New York, 1991.

6. R. L. Ballman, T. Schusman and H. L. Toor, "Injection Molding," *Industry Engineering Chemistry,* vol. 51, pp847-850, 1959.

7. H. Belofsky, *Plastics: Product Design and Process Engineering*, Hanser Publishers, New York, 1995.

8. J. L. Berger and C. G. Gogos, "A numerical Simulation of the Cavity Filling Process with PVC in Injection Molding," *Polymer Engineering and Science,* vol. 13, pp102-108, 1973.

9. T. W. Chan and A. I. Isayev, "Measurement and Prediction of Nonisothermal Crystallization," SPE *ANTEC Conference Paper*, pp1148-51, 1992.

10. T. W. Chan and A. I. Isayev, "Quiescent Polymer Crystallization: Modeling and Measurements," *Polymer Engineering and Science,* vol. 34, pp461-471, 1994.

11. H. H. Chiang, C. A. Hieber and K. K. Wang, "A Unified Simulation of the Filling and Post-filling Stage in Injection molding: Part I. Formulation," *Polymer Engineering and Science,* vol. 31, pp116-124, 1991.

12. H. H. Chiang, C. A. Hieber and K. K. Wang "A Unified Simulation of the Filling and Post-filling Stage in Injection molding: Part II. Experimental Verification," *Polymer Engineering and Science*, vol. 31, pp125-132, 1991.

REFERENCES
(Continued)

13. C. A. Cuvelier, A. Segal and A. A. Vansteennhoven, *Finite Element Methods and Navier-Stokes Equations*, D. Reidel Publishing Company, Dordrecht, Holland, 1986.

14. J. D. Domine, and C. G. Gogos, "Simulations of Reactive Injection Molding," *Polymer Engineering and Science*, vol. 20, pp847-858, 1980.

15. J. Donea, "A Taylor-Galerkin Method for Convective Transport Problems," *International Journal for Numerical Methods in Engineering,* vol. 20, pp101-119, 1984.

16. G. Eder and H. Janeschitz-Kriegl, "Theory of Shear Induced Crystallization of Polymer Melts," *Colloid & Polymer Science,* vol. 266, pp1087-1094, 1988.

17. G. Eder, H. Janeschitz-Kriegl and S. Liedauer, "Crystallization Process in Quiescent and Moving Polymer Melts under Heat Transfer Conditions," *Progress in Polymer Processing*, vol. 15, pp629-714, 1990.

18. G. Eder and A. Wlochowicz "Kinetics of Non-Isothermal Crystallization of Polyethylene and Polypropylene," *Polymers, vol.* 24, pp1593-95, 1983.

19. J. D. Ferry, *Viscoelastic Properties of Polymers*, 3rd edition, Wiley, New York, 1980.

20. P. J. Flory, "Theory of Elastic Mechanisms of Fibrous Proteins," *Journal of American Chemistry Society*, vol. 18, pp5222-35, 1956.

21. D. M. Gao, K. T. Nguyen, A Garcia-Rejon and G. Salloum, "Numerical Modeling of the Mould Filling Stage in Gas-Assisted Injection Molding," *International Polymer Processing*, vol. 12, pp267-277,1997.

22. Y. K. Godovsky and G. L. Slonimsky, "Kinetics of Polymer Crystallization from the Melt," *Journal of Applied Polymer Science,* vol. 12, pp1053-80,1974.

23. C. G. Gogos and C. F. Huang and L. R. Schmidt, "The process of Cavity Filling Including the Fountain Flow in Injection Molding," *Polymer Engineering and Science*, vol. 26, pp1457-66, 1986.

24. X. Guo, A. L. Isayeve and L. Guo, "Crystallinity and Microstructure in Injection Molding of Isotactic Polypropylenes. Part I: A New Approach to Modeling and Model Parameters," *Polymer Engineering and Science*, vol. 39, pp 2096-2114, 1999.

REFERENCES
(Continued)

25. X. Guo, A. L. Isayev and M. Demiray, "Crystallinity and Microstructure in Injection Molding of Isotactic Polypropylenes. Part II: Simulation and Experiment," *Polymer Engineering and Science*, vol. 39, pp 2132-2149, 1999.

26. T. W. Haas and B. Maxwell, "Effects of Shear Stress on the Crystallization of Linear Polyethelene and Polybutene-1," *Polymer Engineering and Science,* vol. 9, pp225-241, 1969.

27. A. Hammami and A. K. Mehrotra, "Re-Examination of a Proposed Model for Nonisothermal Crystallization Kinetics," *Polymer Engineering and Science*, vol. 35, pp170-2, 1995.

28. A. Hammami and J. Spruiell, "Quiescent Non-isothermal Crystallization Kinetics od Isotactic Polypropylenes," *Polymer Engineering and Science,* vol. 35, pp797-804, 1995

29. S. Han and K. K. Wang, "Shrinkage Prediction for Slowly Crystallizing Thermoplastic Polymers in Injection Molding," *International Polymer Processing,* vol. 12, pp228-237, 1997.

30. F. H. Harlow and J. E. Welch, "Numerical Calculation of Time-Dependent Viscous Incompressible Flow of Fluid with Free Surface," *The Physics of Fluids*, vol. 3, pp2128-89, 1965.

31. D. H. Harry and R. G. Parrot, "Numerical Simulation of Injection Molding Filling," *Polymer Engineering and Science*, Vol. 10, pp209-214, 1970.

32. J. F. Hetu, D. M. Gao, A. Garcia-Rejon and G. Salloum, "3D Finite Element Method for the Simulation of the Filling Stage in Injection Molding," *Polymer Engineering and Science,* vol. 38, pp223-36, 1998.

33. C. A. Hieber and S. F. Shen, "A Finite Element/Finite Difference Simulation of the Injection Molding Process," *Journal of Non-Newtonian Fluids*, vol. 7, pp1-11, 1980.

34. C. A. Hieber, S. F. Shen, K. K. Wang and A. I. Isayev, "Filling Thin Cavities of Variable Thickness: A Numerical and Experimental Investigation." *Polymer Engineering and Science,* vol. 23, pp20-26, 1983.

35. C. W. Hirt, J. L. Cook and T. D. Bulter, "A Lagrangian Method for calculating the Dynamics of an Incompressible Fluid Free Surface," *Journal of Computational Physics,* vol. 5, pp103-124, 1970.

REFERENCES
(Continued)

36. C. W. Hirt and B. D. Nichols, "Volume of Fluid (VOF) Method for the Dynamics of Free Boundaries," *Journal of Computational Fluids,* vol. 39, pp201-225, 1981.

37. J. D. Hoffman, G. T. Davis and J. I. Lauritzen "Crystalline and Non Crystalline Solids," *Treatise on Solid state Chemistry*, J. B. Hannay., Plenum., New York, 1976.

38. C. M. Hsiung, M. Cakmak and J. L. White, "Crystallization Phenomena in the Injection Molding of Poly Ether Ehter Ketone and Its Influence on Mechanical Properties," *Polymer Engineering and Science,* vol. 30, pp967-80, 1990.

39. C. M. Hsiung and M. Cakmak, "Computer Simulations of Crystallinity Gradients Developed in Injection Molding of Slowly Crystallizing Polymers," *Polymer Engineering and Science* , vol. 31, pp1372-85, 1991.

40. A. I. Isayev, *Modeling of Polymer Processing, Recent Developments*, Hanser Publishers, New York, 1991.

41. A. I. Isayev, T. W. Chan, M. Gmerek and K. Shimojo, "Injection Molding of Semicrystalline Polymers I. Characterization," *Journal of Applied Polymer Science,* vol. 55, pp807-819, 1995.

42. A. I. Isayev, T. W. Chan, K. Shimojo and M. Gmerek, "Injection Molding of Semicrystalline Polymers II. Modeling and Experiments," *Journal of Applied Polymer Science* , vol. 55, pp820-838, 1995.

43. A. I. Isayev and C. A. Hieber, "Toward a Viscoelastic Modeling of the Injection Molding of Polymers," *Rheology Acta,* vol. 19, pp168-182, 1980.

44. P. Jog and V. M. Nadkarni, "Crystallization Kinetics of Polyphenylene Sulfide," *Journal of Applied Polymer Science* , vol. 30, pp997-1009, 1985.

45. M. R. Kamal, E. Chu and P. G. Lafleur, "Computer Simulation of Injecton Mold Filling for Viscoelastic Melts with Fountain Flow," *Polymer Engineering and Science,* vol. 26, pp190-196, 1986.

46. M. R. Kamal and S. Kenig, "The Injection Molding of Thermoplastics, Part 1. Theoretical Model," *Polymer Engineering and Science,* vol. 12, pp295-301, 1972.

REFERENCES
(Continued)

47. M. R. Kamal and S. Kenig, "The Injection Molding of Thermoplastics, Part 2. Experimental Tests of the Model," *Polymer Engineering and Science,* vol. 12, pp302-308, 1972.

48. M. R. Kamal, M. R., Y. Kuo and P. H. Daon, "Injection Molding Behavior of Thermoplastics in Thin Rectangular Cavities," *Polymer Engineering and Science,* vol. 15, pp863-868, 1975.

49. M. R. Kamal and P. G. Lafleur, "A Structure-Oriented Computer Simulization of Injection Molding of Viscoelastic Crystalline Polymers. Part II: Model Prediction and Experimental Results," *Polymer Engineering and Science,* vol. 26, pp103-110, 1986.

50. M. R. Kamal and T. D. Papathanasiou, "Filling of a Complex -Shaped Mold With a Viscoelastic Polymer. Part II: Comparison with Experimental Data," *Polymer Engineering and Science*, vol. 33, pp410-17, 1993.

51. S. P. Kim and S. C. Kim, "Crystallization Kinetics of Poly(ethylene terephthalate): Memory Effect of Shear History," *Polymer Engineering and Science,* vol. 33, pp83-91, 1993.

52. W. R. Krigbaum and R. J. Reo, "Diffraction Study of Crystallite Orientation in Stretched Polychloroprene Vulcanizates," *Journal of Polymer Science*, A2, pp4391-414, 1964.

53. Y. Kuo and M. R. Kamal, "The Fluid Mechanics and Heat Transfer of Injection Mold Filling of Thermoplastic Materials," *AIChE Journal*, vol. 22, pp661-673, 1976.

54. P. G. Lafleur and M. R. Kamal, "A Structure-Oriented Computer Simulation of the Injection Molding of Viscolastic Crystalline Polymers, Part I: Model with Fountain Flow, Packing, Solidification," *Polymer Engineering and Science,* vol. 26, pp92-102, 1986.

55. R. R. Lagasse and B. Maxwell, "An Experimental Study of the Kinetics of Polymer Crystallization During Shear Flow," *Polymer Engineering and Science*, vol. 16, 189-199, 1976.

56. M. Lambrigger, "Evaluation of data on the Kinetics of Isothermal Polymer Crystallization," *Polymer Engineering and Science*, vol. 36, pp98-99, 1996.

REFERENCES
(Continued)

57. H-S, Lee, H.-C. Sin and S-G. Kim, "Iterative Boundary Pressure Reflection Method for the Simulation of Injection Molding Filling," *Polymer Engineering and Science,* vol. 30, pp1513-22, 1990.

58. C. Lekakou, "Mathematical Modeling and Computer Simulations of the Flow, Nematic Phase Orientation, and Heat Transfer in Thermotropic Liquid Crystalline Polymers," *Polymer Engineering and Science,* vol. 37, pp529-540, 1997.

59. S. Liedauer, G. Eder, H. Janeschitz-Kriegl, P. Jerschow, W. Geymayer and E. Ingolic, "On the Kinetics of Shear Induced Crystallization in Polypropylene," *International Polymer Processing,* vol. 8, pp236-244, 1993.

60. T. Liu, Z. Mo, S. Wang and H. Zhang, "Non-isothermal Melt and Cold Crystallization Kinetics of Poly(aryl Ether Ether Ketone Ketone)," *Polymer Engineering and Science,* vol. 37, pp568-574, 1997.

61. L. Mandelkern, *Crystallization of polymers*, McGraw-Hill, New York, 1964.

62. L. T. Manzione, "Simulation of Cavity Filling and Curing in Reaction Injection Molding," *Polymer Engineering and Science*, vol. 21, p 1234-1243, 1981.

63. H. Mavridis, A. N. Hrymak, "Finite Element Simulation of Fountain Flow in Injection Molding," *Polymer Engineering and Science,* vol. 26, pp449-454, 1993.

64. J. Moitzi and P. Skalicky, "Shear-Induced Crystallization of Isotactic Polypropilene Melts: Isothermal WAXS Experiments with Synchrotron Radiation," *Polymers*, vol. 34, pp 1993.

65. K. Nakamura, T. Watanabe, "Some Aspects of Non-isothermal Crystallization of Polymers. I. Relationship between Crystallization Temperature, Crystallinity, and Cooling Conditions," *Journal of Applied Polymer Science*, vol. 26, pp1077-91, 1972.

66. K. A. Narh, E. Roa, M. D. Saindon and C. Cohen, Cornell Injection Molding Program, *Technical Reports No. 84*, College of Engineering, Cornell University, Ithaca, NY, 1995a.

67. K. A. Narh, E. Roa, M. D. Saindon, C. Cohen and K. K. Wang, "Rheo-Kinetic Measurement for the Determination of Stress-Induced Crystallinity in Polyehtylene Terephthalate," *Proc. SPE ANTEC'95,* pp2932-36 (1995b)

REFERENCES
(Continued)

68. T. A. Osswald and G. Menges, *Materials Science of Polymers for Engineers*, Hanse Publishers, New York, 1995.

69. T. Ozawa, "Kinetics of Nonisothermal Crystallization," *Polymer*, vol. 12, pp150-158, 1971.

70. T. D. Papathanasiou and M. R. Kamal (1993). "Filling of a Compex-Shaped Mold with a Viscoelastic Polymer. Part I. The Mathematical Model," *Polymer Engineering and Science*, vol. 33, pp400-40, 1993.

71. R. M. Patel and J. E. Spruiell, "Crystallization Kinetics During Polymer Processing--Analysis of Available Approaches for Process Modeling," *Polymer Engineering and Science*, vol. 31, pp730-738, 1991.

72. J. C. Robb and F. W. Peaker, Eds., *Progress in High Polymers*. London, Heywood, 1921.

73. M. E. Ryan and T. S. Chung, "Conformal Mapping Analysis of Injection Molding," *Polymer Engineering and Science*, vol. 20, pp642-650, 1980.

74. T. Sato and S. M. Richardson, "Numerical Simulation of the Fountain flow Problem for Viscoelastic Fluids," *Polymer Engineering and Science*, vol. 35, pp805-812, 1995.

75. W. Schneider and A. Koppel, "Non-Isothermal Crystallization Crystallization of Polymers." *International Polymer Processing,* vol. 2, pp151-154, 1988

76. L. R. Schmidt, "Glass Bead-Filled Polypropylene. Part I: Mold filling Studies during Injection Molding," *Polymer Engineering and Science*, vol. 17, pp666-670, 1977.

77. C. H. Sherwood and F. P. Price, "Effect of Shear on the Crystallization Kinetics of Poly(ehtylene Oxide) and Poly (ε–Caprolactone) Melts," *Journal of Polymer Science,* vol. 63, pp77-94, 1978.

78. W. L. Sifleet, N. Dinos and J. R. Collier, "Unsteady-State Heat transfer in a Crystallizing Polymer," *Polymer Engineering and Science,* vol. 13, pp10-16, 1973.

79. R. S. Spencer and G. D. Gilmore, "Flow Phenomenon In the Injection Molding of Polystyrene," *Modern Plastics*, vol. 2, pp143-6, 1950.

REFERENCES
(Continued)

80. L. Sridha, "Measurement and Modeling of Thermal Contact Resistance at a Plastic-Metal Interface," PhD dissertation, Mechanical Engineering Department, New Jersey Institute of Technology, 1999.

81. S. Srivivas, J. R. Babu, J. S. Riffle and G. L. Wilkes, "Kinetics of Isothermal and Nonisothermal Crystallization of Nocel Poly(Arylene Ehter Ether Sulfide)s," *Polymer Engineering and Science*, vol. 37, pp497-510, 1997.

82. R. B. Staub, "Effect of Basic Polymer Properties on Injection Molding Behavior," *SPE Journal*, vol. 17, pp345-348, 1961.

83. R. S. Stein, "Optical Studies of the Stress-Induced Crystallization of Polymers," *Polymer Engineering and Science*, vol. 16, pp152-157, 1976.

84. J. F. Stevenson, "A Simplified Method for Analyzing Mold Filling Dynamics: Part I. Theory," *Polymer Engineering and Science*, vol. 18, pp577-582, 1978.

85. Z. Tadmor, "Molecular Orientation in Injection Molding," *Journal of Applied Polymer Science*, vol. 18, pp 1753-1772,1974.

86. Z. Tadmor and C. G. Gogos, *Principles of Polymer Processing*, New Yok, Wiley Interscience, 1979.

87. V. Tan and C. G. Gogos, "Flow-Induced Crystallization of Linear Polyethylene Above Its Normal Melting Point," *Polymer Engineering and Scienc,* vol. 16, pp512-525, 1976.

88. V. Tan and M. R. Kamal. "The effect of Processing Variables on the Distribution of Morphological Zones and Orientation in Injection Molded Polyethylene," Proceedings of International Polymer Processing, pp665-593, MIT, Cambridge, MA,1977.

89. P. Thienel, and G. Menges, "Mathematical and Experimental Determination of Temperature, Velocity and Pressure Fields in Flat Molds During the Filling Process in Injection Molding of Thermoplastics," *Polymer Engineering and Science,* vol. 18, pp314-320, 1978.

90. E. Thompson, "Use of Pseudo-Concentration to Follow Creeping Viscous Flows During Transient Analysis," *International Journal for Numerical Methods in Fluids*, vol. 6, pp749-761, 1986.

REFERENCES
(Continued)

91. G. Titomanlio, V. Speranza and V. Brucato, "On the Simulation of Thermoplastic Injection Molding Process," *International Polymer Processing*, vol. 12, pp45-53, 1997.

92. A. S. Usmani, J. T. Cross and R. W. Lewis, "A Finite Element Model for the Simulations of Mould Filling in Metal Casting and the Associated Heat Transfer," *International Journal for Numerical Methods in Engineering*, vol. 35, pp787-806, 1992.

93. Wijigaarden, H. V., J. F. Dijksman, "Non-isothermal Flow of a Molten Polymer in a Narrow Rectangular Cavity," *Journal of Non-Newtonian Fluids*, vol. 11, pp175-179, 1982.

94. Williams, G. and H. A. Lord, "The Injection Molding of Thermoplastic Materials, I. Flow of Plastic Materials in Hot and Cold Walled Circular Channels," *Polymer Engineering and Science*, vol. 15, pp553-561, 1975.

95. Wu, P. C., C. F. Huang and C. G Gogos, "Simulation of Mold Filling Process," *Polymer Engineering and Science,* vol. 14, pp223-229, 1974.